Effect of mineral additions on the microstructure and properties of blended cement matrices for fibre-reinforced cement

Julian Eduardo Mejia Ballesteros [a,*], Holmer Savastano Jr. [a], Juliano Fiorelli [a], Moises Frias Rojas[b,*]

[a] University of São Paulo – Faculty of Animal Science and Food Engineering, Department of Biosystems Engineering. Duque de Caxias Norte, 225, 13630-000, Pirassununga, SP, Brazil.

[b] Eduardo Torroja Institute for Construction Science (IETcc-CSIC), 28033 Madrid, Spain.

*Corresponding author: E-mail address: julian.mejia@usp.br

Abstract

This first-ever detailed study of the effect of three mineral additions (limestone, rice husk ash and activated coal mining waste) differing in composition and properties explored the behaviour of blended cements with a 25 % replacement ratio. The aim was to select the optimal addition for improving the performance of natural fibre-reinforced cements. The pozzolanic, physical and mechanical properties as well as the pore structure of the blended cement matrices were examined. The findings showed that although rice husk ash is characterised by high pozzolanicity, it had a less favourable effect on the cement than expected, yielding porous, poorly compacted and hence weak matrices. The activated coal mining waste showed better performance, reaching similar strength to control mortar, better pore size refinement and an important reduction in mean pore size of 60% compared to control mortar after 60 days of curing. In light of those findings, this aluminosilicate addition is proposed as the most apt of the three studied for improving the quality of fibre-reinforced cements.

Keywords: activated coal mining waste, blended cement, pozzolanic reaction, properties, rice husk ash

1. Introduction

Worldwide economic development, with its attendant consumption of non-renewable natural resources and generation of polluting by-products, is exerting ever greater pressure on the environment. The construction industry is hardly exempt from responsibility for this situation. The production and use of

huge amounts of ordinary portland cement, its strategic material par excellence [1], are associated with the release of vast quantities of greenhouse gases [2,3]. From 5 % to 8 % of anthropogenic CO_2, to which global warming is primarily attributed [4], can be traced to portland cement manufacture, given the use of limestone as its main raw material [5,6]: from 800 kg to 900 kg of the gas are generated per tonne of clinker produced [7,8].

With a view to mitigating this environmental and social problem, the cement-based product industry is focusing its research and development effort on viable and innovate technologies that reduce its environmental footprint. The use of alternative fuels, carbon capture and storage, modifications to production systems and the partial replacement of portland clinker have emerged as potential alternatives [9,10]. The fourth option is not only regarded as the most cost-effective and practical [5] approach, but is reinforced by the circular economy principles that inform international policies prioritising the reuse of waste as a supplementary cementitious material [10,11]. For a number of years, research has been underway on alternative pozzolans deriving from agroindustrial waste [12,13] such as sugar cane bagasse, barley and rice husk [3,14] and bamboo [15] or inorganic materials, including fired clay plant rejects [16] and kaolinite-containing paper sludge [17] and coal mining waste [18-20]. When heated under pre-set, controlled conditions, all these materials are converted into pozzolanic supplementary cementitious materials [21-24].

This study pursued a deeper understanding of the effect of three mineral additions on eco-efficient binary cement performance: natural limestone, traditionally used to manufacture commercial cement; rice husk, an agroindustrial product, and kaolinite-based coal mining waste. Stockpiling the latter two generates severe environmental problems and constitutes a human health hazard.

Annual rice output is upward of 600 million tonnes globally [25,26], 20% of which is rice husk (RH) [27]. The world also produces over 7.4 billion tonnes of coal per year [28], generating waste from mining and washing [18,29] amounting to up to 40% of total output, depending on the industrial process involved [30]. The ash resulting from burning rice husk (RHA) is characterised by an 80% to 90% amorphous silica [21,31] and a low heavy metals content [13] as well as a high specific surface [32]. Thermally activated coal mining waste (ACW), in turn, contains 40% to 50% silica and 20% to 25% alumina [18,30]. When blended with cement, this aluminosilicate- or amorphous silica-rich waste

exhibits high pozzolanicity, i.e., it reacts intensely with portlandite [33-35]. That high pozzolanicity has a direct effect on blended cement matrix performance, interfacial transition zone behaviour and durability [36,37].

Products such as water tanks, flat boards and corrugated roof tiles are made from mineral-additioned, fibre-reinforced cement. In 2010 this $280 million industry (worldwide) was estimated to be growing at a rate of 10 % yearly [38], with Brazil as a major producer and consumer of its sustainable products [39]. One line of research focuses on natural fibres as an alternative to the reinforcing materials traditionally used (minerals such as asbestos, or synthetics such as polypropylene and polyvinyl alcohol) to manufacture eco-efficient, innovative, sustainable, inexpensive composites [35] able to perform as well or better than the classical materials. The use of such lignocellulose material to reinforce cement is constrained, however [41], by the high alkalinity of the matrix, which raises the pH in the system water. When absorbed by the highly hydrophilic the fibre, the water prompts alkaline hydrolysis-driven degeneration of the cellulose [42], the component that strengthens fibre-reinforced cement.

This study aimed primarily to enhance the scientific-technical knowledge of binary cement pastes and mortars bearing limestone, RHA or ACW to determine the properties that would endorse their application as fibre reinforcement in high performance cements. The replacement ratio applied, 25 %, was chosen because it is the standard ratio used in Brazil for limestone additions to portland cement [43]. The chemical properties (pozzolanicity) of the starting materials as well as the physical (workability, setting, expansion, heat of hydration) and mechanical (flexural and compressive strength) properties and microporosity of the products were analysed.

2. Material and methods

2.1 Materials

The experiments were conducted with a high early strength ASTM-C150 standard [44] Type III portland cement (PC) manufactured by InterCement Brasil (Estrutur Cauê) with a clinker content of

over 95 % and a maximum particle size of 15.34 μm. The three mineral additions used to prepare the binary cements were: a commercial dolomitic limestone (brand name Itaú), the mineral addition most commonly used in Brazil, with a maximum particle size of 30.36 μm; a silicoaluminous coal mining waste (CW) generated by an open-pit mine, and siliceous rice husk (RH), both furnished by private companies. Prior to blending, the two latter additions were thermally activated in a muffle furnace at 600 °C for 2 h, the optimal conditions for converting this inert waste into economically, energetically and environmentally viable cementitious products [24,45]. The RHA and ACW were subsequently ground and sieved to under 90 μm.

2.2 Experimental methods

2.2.1 Instrumental techniques

The elemental composition of the raw materials was determined on a Bruker S8 Tiger X-ray fluorescence spectrometer, fitted with a 4 kW intermediate X-ray tube and four analyser crystals (LiF (220), LiF (200), PET and XS-55).

Crystalline mineralogical phases were identified on a Bruker D8 Advance X-ray diffractometer with a 2.2 kW Cu anode X-ray tube operating at 3 kW, 30 kV and 30 mA. Diffractograms were recorded at 2θ angles of 5° to 70°, using a 0.5 sec count time per step and a step size of 0.01973°.

Thermogravimetric analyses (TG/DTG) were conducted on a TA SAT1600 analyser, with the following settings: N_2 atmosphere flow, 100 mL·min^{-1}; temperature range, 20 °C to 1000 °C; ramping rate, 10 °C·min^{-1}.

Porosity and pore size distribution were found on a Micrometrics Autopore IV mercury porosimeter accommodating pressures of up to 227.5 MPa. Specimens measuring approximately 1x1x1 cm were prepared and dried at 40 °C for 24 h.

Mortar morphology was determined on samples approximately 1x1 cm embedded in epoxy resin and meticulously polished for backscattering electron microscopic observation under a Hitachi S4800

scanning electron microscope (SEM) fitted with a Bruker XFlash 5030 Detector energy-dispersive X-ray spectrometer.

2.2.2 Methods

2.2.2.1 Chemical analysis

The pozzolanicity of the additions was found with the saturated lime test. In keeping with this accelerated chemical method, 1 g of sample was introduced in 75 mL of a saturated lime solution and heated in a laboratory kiln at 40 °C for 1 d, 7 d, 28 d or 90 d. The difference in the CaO content (mmol/L) in the solution containing the sample and the control solution (17.68 mmol/L) at each test time defined the amount of lime fixed by the pozzolan.

Cement pozzolanicity was determined using the Frattini procedure-based specifications laid down in Spanish and European standard UNE-EN 196-5 [46], in which the points on the (8 d and 15 d) hydroxy ion versus calcium oxide plots are compared to the respective calcium oxide solubility isotherm at 40 °C.

2.2.2.2 Physical analysis

The normal consistency of the blended pastes was found with a Vicat apparatus as described in Spanish and European standard UNE-EN 196-3 (part 5) [47].

Cement setting was evaluated as prescribed in standard UNE-EN 196-3 (part 6) [47] using an automatic Ibertest Vicat apparatus.

The volume stability test was conducted as described in standard UNE-EN 196-3 (part 7) [47].

Heat of hydration was determined during the first 95 h of hydration with the Langavant method as per standard UNE-EN 196-9 [48] on an Ibertest IB32-101E calorimeter fitted with WinLect32 software.

146
2.2.3 Preparation of blended cement matrices
147

148 Prismatic specimens (1x1x6 cm) prepared with 500 g of binder consisting in 75 wt% of ASTM Type
149 III portland cement and 25 wt% of one of the mineral additions (limestone, RHA or ACW) at a
150 constant water/binder ratio of 0.5 were cured in water for 2 d, 7 d, 28 d or 90 d. The specimens were
151 subsequently immersed in acetone for 24 h and vacuum dried for a further 24 h in to detain cement
152 hydration.
153

154 Cement mortars were prepared with the same 25 % replacement ratio as specified above and a
155 water/binder ratio of 0.5. Further to the recommendations in place [49], mechanical strength was
156 measured on 4x4x16 cm prismatic specimens. The fines used consisted in standardised natural sand
157 with a silica content of at least 98 % and a particle size of under 2 mm. The mean mechanical strength
158 values were analysed statistically to the Tukey randomised design procedure (significance level, 0.05)
159 using SAS version 9.3 software.
160

161 **3 Results and discussion**
162

163 3.1 Chemical and mineralogical characterisation of starting materials
164

165 The chemical composition of the starting materials is given in Table 1. Calcium oxide was the
166 majority component in the portland cement (59 %) [50] and limestone (44 %) [51]. As the acid
167 components (SiO_2 + Al_2O_3 + Fe_2O_3) in the limestone summed less than 3 % of the total mass, their
168 chemical reactivity with the hydrated lime [$Ca(OH)_2$] present in the cement was ruled out. The
169 chemical composition of RHA consisted primarily in amorphous silicon oxides (~90 %) [52], whilst
170 the aluminosilicates present in the ACW amounted to nearly 82 % of the total, a value comparable to
171 that reported for commercial metakaolin [53] and much higher than found for thermally activated
172 paper sludge (metakaolinite) [17]. The acid oxides (SiO_2 + Al_2O_3 + Fe_2O_3) in both RHA and ACW

accounted for over 85 % of the total, a composition commonly observed in pozzolans [15,35,52] and a value much higher than the minimum (≥70 %) specified in U.S. standard ASTM C618-17 [54] to qualify as a class N pozzolan. Of the minority elements (expressed in ppm) present, strontium, fluoride and chlorides in RHA and chromium and vanadium in ACW exhibited concentrations of over 100 ppm.

Table 1. X-ray fluorescence-based elemental composition of the starting materials (%).

Oxide	Portland cement	Limestone	RHA	ACW
SiO_2	18.53	1.79	89.71	56.63
Al_2O_3	4.75	0.61	0.14	25.29
Fe_2O_3	2.79	0.28	0.19	4.64
MnO	0.01	0.03	0.17	0.08
MgO	3.42	8.48	0.85	0.77
CaO	58.97	44.13	1.76	4.20
Na_2O	0.91	0.38	0.04	0.17
SO_3	4.58	0.08	0.35	0.27
K_2O	1.40	0.13	3.65	3.09
TiO_2	0.10	0.02	0.01	1.17
P_2O_5	0.20	0.10	1.40	0.14
LoI*	4.00	43.97	1.64	3.09
TOTAL	99.7	100.0	99.9	99.5
Minority element		Concentration (ppm)		
Sr	680	319	32	-
Ni	77	1	11	65
Cr	229	36	46	210
V	31	5	1	162
Zn	102	-	17	25
Pb	1	-	-	4
Cl	224	56	167	46
Zr	-	4	-	-
Y	5	2	-	-
Rb	10	3	-	-
F	1176	650	-	-
As	-	-	-	2
Co	-	-	-	24
Mo	-	-	-	21

*LOI: Loss on ignition (950º C)

The XRD patterns for the starting PC, limestone, RHA and ACW are reproduced in Fig. 1a, b, c and d, respectively. The main anhydrous phases in portland cement, clearly visible in Fig. 1a, included C_3S (a), C_2S (b), C_3A (ac), C_4AF (f), $CaCO_3$ (c), $CaSO_4.1/2H_2O$ (ba) and MgO in the form of periclase (pe), as expected for this material [55,56]. Traces of $Ca(OH)_2$ (p), one of the main hydrated phases in

hydrated cement, were also found, denoting minor cement hydration during storage as a result of Brazil's high relative humidity in certain seasons of the year.

The pattern for limestone (Fig. 1b) contained diffraction lines characteristic of calcite at 29.4° (2θ) and 30.9° (2θ) [57]. The diffractogram for RHA (Fig. 1c) showed a very wide band in the 10° to 40° range, denoting the highly amorphous nature of this agroindustrial ash [58], which would therefore be expected to exhibit greater reactivity with the lime present in cement. Traces of crystalline phases such as quartz (Q) at 26.6° (2θ) and calcite (c) at 29.4º (2θ) were also identified. The diffractogram for ACW (Fig. 1d) contained crystalline mineralogical phases, mainly quartz at 20.8° and 26.6° and smaller proportions of mica (m) at 8.8° and calcite (c). These findings were consistent with the values reported in the literature [24].

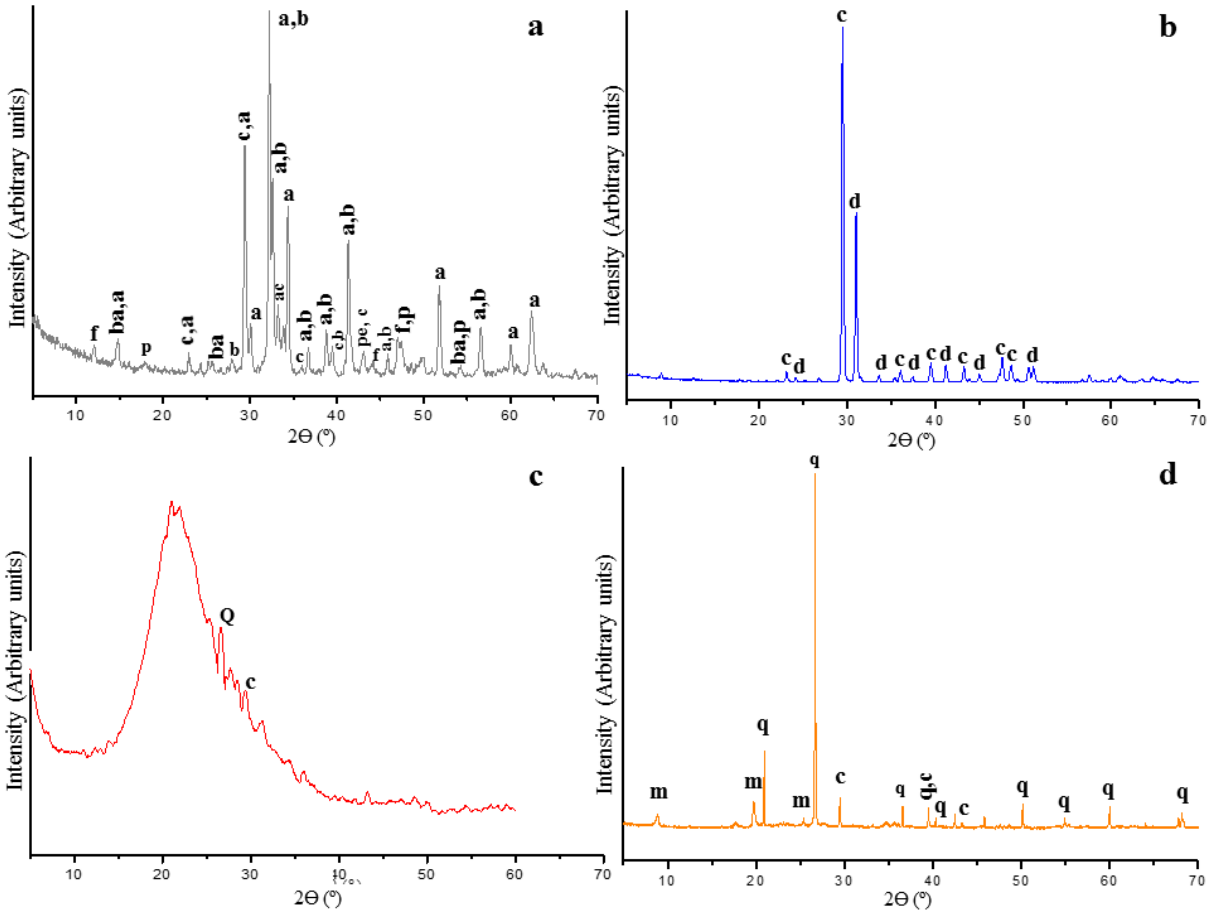

Fig. 1. XRD patterns for: (a) PC; (b) limestone; (c) RHA; and (d) ACW.

198 The thermogravimetric analyses (DTG) for the starting materials are shown in Fig. 2. Thermal
199 behaviour varied depending on the nature of the sample. Four significant weight loss bands were
200 identified for PC (Fig. 2a). The first, at 105 °C, with a mass loss of 0.56 %, might be related to
201 ettringite and C-S-H gel dehydroxylation [60] given that, as noted earlier, the cement showed signs of
202 hydration. The band at 238 °C (mass loss of around 0.24 %) was attributed to dehydroxylation of the
203 half molecule of water in bassanite [61]. A band appearing at around 395 °C was associated with the
204 dehydroxylation of portlandite (a phase previously identified by XRD) dehydroxylation [60,62], with a
205 mass loss of 0.62 %. The most intense band, at 714 °C, with a 2.83 % weight loss, was due to
206 carbonate decarbonation [63]. The DTG curve for calcite (Fig. 2b) was indicative of a highly stable
207 material at temperatures of up to 650 °C, with significant (44.4 %) mass loss at 650 °C to 850 °C,
208 peaking at 825 °C, attributable to decarbonation of dolomite, first, and subsequently of calcite [57].
209 Due to the overlap in this area of the graph, loss could not be quantified separately for the two
210 carbonates. RHA (Fig. 2c) exhibited a peak at 45 °C, denoting loss of moisture related to the high
211 volume and low density of rice husk ash particles [58,64,65]. The mass loss (0.54 %) observed in the
212 530 °C to 630 °C range, with a peak at 605 °C, would be the result of a number of effects: the
213 presence of traces of organic and volatile matter generated during calcination [66,67], gradual
214 decomposition of unburnt lignin [68] from temperatures of around 400 °C to 800 °C [68,69] and the
215 presence of calcite, identified by XRD. The peak at 895 °C would be associated with the
216 crystallisation of amorphous silica. Two bands located in the 250 °C to 450 °C range on the curve for
217 ACW (Fig. 2d) were attributable to the presence of unburnt coal waste and traces of kaolinite, with a
218 mass loss of 0.48 %, whilst the most intense band at 660 °C, indicative of a loss of 1.48 %, was due to
219 carbonate decarbonation.
220

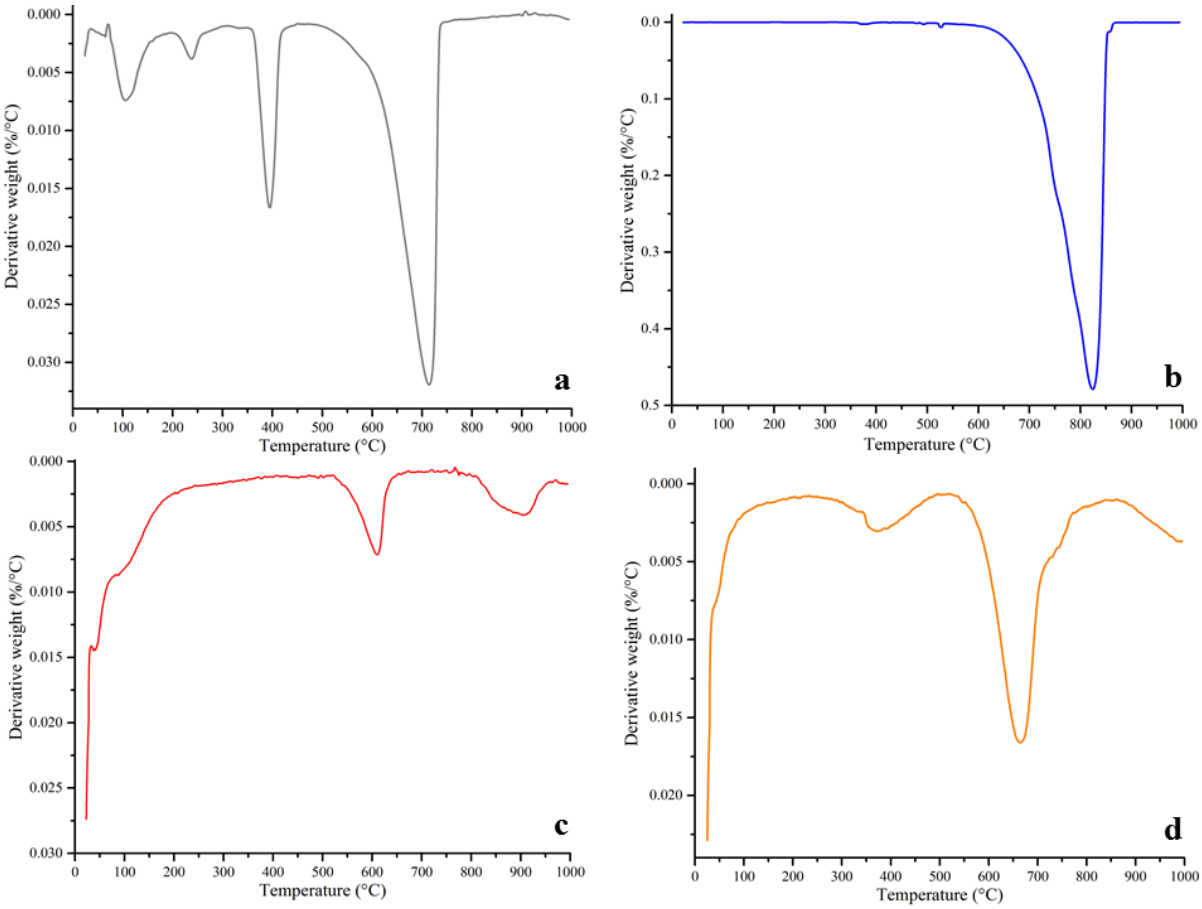

Fig. 2. DTG curves for: (a) cement; (b) limestone; (c) RHA; and (d) ACW.

3.2 Material pozzolanicity

3.2.1 Pozzolanic activity of the mineral additions

The 1 d, 7 d, 28 d and 90 d saturated lime solution test findings for additions RHA and ACW are shown in Fig. 3. Inasmuch as limestone exhibited no chemical capacity to react with lime [$Ca(OH)_2$], it was not tested for pozzolanicity.

The 90 d findings showed that both RHA and ACW fixed 90 % of the total lime available. The fixation rate varied, however, particularly in the first 7 d: RHA consumed 83 % of the lime in the first 24 h, double the amount fixed by ACW. That difference may play a significant role in blended cement matrix strength development.

The differences in pozzolanic behaviour between the two mineral additions would be primarily explained by the greater fineness, larger surface area and higher amorphous silica content in RHA [32,64,70,71] and corroborated by studies conducted on other pozzolans with similar chemical compositions [1,15,72].

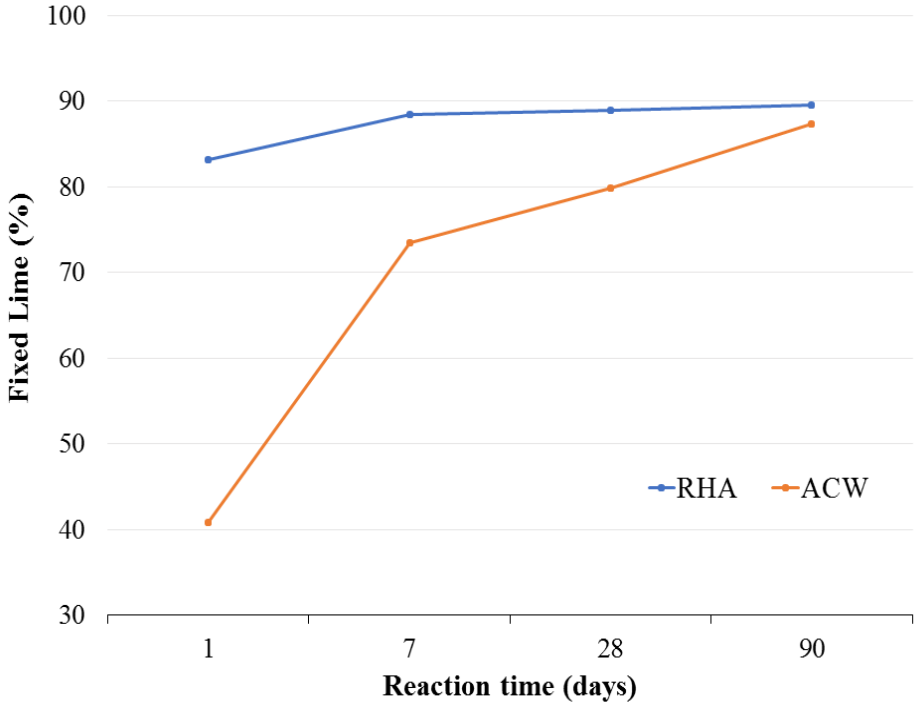

Fig. 3. RHA and ACW pozzolanicity versus time.

3.3.2 Blended paste pozzolanicity

The 8 d and 15 d Frattini test findings for the cement pastes (Fig. 4) reflected the reactivity of the pozzolans with the calcium hydroxide released during portland cement hydration. Further to Spanish and European standard UNE-EN 196-5 [46], a cement is regarded as pozzolanic (Type IV) if the value obtained lies below the solubility curve, as was observed for active pozzolans RHA and ACW. Even after 8 d the blended cements with 25 % replacement ratios met this pozzolanicity requirement. The RHA blends were more reactive with $Ca(OH)_2$ and exhibited a greater decline in the Ca^{2+} concentration than the ACW materials, corroborating the pure pozzolan/lime system findings

discussed above. The PC and PC+limestone pastes exhibited no pozzolanicity at either of the test times.

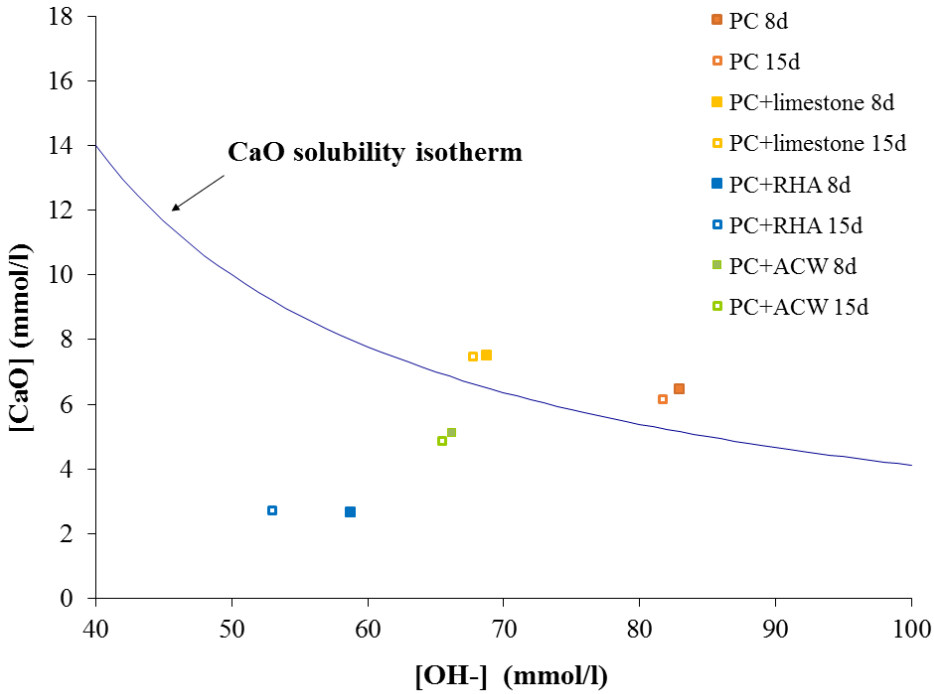

Fig. 4. Blended paste pozzolanicity further to the Frattini test.

3.4 Hydrated phases in the blended pastes

XRD (Figs. 5-8) and TG/DTG (Fig. 9) techniques were deployed to identify and monitor the mineralogical phases in 2 d, 28 d and 90 d prismatic cement paste specimens.

The 2 d reference PC (Fig. 5) contained crystalline mineralogical phases typical of anhydrous cement, such as C_3S (a), C_3S (b), C_3A (ac), $CaCO_3$ (c) and C_4AF (f), as well as the hydrated mineralogical phases $Ca(OH)_2$ (p) and ettringite (e). As hydration progressed (28 d to 90 d), the intensity of the alite and belite bands especially, as well as the tricalcium aluminate line, declined. That was attendant upon a rise in the intensity of the diffraction lines for portlandite and the appearance of monocarboaluminates (ca) after 28 d. The binary cement pastes prepared with limestone (Fig. 6) behaved in much the same manner as the reference cement, except that they contained higher proportions of calcite ($CaCO_3$) and dolomite [$MgCa(CO_3)_2$]. The pastes bearing 25 % RHA (Fig. 7)

contained many of the same anhydrous mineralogical phases as the two preceding pastes, although intensity was much lower in the portlandite band, particularly in the 90 d material, and slightly higher in the ettringite diffraction line. No monocarboaluminate formation was detected in this binary cement. The decline in portlandite was the expected result of the rice husk ash-driven formation of (primarily) C-S-H gel [73]. The anhydrous alite and belite phase content was greater than in the non-pozzolanic cement pastes, denoting lower cement particle hydration, either because the RHA absorbed significant amounts of water or because the anhydrous cement particles acted as precipitation sites for the hydrated phases [3,6]. The more intense portlandite band on the pattern for the cement pastes containing ACW (Fig. 8) than observed for the RHA material was the result of the slower rate of the pozzolanic reaction mentioned earlier. Considerable amounts of monocarboaluminate were observed to form beginning in the 28 d pastes, favoured by the extra supply of reactive alumina sourced from the ACW [29].

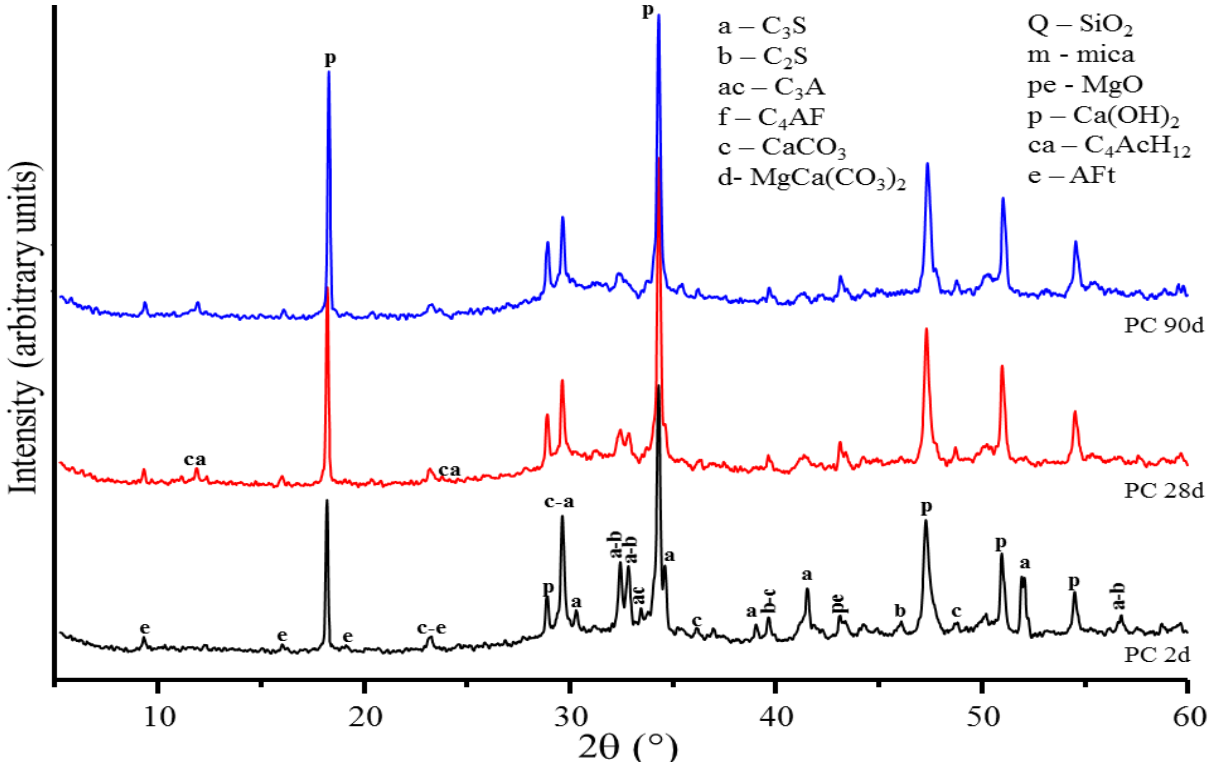

Fig. 5. Reference cement paste (PC) mineralogy versus reaction time.

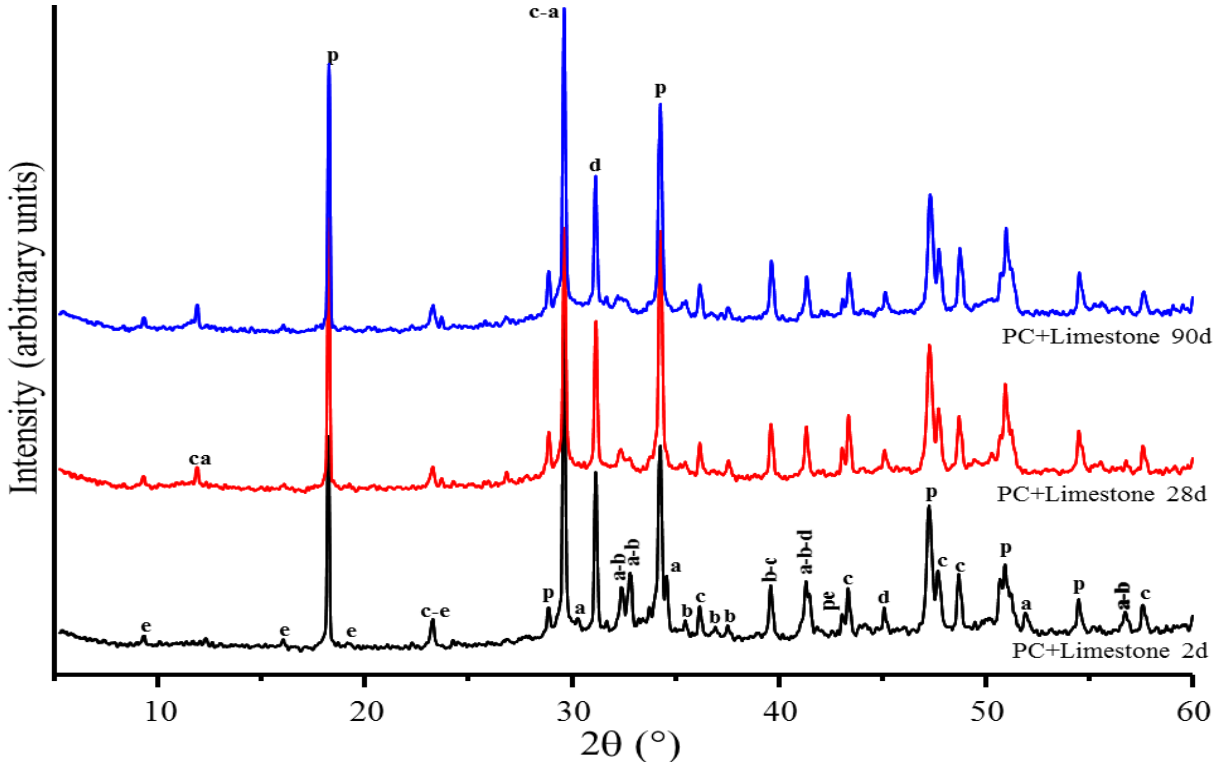

Fig. 6. Mineralogy of 25 % limestone cement paste versus reaction time.

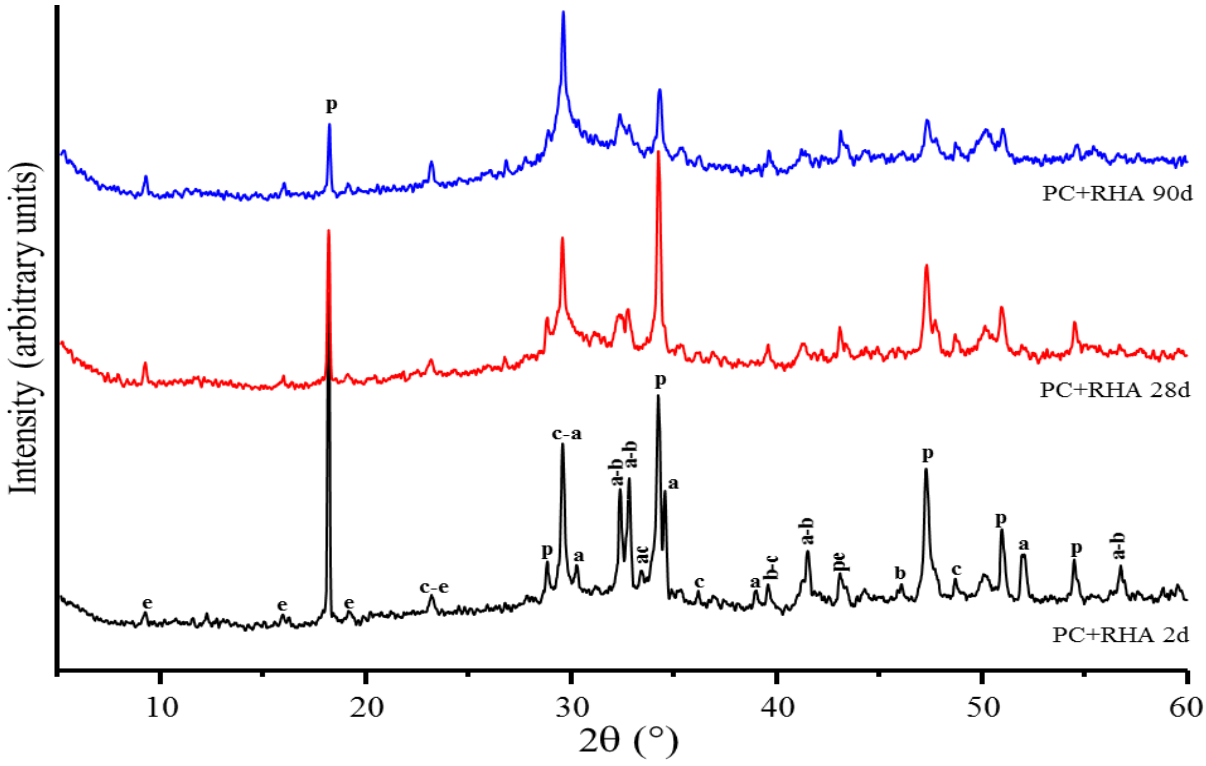

Fig. 7. Mineralogy of 25 % RHA cement paste versus reaction time.

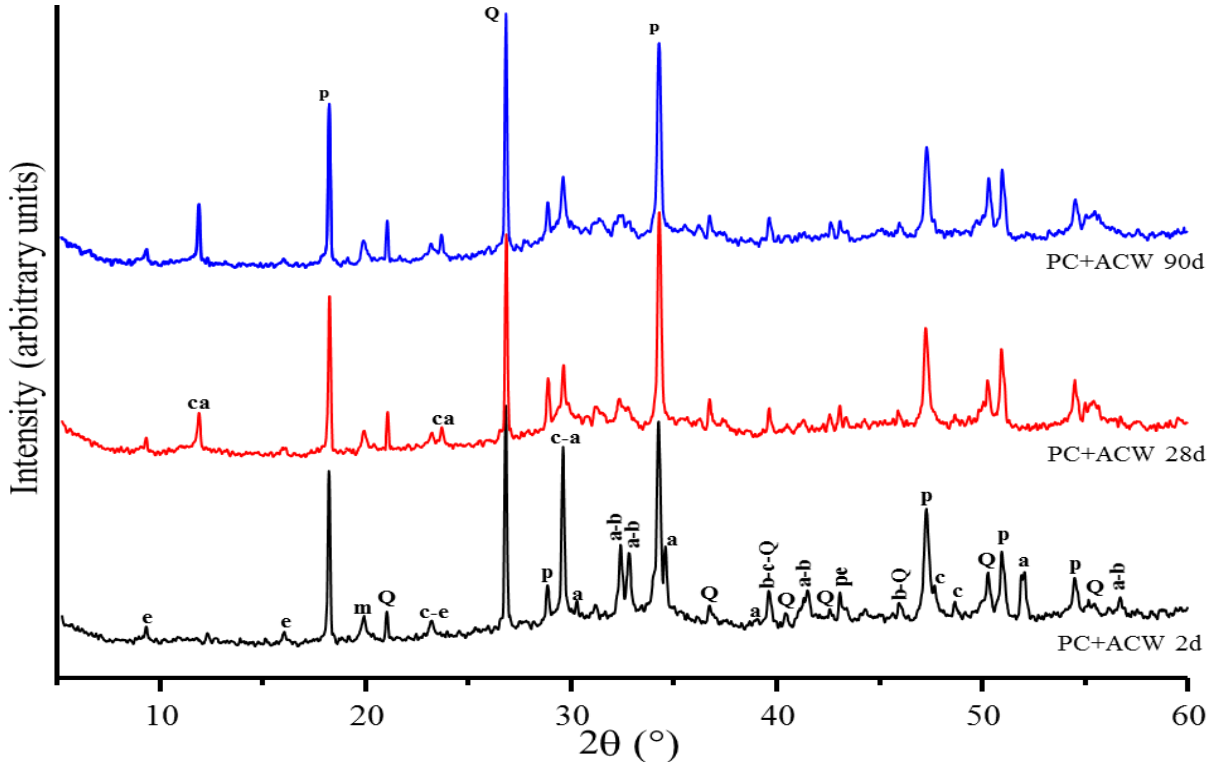

Fig. 8. Mineralogy of 25 % ACW cement paste versus reaction time.

Table 2 gives the percentage weight loss for the cements studied in the three temperature ranges with the steepest declines (further to the DTG curves in Fig. 9), namely 50 °C to 300 °C, 400 °C to 500 °C and 500 °C to 750 °C.

The main hydrated phases in cement dehydroxylated in the first range [20,74], where weight loss was observed to rise with curing time in all the cements analysed, with 90 d losses of 11 % to 16 %. The shallowest decline was recorded for the paste bearing 25 % limestone due to the filler effect of the addition, which nonetheless also reacted chemically with the aluminates in the cement to form hexagonal carboaluminate phases [75]. Weight loss was steepest in the 25 % RHA paste, which contained the most reactive pozzolan.

The bands for C-S-H gel and ettringite overlapped at 103 °C. At 2 days of hydration, a minor band overlapped with the main band at 145 °C, possibly attributable to the steadily intensifying dehydroxylation of metastable hexagonal compounds, C_4AH_{13} and C_4AcH_{12} [61,76,77], in the PC, PC+limestone and especially the PC+ACW pastes. As noted earlier, the higher content of these phases in the ACW-bearing material would be due to the additional source of reactive alumina present in the

306 addition (recycled metakaolinite). A band initially observed at 236 °C in the ACW paste that shifted to
307 260 °C in the 90 day cement was generated by the dehydroxylation of layered double hydroxide
308 (LDH)-like structures, a hydrated phase typical of the pozzolanic reaction between the recycled
309 metakaolin (MK) in coal waste and portlandite [29].

310 In the 400 °C to 500 °C range, a weight loss band characteristic of portlandite dehydroxylation was
311 observed in all the cement pastes, although the pattern followed varied with the mineral addition.
312 Pursuant to the data in Table 2, the percentage of portlandite (H_2O loss x 74/18) in cement PC rose
313 with hydration time, from 15.91 % in the 2 day to 20.20 % in the 90 day paste, whereas in the blended
314 cements $Ca(OH)_2$ content fluctuated differently depending on the pozzolanicity of the additions. In the
315 25 % limestone cement, portlandite rose from 13.40 % to 15.85 %, values higher than the degree of
316 cement replacement (11.93 % to 15.15 %, corresponding to 75% cement), ratifying the filler and (non-
317 pozzolanic) chemical effects of the addition, which would accelerate portland cement particle
318 hydration. In the pastes bearing 25 % RHA, portlandite content fell by 31.86 % between 2 d and 90 d,
319 confirming the high pozzolanicity of the addition (Fig. 3). The pastes with 25 % ACW exhibited
320 portlandite contents of 13 % to 14 %, turning slightly downward between 28 d and 90 d, possibly
321 because ACW pozzolanicity peaked at 28 d. That trend would be masked by greater calcite formation
322 (4.17 % of the CO_2 released), due partly to possible portlandite carbonation during sample handling
323 and storage prior to characterisation.

324 The mass loss observed in all the pastes analysed between 500 °C ad 750 °C (Fig. 9) was reflected in a
325 wide band attributed to calcium carbonate decarbonation [74]. The greatest loss of CO_2 (Table 2) was,
326 as expected, observed for the paste with 25 % limestone, followed by paste PC, paste 25 % RHA and
327 paste 25 % ACW in that order, although the values for the latter two lay in a fairly narrow range, from
328 3.8 % to 4.45 %. In both cases, the calcite band was observed to split, with a small band appearing at a
329 lower temperature, associated with the formation of less crystalline calcite generated during partial
330 portlandite carbonation [78]. This was much more visible in the 25 % ACW pastes.

331 Table 2. Weight loss and portlandite content by curing time.

Temperature range	Curing age	Weight loss	$Ca(OH)_2$

	°C	días	%	%
PC	50-300	2	9.88	-
		28	12.83	-
		90	14.06	-
	400-500	2	3.87	15.91
		28	4.73	19.45
		90	4.94	20.20
	500-750	2	5.35	-
		28	4.09	-
		90	4.08	-
PC + limestone	50-300	2	8.2	-
		28	10.54	-
		90	11.25	-
	400-500	2	3.26	13.40
		28	3.82	15.70
		90	3.85	15.83
	500-785	2	13.71	-
		28	12.99	-
		90	13.79	-
PC + RHA	50-300	2	10.12	-
		28	13.81	-
		90	16.12	-
	400-500	2	2.58	10.61
		28	2.37	9.74
		90	1.76	7.23
	500-750	2	4.15	-
		28	4.26	-
		90	3.99	-
PC + ACW	50-300	2	8.83	-
		28	12.69	-
		90	14.03	-
	400-500	2	3.17	13.03
		28	3.39	13.94
		90	3.28	13.48
	500-820	2	4.45	-
		28	3.87	-
		90	4.17	-

332

333

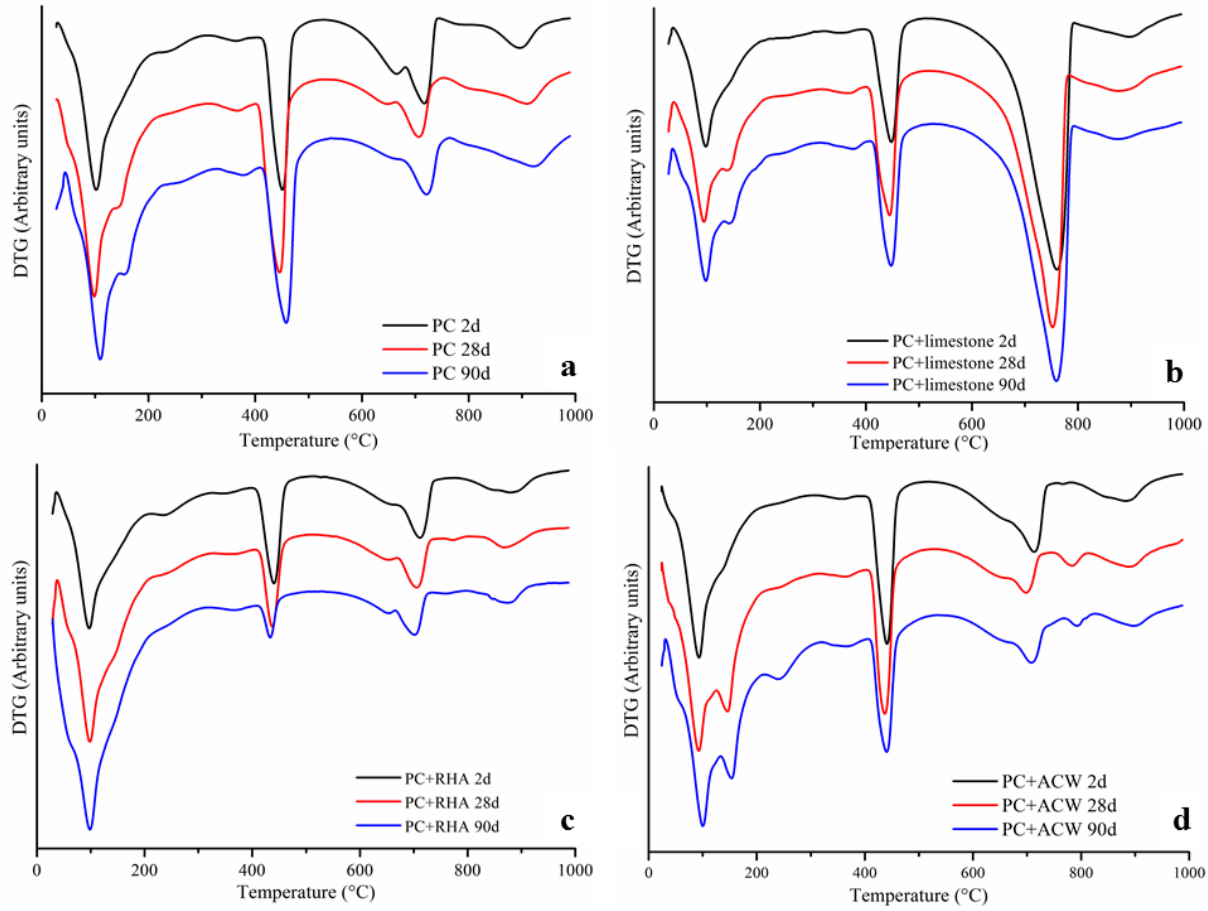

Fig. 9. 2 d, 28 d and 90 d DTG curves for: (a) PC; (b) PC+limestone; (c) PC+RHA; and (d) PC+ACW.

3.5 Physical behaviour of cement pastes

Data on the amount of water required for normal paste consistency, initial setting times and volume stability, parameters specified in the standards in place, are given in Table 3 [47]. Water demand was higher in the pozzolan-additioned pastes than in the reference, with a 98 % gain recorded in cement 25 % RHA and a 12.8 % rise in paste 25 % ACW. Those findings can be explained by the fineness of rice husk ash, which favoured water absorption, and the sorptivity of the clay minerals (MK, micas) present in ACW [79-81]. A rise in water demand as high as observed for RHA would jeopardise mechanical strength. The pastes prepared with limestone exhibited water demand slightly lower (9.4 %) than found in the reference PC.

No significant differences were observed in initial setting time (Table 3) between the control and the 25 % limestone and 25 % ACW pastes. According to prior studies [26], pozzolanic additions should

hasten the setting rate due to the greater early age water absorption induced. That behaviour was not observed for the cements with 25 % ACW (or limestone), however. Adding 25 % RHA, in turn, delayed setting time by approximately 200 min, a finding consistent with earlier reports [79,82] and related to the hydration-retarding effect of minority elements such as Zn, Pb and Ni [30,81]. That explanation was not applicable here, however, for the sum of these retarding elements was much smaller in the RHA studied than in the ACW used and the reference PC. The RHA findings may be associated with the high water sorptivity of the ash itself stemming from its high specific surface, which would delay initial setting time. Such behaviour could have a beneficial side effect, for it could obviate the need for commercial admixtures to prevent setting during the transport of ready-mix concrete. The setting times for all the cements analysed were standard UNE-EN 197-1-compliant [83].

The volume stability findings for the pastes (Table 3) showed that at a replacement ratio of 25 %, none of the minerals posed instability issues and all were consistent with the recommendations in place [83].

Table 3. Water demand for normal consistency, setting time (± 5 min) and volume stability (± 1 mm) for blended cement pastes.

Blend	Water demand (g)	Water penetration (mm)	Initial setting time (min)		Expansion (mm)	
			Measured	Standard requirement	Measured	Standard requirement
PC	164	33	235	≥ 60	0 ± 1	≤ 10
PC+limestone	154	35	245		1 ± 1	
PC+RHA	325	34	435		0 ± 1	
PC+ACW	185	36	255		0 ± 1	

3.6 Heat released and heat of hydration in blended mortars

The inclusion of mineral additions in the cement matrix has a direct impact on heat of hydration and hence on cement matrix durability (curing, shrinkage, cracking), particularly when large volumes of bulk cement are involved. This physical property, recently included in the standards in place [83], must be assessed.

The heat released in the first 95 h of the test is shown in Fig. 10. Heat release varied with the nature of the mineral addition, peaking at 14 h to 18 h. The highest temperature, 38.1 °C, was reached by

reference PC after 14 h, followed by PC+ACW, with 34.4 °C after 15 h. The temperatures recorded for PC+RHA (31.3 °C) and PC+limestone (31.3 °C) were similar, although the peaks were slightly retarded (16 h to 17 h).

The slightly higher early (≤ 10 h) temperatures observed for the mortars prepared with 25 % ACW and RHA than for the PC and 25 % limestone mortars would be associated with the dual pozzolanic and filler effects of the additions [84], although the pozzolanic effect was more visible at later ages [85]. All the additioned mortars, moreover, exhibited a lower peak temperature than the reference, an indication that dilution prevailed over the pozzolanic effect [86,87].

A certain contradiction in the heat release findings merits comment. On the one hand, the ash (comprising primarily reactive silica) is known to be highly pozzolanic, whilst on the other it released less heat than the other additions analysed. Such unexpected behaviour might be related to a shortage of hydration water in this mortar, given the use of a constant water/binder ratio across the board, the considerable lag in its initial setting time and even the diluting effect of the addition [88,89].

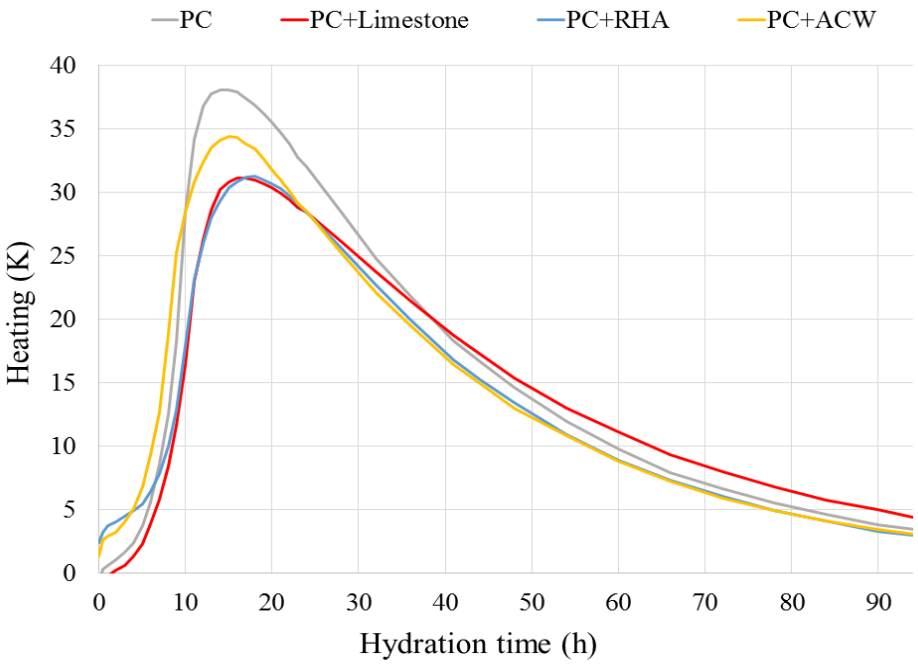

Fig. 10. Heat released in mortars versus time.

390 The heat of hydration curves for the standardized mortars are shown in Fig. 11. The curves were
391 divided into three time frames for more detailed analysis: 0 h to 5 h, 5 h to 24 h and 24 h to 94 h.

392 The mortars containing ACW and RHA generated greater heat of hydration than the reference PC
393 mortar in the first 5 h, whereas the limestone addition had the opposite effect. As noted, in RHA and
394 ACW that early behaviour might be the result of pozzolanic reactions and the formation of nucleation
395 sites that induce the filler effect-mediated growth of hydration products [70,89], whilst in limestone it
396 might be related to dilution.

397 In the second period (5 h to 24 h), the reference mortar exhibited a steep rise in heat of hydration
398 compared to the RHA- and limestone-additioned mortars. The mortar bearing ACW turned at 10 h,
399 when it began to release less heat than the PC mortar. After 30 h, heat of hydration was nearly
400 constant in all the mortars, with only insignificant rises.

401 Standard UNE-EN 197-1 [83] defines a low heat of hydration cement as one where the cumulative
402 41 h value is $\leq$ 270 J/g, whilst very low heat of hydration is defined in standard UNE-EN 14216:2015
403 [90] as <220 J/g. Further to the 41 h cumulative heat of hydration data in Table 4, only the material
404 prepared with 25 % limestone would be regarded as a low heat of hydration cement; given their
405 pozzolanic activity, the others would not be eligible for that category. Those findings may help
406 determine the applications for which each material is best suited.

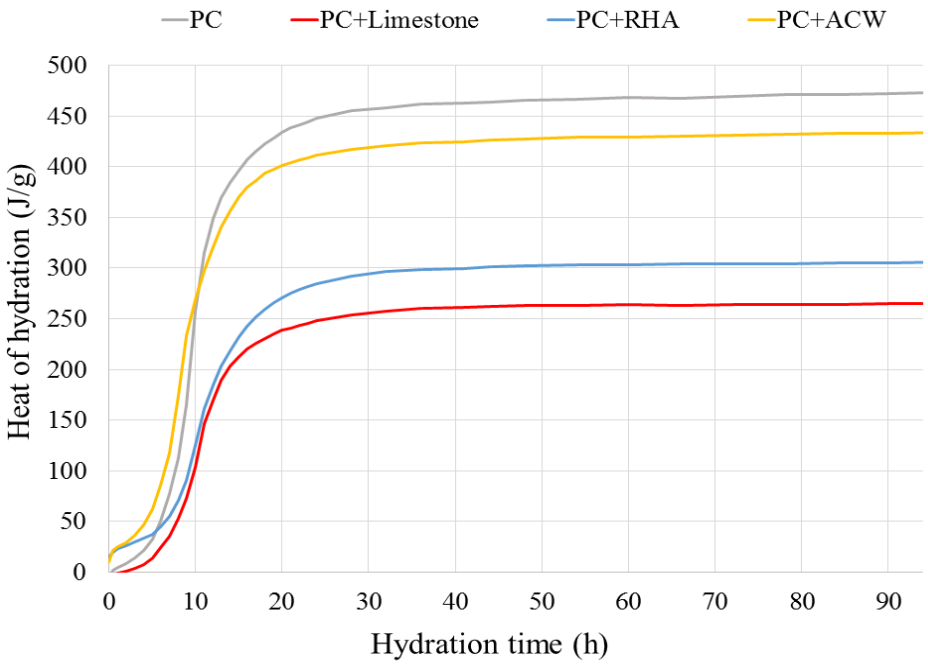

Fig. 11. Heat of hydration in selected mortars versus time

Table 4. Peak heat of hydration at 41 h.

Blend	Heat of hydration	Standard	
	J/g	UNE-EN 197-1	UNE-EN 14216
PC	462.9	< 270 J/g	< 220 J/g
PC+limestone	261.3		
PC+RHA	299.8		
PC+ACW	424.9		

3.7 Mortar mechanical strength

The 7 d and 60 d mean flexural and compressive strength values and standard deviations for the mortars prepared with cements containing 25 % limestone, RHA or ACW relative to the reference mortar (PC) are shown in FigS. 12 and 13.

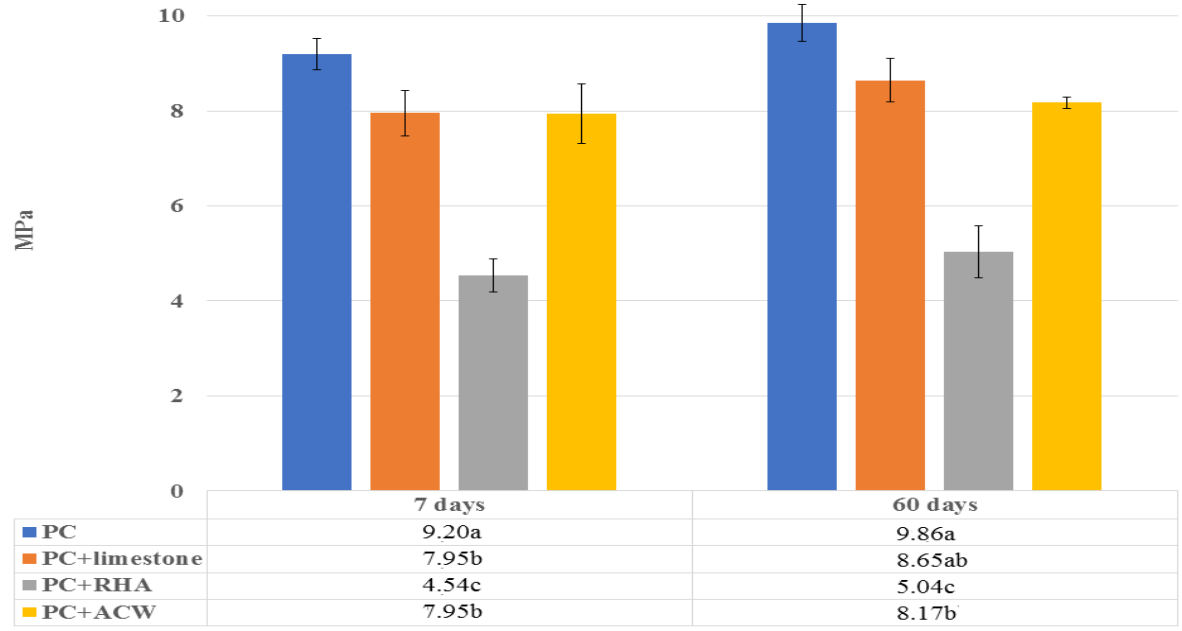

	7 days	60 days
PC	9.20a	9.86a
PC+limestone	7.95b	8.65ab
PC+RHA	4.54c	5.04c
PC+ACW	7.95b	8.17b

Fig. 12. Flexural strength versus curing time
(In each column different letters denote statistically significant difference at p<0.05 (Tukey).)

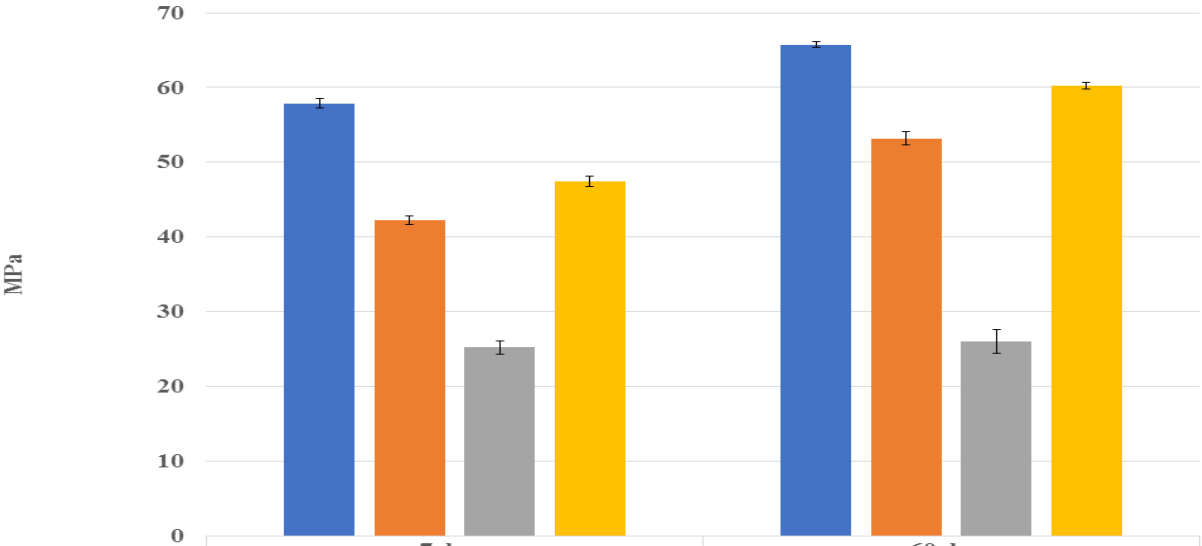

	7 days	60 days
PC	57.90a	65.73a
PC+limestone	42.29b	53.19b
PC+RHA	25.21c	26.03c
PC+ACW	47.41d	60.24d

Fig. 13. Compressive strength versus curing time
(In each column different letters denote statistically significant difference at p<0.05 (Tukey).)

Cement-based materials are known to be brittle in terms of flexural stress [91]. Fig. 12 shows that the replacement of cement with mineral additions in all cases induced a decline in 7 d flexural strength relative to the reference mortar, particularly in mortar PC+RHA, which exhibited a loss of 50.6 %,

whereas the PC+limestone and PC+ACW mortars each declined by 13.6 %. These differences proved to be statistically significant from the reference at $p<0.05$ when tested with the Tukey procedure. In the 60 d materials, the pattern was similar, with slight rises in flexural strength in all four mortars and differences similar to those observed in the 7 day materials.

Compressive strength trends (Fig. 13) resembled the flexural strength patterns. Compressive strength was significantly ($p<0.05$) lower in the three additioned mortars than in the reference. Here, however, the loss was lowest in PC+ACW at both curing ages. In the 7 d mortars, compressive strength was 27 % lower in PC+limestone, 56.5 % lower in PC+RHA and 18.1 % lower in PC+ACW than in the reference, while at 60 d the loss for the limestone-additioned mortar was 19.1 % and for the ACW 8.3 %. The loss in the RHA mortar intensified with time, however, to 60.4 % compared to the PC.

Similar mechanical strength patterns with the partial replacement of cement have been reported by a number of authors for other pozzolanic materials [1,22,75], for replacement of a percentage of cement impacts early age strength due to the dilution effect [92]. At later ages, cement hydration or pozzolanic reactions yield essentially primary and secondary C-S-H gels, raising mechanical strength [22,25,26,75]. Other factors also have a direct impact, such as the matrix densification [22,26] resulting from portlandite precipitation and reduced pore size.

The 25 % RHA pastes had lower strength at all curing ages due to their high specific surface, which increased [32] the amount of water needed to reach normal consistency. Since all the mortars were prepared with a fixed w/b ratio of 0.5, the result in PC+RHA was hydrated phase-low, poorly compacted, porous matrices, all of which translated into considerably lower strength than in the reference. Those findings were corroborated by the SEM micrographs of the 60 d mortars in Fig. 14, which clearly show the lesser density and greater porosity in the 25 % RHA than in the other mortars.

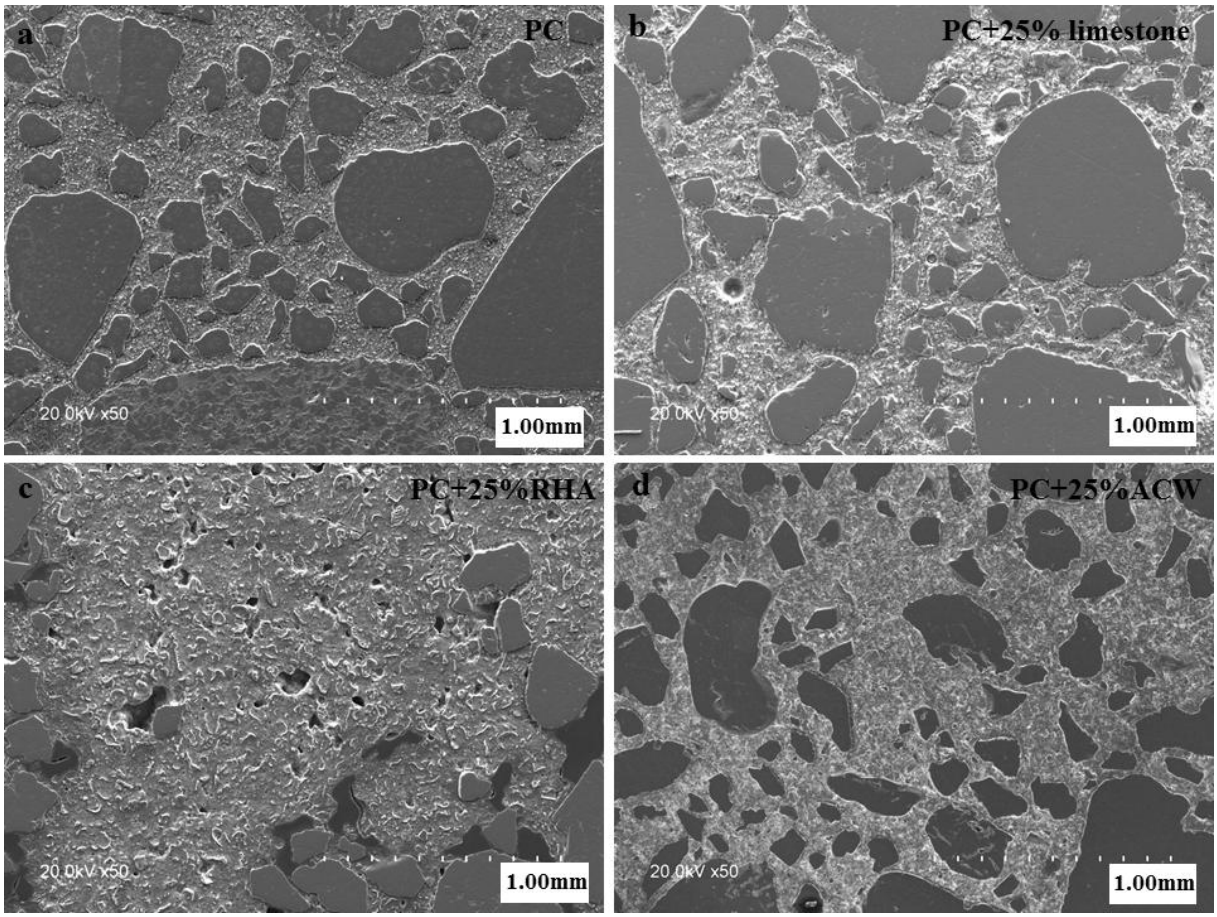

Fig. 14. Micrographs of 60 d mortars for (a) cement; (b) PC+limestone; (c) PC+RHA; and (d) PC+ACW.

3.8 Mortar microporosity

Total porosity, capillary pore (10-0.01 μm) and gel pore (<0.01 μm) data for the 7 d and 60 d mortars are listed in Table 5. The 7 d total porosity was similar in mortars PC, PC+limestone and PC+ACW and varied only slightly in the 60 d materials. In contrast, 7 d 25 % RHA exhibited total porosity of 23 %, which declined significantly to 16.6 % at the later age. That could be related to the lower compressive strength and greater porosity of this mortar, both in turn associated with pozzolan RHA's higher water demand (Table 3).

At 11 % to 11.5 %, capillary porosity (10 μm to 0.01 μm) was lower in the 7 d, 25 % RHA and 25 % ACW mortars than in the PC and 25 % limestone mortars (12.2 % to 12.8 %). Of the 60 d materials, only mortar PC exhibited a slight decline in capillary porosity relative to the early age value. Nor were

significant changes observed in the gel pores in the range 0.01 μm to 0.0068 μm (instrumental limit), with values of under 0.8 %. As earlier studies have shown [93], cement replacement alters the matrix pore system. The inclusion of pozzolanic materials in cement might be reasonably assumed to minimise total porosity and refine pore size [94,95], depending on the pozzolanic reactions and the filler effect [96]. That pattern was observed for the ACW pastes. The contrary was found for the RHA blends, again as a result of its high water demand, which would favour the formation of a more porous matrix, as shown in the SEM micrographs (Fig. 14) [95,97,98].

The particle size distribution curves (Fig. 15) confirmed those findings. Pore sizes of 0.004 μm to 0.005 μm clearly present in the 60 d, 25 % RHA and ACW mortars, and especially in the latter, were associated with the formation of C-S-H gels during the pozzolanic reaction. These data are wholly consistent with the mean pore diameter (4V/A) values listed in Table 6. As the table shows, the smallest pore sizes at both ages were observed for PC+ACW. That pore refinement capacity could have beneficial effects for the interfacial transition zone and mechanical performance in fibre-reinforced cements.

Table 5. Seven d and 60 d total, capillary and gel porosity.

		PC	PC+limestone	PC+RHA	PC+ACW
Total porosity (%)	7 d	13.96	13.94	23.04	12.26
	60 d	12.65	14.34	16.63	12.53
Capillary porosity (%)	7 d	12.25	12.84	11.51	10.92
	60 d	11.63	13.48	12.77	11.40
Gel porosity (%)	7 d	0.39	0.25	0.22	0.62
	60 d	0.21	0.19	0.74	0.45

Table 6. Seven d and 60 d mean pore diameter.

Blend	Mean pore diameter (4V/D) μm	
	7 d	60 d
PC	0.0554	0.0527
PC+limestone	0.0636	0.0565
PC+RHA	0.1265	0.0448
PC+ACW	0.0378	0.0362

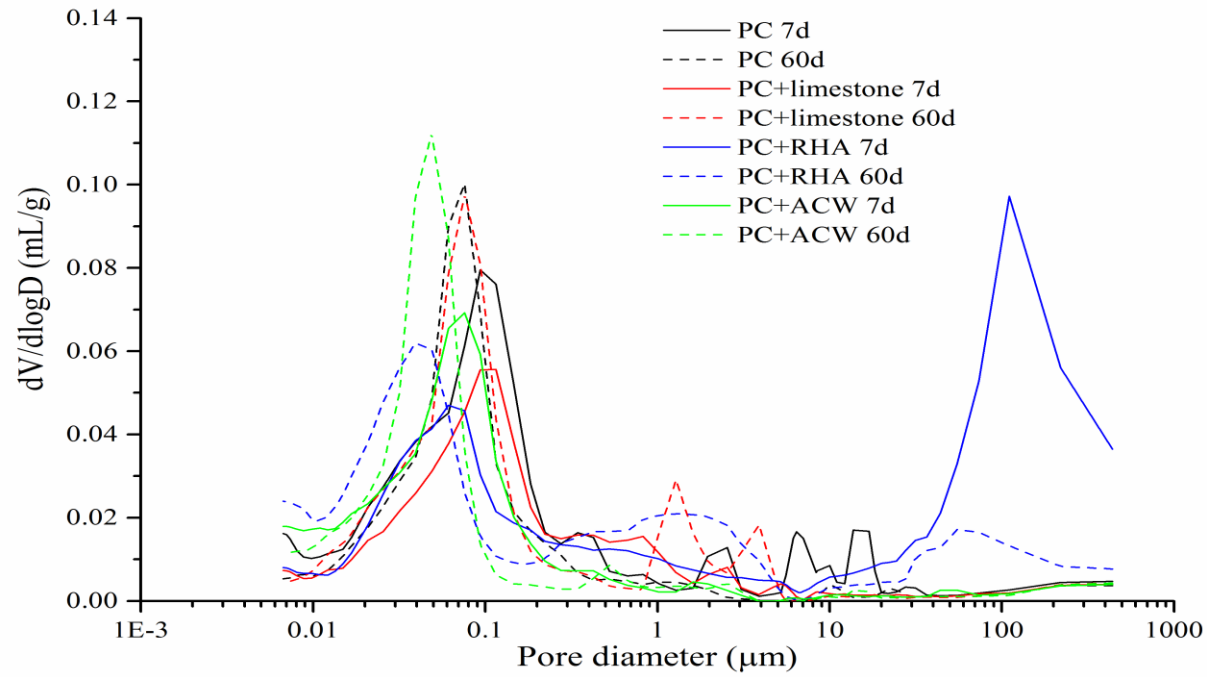

Fig. 15. 7 d and 60 d pore size distribution curves.

4. Conclusions

The conclusions drawn from the present study are summarised below.

1. After activation at 600 °C for 2 h in a muffle furnace, RHA and ACW absorb 90 % of the lime in the pozzolan/lime system within 90 d. That capacity might support their use in the enhancement of vegetable fibre-reinforced cement durability. The reaction rate varies substantially, however, with RHA proving to be a more active pozzolan in the short run. These values are consistent with the 8 day test scores observed for the respective cements, according to which they are pozzolanic.

2. C_4AcH_{12} is a crystalline phase present in 28 d reference, PC+limestone and PC+ACW pastes, along with ettringite and C-S-H gels. When cement is partially replaced by ACW, the proportion of the aforementioned hexagonal phase rises due to the reactive alumina sourced from the pozzolan, an effect that could induce cement/fibre interface densification.

3. Cements bearing 25 % RHA exhibit a 98 %, and materials with 25 % ACW a 13 %, higher water demand than the reference, whereas in 25 % limestone cement demand is around 9 % lower.

Initial setting time is significantly delayed, by 200 min relative to the reference paste, in 25 % RHA-additioned binder. Volume stability is not altered by the replacement of 25 % of the cement with any of these mineral additions. Both in terms of initial setting time and volume stability, the three blended cement pastes meet the requirements laid down in the standards in place.

4. Blending the mineral additions studied into the cement at a rate of 25 % beneficially lowers both total heat and heat of hydration. The steepest declines are observed for the limestone and RHA additions. Of the blended cements studied, only the PC+limestone qualifies as a low heat of hydration material ($\leq$ 270 J/g), thanks to its nil pozzolanicity.

5. The mortars containing 25 % additions exhibit lower mechanical strength than the reference. In the 60 d materials, compressive strength is 19 % lower in blends containing limestone, 8 % lower in those with ACW and 60 % lower in the RHA mortars. Further to the SEM micrographs, the mortars with 25 % RHA have very porous, poorly compacted morphologies.

6. The replacement of cement by these mineral additions at a rate of 25 wt% alters microporosity in different ways depending on the chemical, physical and pozzolanic characteristics of the addition. The cements prepared with 25 % ACW perform best in terms of microporosity, with a visible refinement of the pore system. The mean pore diameter in the ACW material is 31.3 % smaller than in the reference cement.

By say of summary of all foregoing, the use of mineral additions to manufacture binary cements and their effects on new cement performance depend not only on the chemical, mineralogical and pozzolanic properties of the additions, but also on the replacement ratio (25 % in this study). This study found that with a high replacement ratio (25 %), RHA, known for its high pozzolanicity, comparable to that of silica fume, yields poorly compacted, highly porous matrices. Adding 25 % limestone, in contrast, favours cement hydration nucleation and lowers water demand and heat of hydration. ACW additioned paste exhibits both high strength and a refined pore structure, an indication that of the three mineral additions studied, it would be the one most apt for fibre-reinforced cement applications.

Acknowledgements

This research was funded by the Spanish Ministry of Economy and Competitiveness (BIA2015-65558-C3-1-2-3R) (MINECO/FEDER)), the National Research Council's I-COOP Programme (ref: COOPA20089-2015) and CNPq (project #306386/2013-5). The backing afforded by the Commission on In-service Training for Higher Education Personnel (CAPES) and the Framework Partnering Agreement between IETcc/CSIC (Spain) and FZEA/USP (Brazil) (ref: 2013040043) is gratefully acknowledged. Funding was also provided by FAPESP under Theme Project #2012/51467-3.

References

[1] M. Frías, O. Rodríguez, M.I. Sánchez de Rojas, E. Villar-Cociña, M.S. Rodrigues, H.J. Savastano, Advances on the development of ternary cements elaborated with biomass ashes coming from different activation process, Constr. Build. Mater. 136 (2017) 73-80. doi: 10.1016/j.conbuildmat.2017.01.018

[2] F.A. Silva, R.D. Toledo Filho, J.M.F. de Almeida, E.D.M.R. Fairbairn, Physical and mechanical properties of durable sisal fiber–cement composites, Constr. Build. Mater. 24 (2010) 777-785. doi: 10.1016/j.conbuildmat.2009.10.030

[3] H. Mikulčić, J.J. Klemeš, M. Vujanović, K. Urbaniec, N. Duić, Reducing greenhouse gasses emissions by fostering the deployment of alternative raw materials and energy sources in the cleaner cement manufacturing process, J. Clean. Prod. 136 (2016) 119-132. doi 10.1016/j.jclepro.2016.04.145

[4] E. Benhelal, G. Zahedi, E. Shamsaei, A. Bahadori, Global strategies and potentials to curb CO2 emissions in cement industry, J. Clean. Prod. 51 (2013) 142-161. doi 10.1016/j.jclepro.2012.10.049

[5] K.H. Yang, Y.B. Jung, M.S. Cho, S.H. Tae, Effect of supplementary cementitious materials on reduction of CO2 emissions from concrete, J. Clean. Prod. 103 (2015) 774-783. doi: 10.1016/j.jclepro.2014.03.018

[6] R. Kajaste, H. Markku, Cement industry greenhouse gas emissions–management options and abatement cost, J. Clean. Prod. 112 (2016) 4041-4052. doi: 10.1016/j.jclepro.2015.07.055

[7] A. Hasanbeigi, C. Menke, L. Price, The CO2 abatement cost curve for the Thailand cement industry, J. Clean. Prod. 18 (2010) 1509-1518. doi: 10.1016/j.jclepro.2010.06.005

[8] A. Teklay, C. Yin, L. Rosendahl, Flash calcination of kaolinite rich clay and impact of process conditions on the quality of the calcines: a way to reduce CO2 footprint from cement industry, Appl. Energy. 162 (2016) 1218-1224. doi: 10.1016/j.apenergy.2015.04.127

[9] S.O. Ogbeide, Developing an optimization model for CO2 reduction in cement production process, J. Eng. Sci. Technol. Rev. 3 (2012) 85-88.

[10] Y. Wang, S. Höller, P. Viebahn P, Z. Hao, Integrated assessment of CO2 reduction technologies in China's cement industry, Int. J. Greenh. Gas. Con. 20 (2014) 27-36. doi: 10.1016/j.ijggc.2013.10.004

[11] M. Smol, J. Kulczycka, A. Henclik, K. Gorazda, Z. Wzorek, The possible use of sewage sludge ash (SSA) in the construction industry as a way towards a circular economy, J. Clean. Prod. 95 (2015) 45-54. doi: 10.1016/j.jclepro.2015.02.051

[12] E. Aprianti, P. Shafigh, S. Bahri, J.N. Farahani, Supplementary cementitious materials origin from agricultural wastes e a review, Constr. Build. Mater. 74 (2015) 176-187. doi: 10.1016/j.conbuildmat.2014.10.010

[13] A.P. Gursel, H. Maryman, C. Ostertag, A life-cycle approach to environmental, mechanical, and durability properties of "green" concrete mixes with rice husk ash, J. Clean. Prod. 112 (2016) 823-836. doi: 10.1016/j.jclepro.2015.06.029

[14] S.D. Carreño, R.G.C. García, O.O.R. Ortiz, Laboratory processing of Colombian rice husk for obtaining amorphous silica as concrete supplementary cementing material, Constr. Build. Mater. 96 (2015) 65-75. doi: 10.1016/j.conbuildmat.2015.07.178

[15] L. Rodier, K. Bilba, C. Onésippe, M.A. Arsène, Study of pozzolanic activity of bamboo stem ashes for use as partial replacement of cement, Mater. Struct. 50 (2017) 87. doi: 10.1617/s11527-016-0958-6

[16] S. Subaşı, H. Öztürk, M. Emiroğlu, Utilizing of waste ceramic powders as filler material in self-consolidating concrete, Constr. Build. Mater. 149 (2017) 567-574. doi 10.1016/j.conbuildmat.2017.05.180

[17] M. Frías, O. Rodríguez, M.I. Sánchez de Rojas, Paper sludge, an environmentally sound alternative source of MK-based cementitious materials. a review, Constr. Build. Mater. 74 (2015) 37-48. doi: 10.1016/j.conbuildmat.2014.10.007

[18] I. Vegas, M. Cano, I. Arribas, M. Frias, O. Rodríguez, Physical–mechanical behavior of binary cements blended with thermally activated coal mining waste, Constr. Build. Mater. 99 (2015) 169-174. doi: 10.1016/j.conbuildmat.2015.07.189

[19] S. Hesami, A. Modarres, M. Soltaninejad, H. Madani, Mechanical properties of roller compacted concrete pavement containing coal waste and limestone powder as partial replacements of cement, Constr. Build. Mater. 111 (2016) 625-636. doi: 10.1016/j.conbuildmat.2016.02.116

[20] M. Frías, O. Rodriguez, R.V. de la Villa, R. García, S.R. Martínez, L.J.C. Fernández, I. Vegas. The Influence of Activated Coal Mining Wastes on the Mineralogy of Blended Cement Pastes, J. Am. Ceram. Soc. 99 (2016) 300-307. doi: 10.1111/jace.13840

[21] M.F.M. Zain, M.N. Islam, F. Mahmud, M. Jamil, Production of rice husk ash for use in concrete as a supplementary cementitious material, Constr. Build. Mater. 25 (2011) 798–805. doi: 10.1016/j.conbuildmat.2010.07.003

[22] M.C. Juenger, R. Siddique, Recent advances in understanding the role of supplementary cementitious materials in concrete, Cem. Concr. Res. 78 (2015) 71-80. doi: 10.1016/j.cemconres.2015.03.018

[23] R. García, R.V. de la Villa, M. Frías, O. Rodriguez, S.R. Martínez, L.C. Fernández, E.C. Villar, Mineralogical study of calcined coal waste in a pozzolan/Ca(OH)2 system, Appl. Clay. Sci. 108 (2015) 45-54. doi: 10.1016/j.clay.2015.02.014

[24] R.G. Giménez, R.V. de la Villa, M. Frías, From coal-mining waste to construction material: a study of its mineral phases, Environ. Earth. Sci. 75 (2016) 478. doi: 10.1007/s12665-016-5494-8

[25] M. Jamil, A.B.M.A. Kaish, S.N. Raman, M.F.M. Zain, Pozzolanic contribution of rice husk ash in cementitious system, Constr. Build. Mater. 47 (2013) 588–593. doi: 10.1016/j.conbuildmat.2013.05.088

[26] W. Yang, Y. Xue, S. Wu, Y. Xiao, M. Zhou, Performance investigation and environmental application of basic oxygen furnace slag–Rice husk ash based composite cementitious materials, Constr. Build. Mater. 123 (2016) 493-500. doi: 10.1016/j.conbuildmat.2016.07.051

[27] L.R. Hickert, P.B.C. de Souza, C.A. Rosa, M.A.Z. Ayub, Simultaneous saccharification and co-fermentation of un-detoxified rice hull hydrolysate by Saccharomyces cerevisiae ICV D254 and Spathaspora arborariae NRRL Y-48658 for the production of ethanol and xylitol, Bioresour. Technol. 143 (2013) 112-116. doi: 10.1016/j.biortech.2013.05.123

[28] Statistical Review of Word Energy. https://www.bp.com/en/global/corporate/search.html?q=bp-statistical-review-of-world-energy-2017-underpinning-data&_charset_=UTF-8, 2017 (accessed 12 November 2017).

[29] M. Frías, R.V. de la Villa, M.I. Sanchez de Rojas, C. Medina, A.V. Juan. Scientific aspects of kaolinite based coal mining wastes in pozzolan/Ca (OH)2 system, J. Am. Ceram. Soc. 95 (2012) 386-391. doi: 10.1111/j.1551-2916.2011.04985.x

[30] L. Haibin, L. Zhenling, Recycling Utilization Patterns of Coal Mining Waste in China, Resour., Conserv. Recycl. 54 (2010) 1331–1340. doi: 10.1016/j.biortech.2013.05.123

[31] S. Hesami, S. Ahmadi, M. Nematzadeh, Effects of rice husk ash and fiber on mechanical properties of pervious concrete pavement, Constr. Build. Mater. 53 (2014) 680-691. doi: 10.1016/j.conbuildmat.2013.11.070

[32] R. Walker, S. Pavía, Physical properties and reactivity of pozzolans, and their influence on the properties of lime–pozzolan pastes, Mater. Struct. 44 (2011) 1139-1150. doi: 10.1617/s11527-010-9689-2

[33] W.Xu, Y.L. Tommy, S.A. Memon, Microstructure and reactivity of rich husk ash, Constr. Build. Mater. 29 (2012) 541–547. doi: 10.1016/j.conbuildmat.2011.11.005

[34] G. Marmol, S.F. Santos, H.J. Savastano, M.V. Borrachero, J. Monzó, J. Payá, Mechanical and physical performance of low alkalinity cementitious composites reinforced with recycled cellulosic fibres pulp from cement kraft bags, Ind. Crops. Prod. . 49 (2013) 422-427. doi: 10.1016/j.indcrop.2013.04.051

[35] J. Wei, C. Meyer, Utilization of rice husk ash in green natural fiber-reinforced cement composites: mitigating degradation of sisal fiber, Cem. Concr. Res. 81 (2016) 94-111. doi: 10.1016/j.cemconres.2015.12.001

[36] D.D. Bui, J. Hu, P. Stroeven, Particle size effect on the strength of rice husk ash blended gap-graded Portland cement concrete, Cem. Concr. Compos.. 27 (2005) 357–66. doi: 10.1016/j.cemconcomp.2004.05.002

[37] K.B. Park, S.J. Kwon, X.Y. Wang, Analysis of the effects of rice husk ash on the hydration of cementitious materials, Constr. Build. Mater. 105 (2016) 196-205. doi: 10.1016/j.conbuildmat.2015.12.086

[38] O. Faruk, A.K. Bledzki, H.P. Fink, M. Sain, Progress report on natural fiber reinforced composites, Macromol. Mater. Eng. 299 (2014) 9–26. doi: 10.1002/mame.201300008

[39] World Green Building Council. http://www.worldgbc.org/news-media, 2016 (accessed 10 November 2017).

[40] J.E.M. Ballesteros, S.F. Santos, G. Mármol, H.J. Savastano, J. Fiorelli, Evaluation of cellulosic pulps treated by hornification as reinforcement of cementitious composites, Constr. Build. Mater. 100 (2015) 83-90. doi: 10.1016/j.conbuildmat.2015.09.044

[41] J.E.M. Ballesteros, V. dos Santos, G. Mármol, M. Frías, J. Fiorelli, Potential of the hornification treatment on eucalyptus and pine fibers for fiber-cement applications, Cellulose. 24 (2017) 2275-2286. doi: 10.1007/s10570-017-1253-6

[42] J.H. Morton, T. Cooke, S.A.S. Akers, Performance of slash pine fibers in fiber cement products, Constr. Build. Mater. 24 (2010) 165-170. doi: 10.1016/j.conbuildmat.2007.08.015

[43] S.F. Santos, J.R. de Anchieta, G.H.D. Tonoli, A.E.F.A. de Souza, H.J. Savastano, Effect of colloidal silica on the mechanical properties of fiber–cement reinforced with cellulosic fibers, J. Mater. Sci. 49 (2014) 7497-7506. doi: 10.1007/s10853-014-8455-1

[44] ASTM C150/C150M-11, Standard Specification for Portland Cement, 2011.

[45] R.S. Bie, X.F. Song, Q.Q. Liu, X.Y. Ji, P. Chen, Studies on effects of burning conditions and rice husk ash (RHA) blending amount on the mechanical behavior of cement, Cem. Concr. Compos. 55 (2015) 162-168. doi: 10.1016/j.cemconcomp.2014.09.008

[46] Asociación Española de Normalización y Certificación, UNE EN 196-5, Method of testing cement. Part 5: Pozzolanicity test for pozzolanic cement, 2011.

[47] Asociación Española de Normalización y Certificación, UNE EN 196-3, Method of testing cement. Part 3: Determination of setting times and volume stability, 2009.

[48] Asociación Española de Normalización y Certificación, UNE EN 196-9, Method of testing cement. Part 9: Determination of the heat of hydration. Semiadiabatic method, 2011.

[49] Asociación Española de Normalización y Certificación, UNE EN 196-1, Method of testing cement. Part 1: Determination of strength, 2005.

[50] L. Xu, K. Wu, C. Rößler, P. Wang, H.M. Ludwig, Influence of curing temperatures on the hydration of calcium aluminate cement/Portland cement/calcium sulfate blends, Cem. Concr. Compos. 80 (2017) 298-306. doi: 10.1016/j.cemconcomp.2017.03.016

[51] A. El-Taher, M.A.K.J. Abdelhalim, Elemental analysis of limestone by instrumental neutron activation analysis, J. Radioanal. Nucl. Chem. 299 (2014) 1949-1953. doi: 10.1007/s10967-014-2925-4

[52] H. Huang, X. Gao, H. Wang, H. Ye, Influence of rice husk ash on strength and permeability of ultra-high performance concrete, Constr. Build. Mater. 149 (2017) 621-628. doi: 10.1016/j.conbuildmat.2017.05.155

[53] R. Mirmoghtadaei, M. Mohammadi, N.A. Samani, S. Mousavi, The impact of surface preparation on the bond strength of repaired concrete by metakaolin containing concrete, Constr. Build. Mater. 80 (2015) 76-83. doi: 10.1016/j.conbuildmat.2015.01.018

[54] ASTM C618-17, Standard Specification for Coal Fly Ash and Raw or Calcined Natural Pozzolan for Use in Concrete, 2017. doi: 10.1520/C0618-17

[55] R. Snellings, A. Salze, K.L. Scrivener, Use of X-ray diffraction to quantify amorphous supplementary cementitious materials in anhydrous and hydrated blended cements, Cem. Concr. Res. 64 (2014) 89-98. doi: 10.1016/j.cemconres.2014.06.011

[56] V. Sklivaniti, P.E. Tsakiridis, N.S. Katsiotis, D. Velissariou, N. Pistofidis, D. Papageorgiou, M. Beazi, Valorisation of woody biomass bottom ash in Portland cement: A characterization and hydration study, J. Environ. Chem. Eng. 5 (2017) 205-213. doi: 10.1016/j.jece.2016.11.042

[57] J.M. Valverde, P.E. Sanchez-Jimenez, L.A.M. Perez, Ca-looping for postcombustion CO2 capture: a comparative analysis on the performances of dolomite and limestone, Appl. Energy. 138 (2015) 202-215. doi: 10.1016/j.apenergy.2014.10.087

[58] G.A. Habeeb, H.B. Mahmud, Study on properties of rice husk ash and its use as cement replacement material, Mater. Res. 13 (2010) 185-190. doi: 10.1590/S1516-14392010000200011

[59] J. Salas, P. Castillo, M.I. Sanchez de Rojas, J. Veras, Use or rice husk ash an addition in mortar, Mater. Construcc. 36 (1986) 21-39. doi: 10.3989/mc.1986.v36.i203.888

[60] A.N. Junior, R.D. Toledo Filho, E.D.M.R. Fairbairn, J. Dweck J, CO2 sequestration by high initial strength Portland cement pastes, J. Therm. Anal. Calorim. 113 (2013) 1577-1584. doi: 10.1007/s10973-013-3117-0

[61] N.C. Collier, Transition and decomposition temperatures of cement phases–a collection of thermal analysis data, Ceram-Silikaty. 60 (2016). doi: 10.13168/cs.2016.0050

[62] R. Gabrovšek, T. Vuk, V. Kaučič, Evaluation of the hydration of Portland cement containing various carbonates by means of thermal analysis, Acta. Chim. Slov. 53 (2006) 159-165.

[63] R.G. Giménez, V. de la Villa, S. Goñi, M. Frías, Fly Ash and paper sludge on the evolution of ternary blended cements: mineralogy and hydrated phases, J. Mater. Civil. Eng. 27 (2014) 04014249gi. doi: 10.1061/(ASCE)MT.1943-5533.0001223

[64] C. Rößler, D.D. Bui, H.M. Ludwig, Rice husk ash as both pozzolanic admixture and internal curing agent in ultra-high performance concrete, Cem. Concr. Compos. 53 (2014) 270-278. doi: 10.1016/j.cemconcomp.2014.07.015

[65] R. Pode, Potential applications of rice husk ash waste from rice husk biomass power plant, Renew. Sust. Energ. Rev. 53 (2016) 1468-1485. doi: 10.1016/j.rser.2015.09.051

[66] F. Bondioli, L. Barbieri, A.M. Ferrari, T. Manfredini, Characterization of rice husk ash and its recycling as quartz substitute for the production of ceramic glazes, J. Am. Ceram. Soc. 93 (2010) 121-126. doi: 10.1111/j.1551-2916.2009.03337.x

[67] T.J. Agredo, R. Mejía de Gutiérrez, C.E.G. Escandón, L.O.S. González, Characterization of sugar cane bagasse ash as supplementary material for Portland cement, Ingeniería e Investigación. 34 (2014) 5-10. doi: 10.15446/ing.investig.v34n1.42787

[68] A.C.R. Lim, B.L.F. Chin, Z.A. Jawad, K.L. Hii, Kinetic analysis of rice husk pyrolysis using kissinger-akahira-sunose (KAS) Method, Procedia Eng. 148 (2016) 1247-1251. doi: 10.1016/j.proeng.2016.06.486

[69] M.K.D. Rambo, F.L. Schmidt, M.M.C. Ferreira, Analysis of the lignocellulosic components of biomass residues for biorefinery opportunities, Talanta. 144 (2015) 696-703. doi: 10.1016/j.talanta.2015.06.045

[70] A. Alujas, R. Fernández, R. Quintana, K.L. Scrivener, F. Martirena, Pozzolanic reactivity of low grade kaolinitic clays: Influence of calcination temperature and impact of calcination products on OPC hydration, Appl. Clay. Sci. . 108 (2015) 94-101. doi: 10.1016/j.clay.2015.01.028

[71] S.K. Antiohos, V.G. Papadakis, S. Tsimas, Rice husk ash (RHA) effectiveness in cement and concrete as a function of reactive silica and fineness, Cem. Concr. Res. 61 (2014) 20-27. doi: 10.1016/j.cemconres.2014.04.001

[72] N. Kabay, M.M. Tufekci, A.B. Kizilkanat, D. Oktay, Properties of concrete with pumice powder and fly ash as cement replacement materials, Constr. Build. Mater. 85 (2015) 1-8. doi: 10.1016/j.conbuildmat.2015.03.026

[73] C.L. Pereira, H.J. Savastano, J. Payá, S.F. Santos, M.V. Borrachero, J. Monzó, L. Soriano, Use of highly reactive rice husk ash in the production of cement matrix reinforced with green coconut fiber, Ind. Crops. Prod. 49 (2013) 88-96. doi: 10.1016/j.indcrop.2013.04.038

[74] M. Frías, O.L. Rodríguez, R.J. García, I. Vegas, Influence of activation temperature on reaction kinetics in recycled clay waste–calcium hydroxide systems, J. Am. Ceram. Soc. 91 (2008) 4044-4051. doi: 10.1111/j.1551-2916.2008.02807.x

[75] H.F.W. Taylor, Cement Chemistry, 2nd ed., Thomas Telford, London, 1997.

[76] V.S. Ramachandran, R.M. Paroli, J.J. Beaudoin, A.H. Delgado, Handbook of thermal analysis of construction materials. William Andrew, 2002.

[77] M. Frías, R. García, R.V. de la Villa, E. Villar, The effect of binary pozzolan mix on the mineralogical changes in the ternary activated paper sludge–fly ash–Ca (OH) 2 system, Constr. Build. Mater. 38 (2013) 48-53. doi: 10.1016/j.conbuildmat.2012.08.045

[78] R.O. Largo, R.V. de la Villa, M.I. Sánchez de Rojas, M. Frías, Novel use of kaolin wastes in blended cements, J. Am. Ceram. Soc. 92 (2009) 2443-2446. doi: 10.1111/j.1551-2916.2009.03231.x

[79] K. Ganesan, K, Rajagopal, K. Thangavel, Rice husk ash blended cement: assessment of optimal level of replacement for strength and permeability properties of concrete, Constr. Build. Mater. 22 (2008) 1675-1683. doi: 10.1016/j.conbuildmat.2007.06.011

[80] S.A. Abo-El-Enein, G. El-kady, T.M. El-Sokkary, M. Gharieb, Physico-mechanical properties of composite cement pastes containing silica fume and fly ash, HBRC Journal. 11 (2015) 7-15. doi: 10.1016/j.hbrcj.2014.02.003

[81] M. Frías, H.J. Savastano, E.V. Cociña, M.I. Sánchez de Rojas, S. Santos, Characterization and properties of blended cement matrices containing activated bamboo leaf wastes, Cem. Concr. Compos. 34 (2012) 1019-1023. doi: 10.1016/j.cemconcomp.2012.05.005

[82] A.N. Givi, S.A. Rashid, F.N.A Aziz, M.A.M. Salleh, Contribution of rice husk ash to the properties of mortar and concrete: a review, J. Am. Sci. 6 (2010) 157-165.

[83] Asociación Española de Normalización y Certificación, UNE EN 197-1, Cement - Part 1: Composition, specifications and conformity criteria for common cements, 2011.

[84] O. Rodríguez, M. Frías, M.I. Sanchez de Rojas, Influence of the calcined paper sludge on the development of hydration heat in blended cement mortars, J. Therm. Anal. Calorim. 92 (2008) 865-871. doi: 10.1007/s10973-007-8270-x

[85] K. Aghaee, M. Foroughi, Mechanical properties of lightweight concrete partition with a core of textile waste, Adv. Civil. Eng. 2013 (2013) 1–7. doi: 10.1155/2013/482310

[86] F. Deschner, F. Winnefeld, B. Lothenbach, S. Seufert, P. Schwesig, S. Dittrich, F. Goetz-Neunhoeffer, J. Neubauer, Hydration of Portland cement with high replacement by siliceous fly ash, Cem. Concr. Res. 42 (2012) 1389-1400. doi:10.1016/j.cemconres.2012.06.009

[87] P. Thongsanitgarn, W. Wongkeo, A. Chaipanich, C.S. Poon, Heat of hydration of Portland high-calcium fly ash cement incorporating limestone powder: Effect of limestone particle size, Constr. Build. Mater. 66 (2014) 410-417. doi: 10.1016/j.conbuildmat.2014.05.060

[88] D.G. Snelson, S. Wild, M. O'Farrell, Heat of hydration of Portland cement–metakaolin–fly ash (PC–MK–PFA) blends, Cem. Concr. Res. 38 (2008) 832-840. doi:10.1016/j.cemconres.2008.01.004

[89] F. Han, R. Liu, D. Wang, P. Yan, Characteristics of the hydration heat evolution of composite binder at different hydrating temperature, Thermochim. Acta. 586 (2014) 52-57. doi: 10.1016/j.tca.2014.04.010

[90] Asociación Española de Normalización y Certificación, UNE EN 14216, Cement - Part 1: Composition, specifications and conformity criteria for very low heat special cement, 2015.

[91] M. Halvaei, M. Jamshidi, M. Latifi, Application of low modulus polymeric fibers in engineered cementitious composites, J. Ind. Text. 43 (2014) 511-524. doi: 10.1177/1528083712465881

[92] P. Lawrence, M. Cyr, E. Ringot, Mineral admixtures in mortars: effect of inert materials on short-term hydration, Cem. Concr. Res. 33 (2003) 1939-1947. doi: 10.1016/S0008-8846(03)00183-2

[93] Y. Senhadji, G. Escadeillas, M. Mouli, H. Khelafi, Influence of natural pozzolan, silica fume and limestone fine on strength, acid resistance and microstructure of mortar, Powder Technol. 254 (2014) 314-323. doi: 10.1016/j.powtec.2014.01.046

[94] E. Ghafari, H. Costa, E. Júlio, A. Portugal, L. Durães, The effect of nanosilica addition on flowability, strength and transport properties of ultra high performance concrete, Mater. Des. 59 (2014) 1-9. doi: 10.1016/j.matdes.2014.02.051

[95] C. Nunes, Z. Slížková, M. Stefanidou, J. Němeček, Microstructure of lime and lime-pozzolana pastes with nanosilica, Cem. Concr. Res. 83 (2016) 152-163. doi: 10.1016/j.cemconres.2016.02.004

[96] M. Najimi, J. Sobhani, B. Ahmadi, M. Shekarchi, An experimental study on durability properties of concrete containing zeolite as a highly reactive natural pozzolan, Constr. Build. Mater. 35 (2012) 1023–1033. doi: 10.1016/j.conbuildmat.2012.04.038

[97] A.A. Sabtan, W.M. Shehata, Evaluation of engineering properties of scoria in central Harrat Rahat, Saudi Arabia. Bull. Eng. Geol. Environ. 59 (2000) 219–25. doi: 10.1007/s100640000061

[98] K. Celik, M.D. Jackson, M. Mancio, C. Meral, A.H. Emwas, P.K. Mehta, P.J.M. Monteiro, High-volume natural volcanic pozzolan and limestone powder as partial replacements for portland cement in self-compacting and sustainable concrete, Cem. Concr. Compos. 45 (2014) 136-147. doi: 10.1016/j.cemconcomp.2013.09.003

Table 1

Click here to download Table: Table 1.docx

Table 1. X-ray fluorescence-based elemental composition of the starting materials (%).

Oxide	Portland cement	Limestone	RHA	ACW
SiO_2	18.53	1.79	89.71	56.63
Al_2O_3	4.75	0.61	0.14	25.29
Fe_2O_3	2.79	0.28	0.19	4.64
MnO	0.01	0.03	0.17	0.08
MgO	3.42	8.48	0.85	0.77
CaO	58.97	44.13	1.76	4.20
Na_2O	0.91	0.38	0.04	0.17
SO_3	4.58	0.08	0.35	0.27
K_2O	1.40	0.13	3.65	3.09
TiO_2	0.10	0.02	0.01	1.17
P_2O_5	0.20	0.10	1.40	0.14
LoI*	4.00	43.97	1.64	3.09
TOTAL	99.7	100.0	99.9	99.5
Minority element		Concentration (ppm)		
Sr	680	319	32	-
Ni	77	1	11	65
Cr	229	36	46	210
V	31	5	1	162
Zn	102	-	17	25
Pb	1	-	-	4
Cl	224	56	167	46
Zr	-	4	-	-
Y	5	2	-	-
Rb	10	3	-	-
F	1176	650	-	-
As	-	-	-	2
Co	-	-	-	24
Mo	-	-	-	21

*LOI: Loss on ignition (950º C)

Table 2

Click here to download Table: Table 2.docx

Table 2. Weight loss and portlandite content by curing time.

	Temperature range	Curing age	Weight loss	$Ca(OH)_2$
	°C	días	%	%
PC	50-300	2	9.88	-
		28	12.83	-
		90	14.06	-
	400-500	2	3.87	15.91
		28	4.73	19.45
		90	4.94	20.20
	500-750	2	5.35	-
		28	4.09	-
		90	4.08	-
PC + limestone	50-300	2	8.2	-
		28	10.54	-
		90	11.25	-
	400-500	2	3.26	13.40
		28	3.82	15.70
		90	3.85	15.83
	500-785	2	13.71	-
		28	12.99	-
		90	13.79	-
PC + RHA	50-300	2	10.12	-
		28	13.81	-
		90	16.12	-
	400-500	2	2.58	10.61
		28	2.37	9.74
		90	1.76	7.23
	500-750	2	4.15	-
		28	4.26	-
		90	3.99	-
PC + ACW	50-300	2	8.83	-
		28	12.69	-
		90	14.03	-
	400-500	2	3.17	13.03
		28	3.39	13.94
		90	3.28	13.48
	500-820	2	4.45	-
		28	3.87	-
		90	4.17	-

Table 3

Click here to download Table: Table 3.docx

Table 3. Water demand for normal consistency, setting time (± 5 min) and volume stability (± 1 mm) for blended cement pastes.

Blend	Water demand (g)	Water penetration (mm)	Initial setting time (min)		Expansion (mm)	
			Measured	Standard requirement	Measured	Standard requirement
PC	164	33	235	≥ 60	0 ± 1	≤ 10
PC+limestone	154	35	245		1 ± 1	
PC+RHA	325	34	435		0 ± 1	
PC+ACW	185	36	255		0 ± 1	

Table 4

Table 4. Peak heat of hydration at 41 h.

Blend	Heat of hydration	Standard	
	J/g	UNE-EN 197-1	UNE-EN 14216
PC	462.9	< 270 J/g	< 220 J/g
PC+limestone	261.3		
PC+RHA	299.8		
PC+ACW	424.9		

Table 5

Click here to download Table: Table 5.docx

Table 5. Seven d and 60 d total, capillary and gel porosity.

		PC	PC+limestone	PC+RHA	PC+ACW
Total porosity (%)	7 d	13.96	13.94	23.04	12.26
	60 d	12.65	14.34	16.63	12.53
Capillary porosity (%)	7 d	12.25	12.84	11.51	10.92
	60 d	11.63	13.48	12.77	11.40
Gel porosity (%)	7 d	0.39	0.25	0.22	0.62
	60 d	0.21	0.19	0.74	0.45

Table 6

Click here to download Table: Table 6.docx

Table 6. Seven d and 60 d mean pore diameter.

Blend	Mean pore diameter (4V/D) μm	
	7 d	60 d
PC	0.0554	0.0527
PC+limestone	0.0636	0.0565
PC+RHA	0.1265	0.0448
PC+ACW	0.0378	0.0362

Figure 1

Click here to download high resolution image

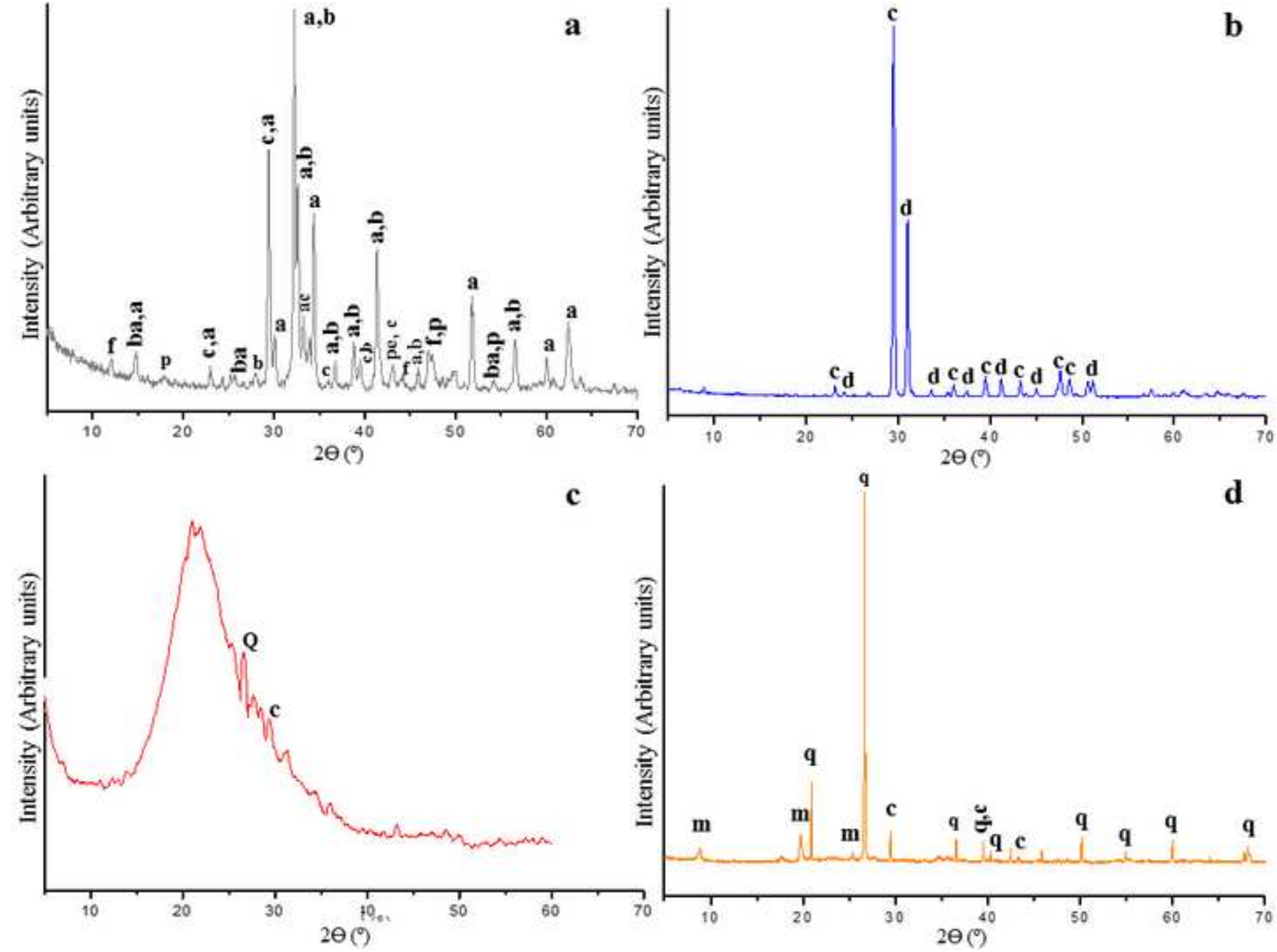

Figure 1a

Click here to download high resolution image

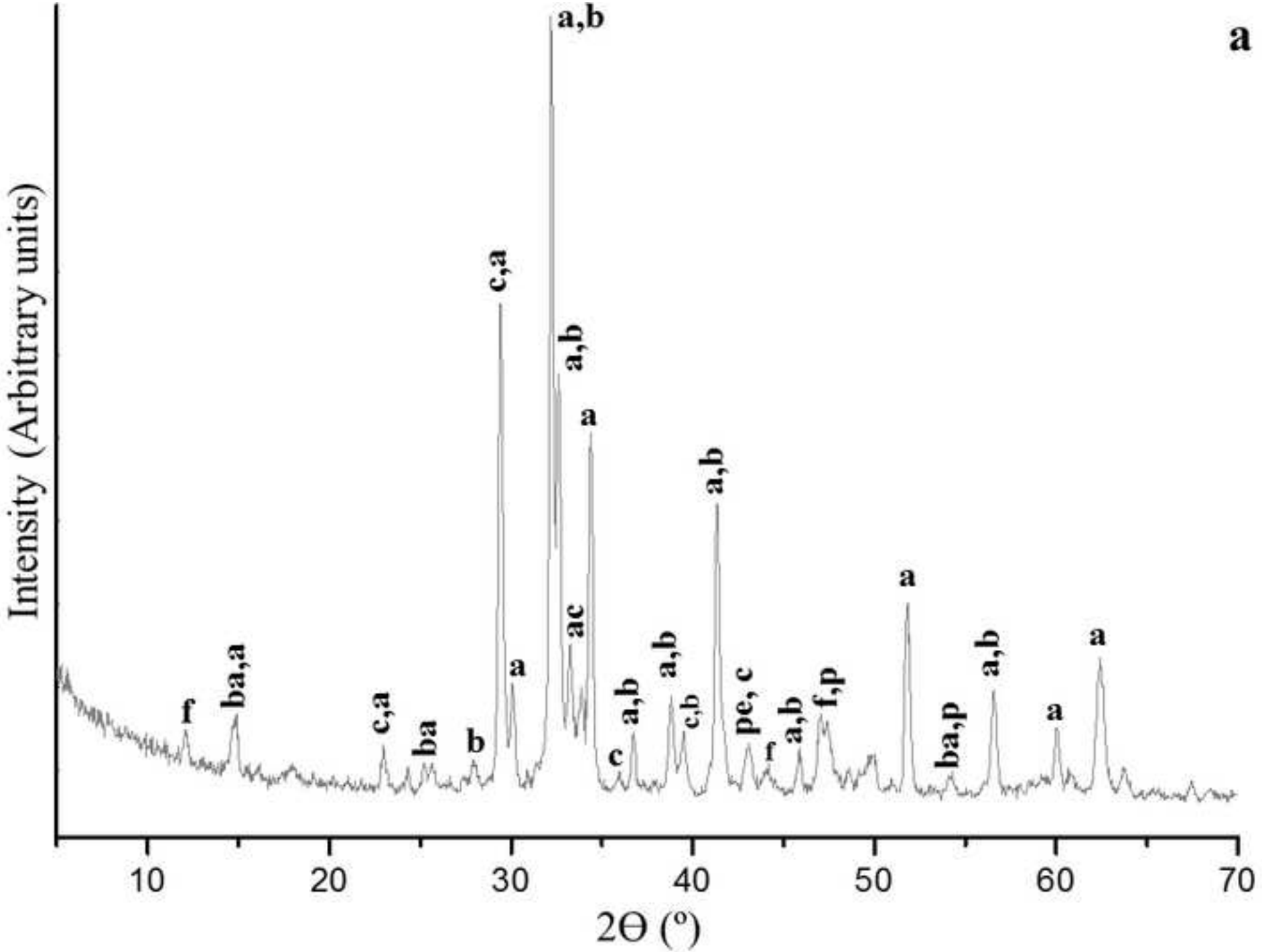

Figure 1b

Click here to download high resolution image

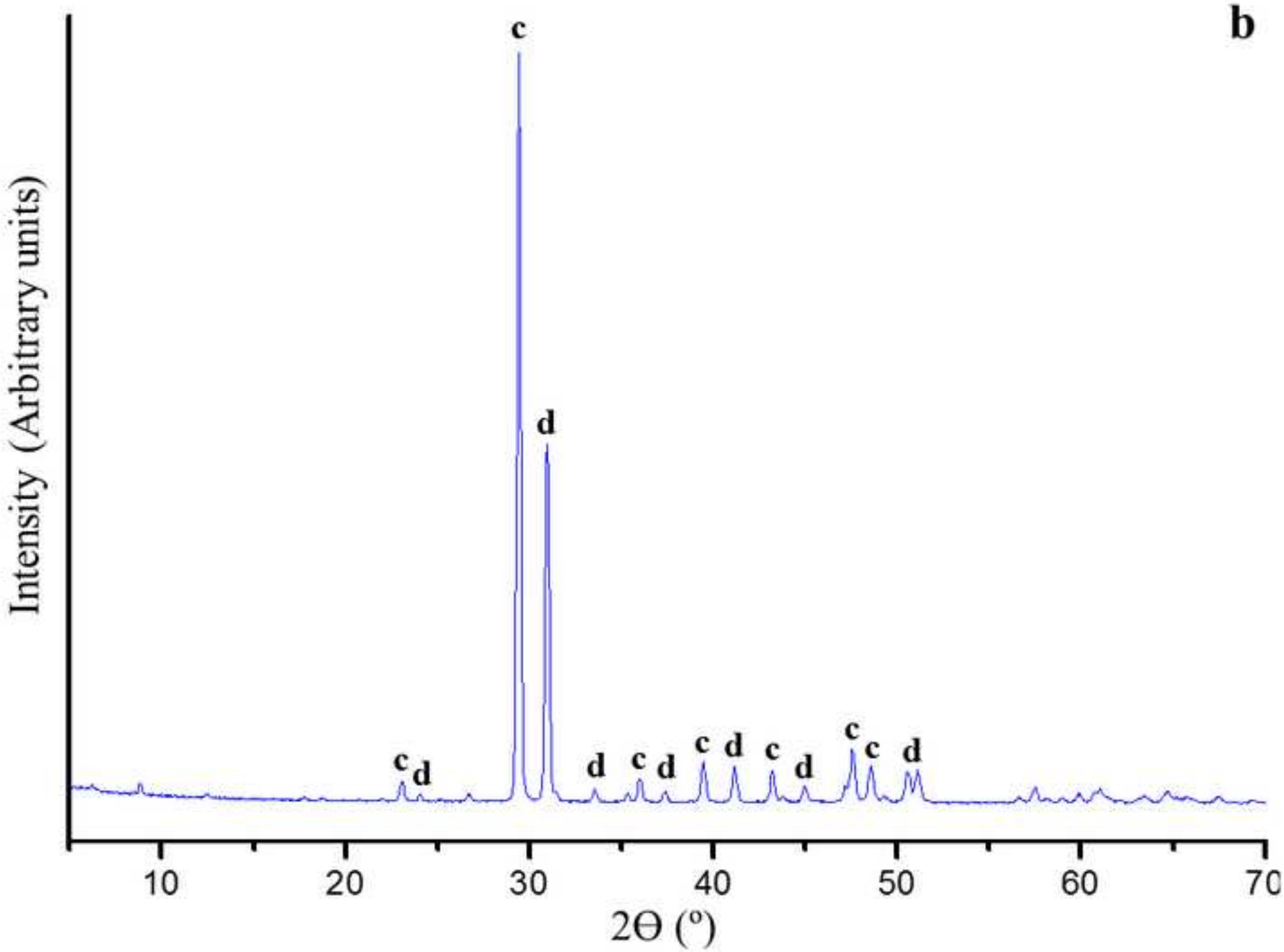

Figure 1c

Click here to download high resolution image

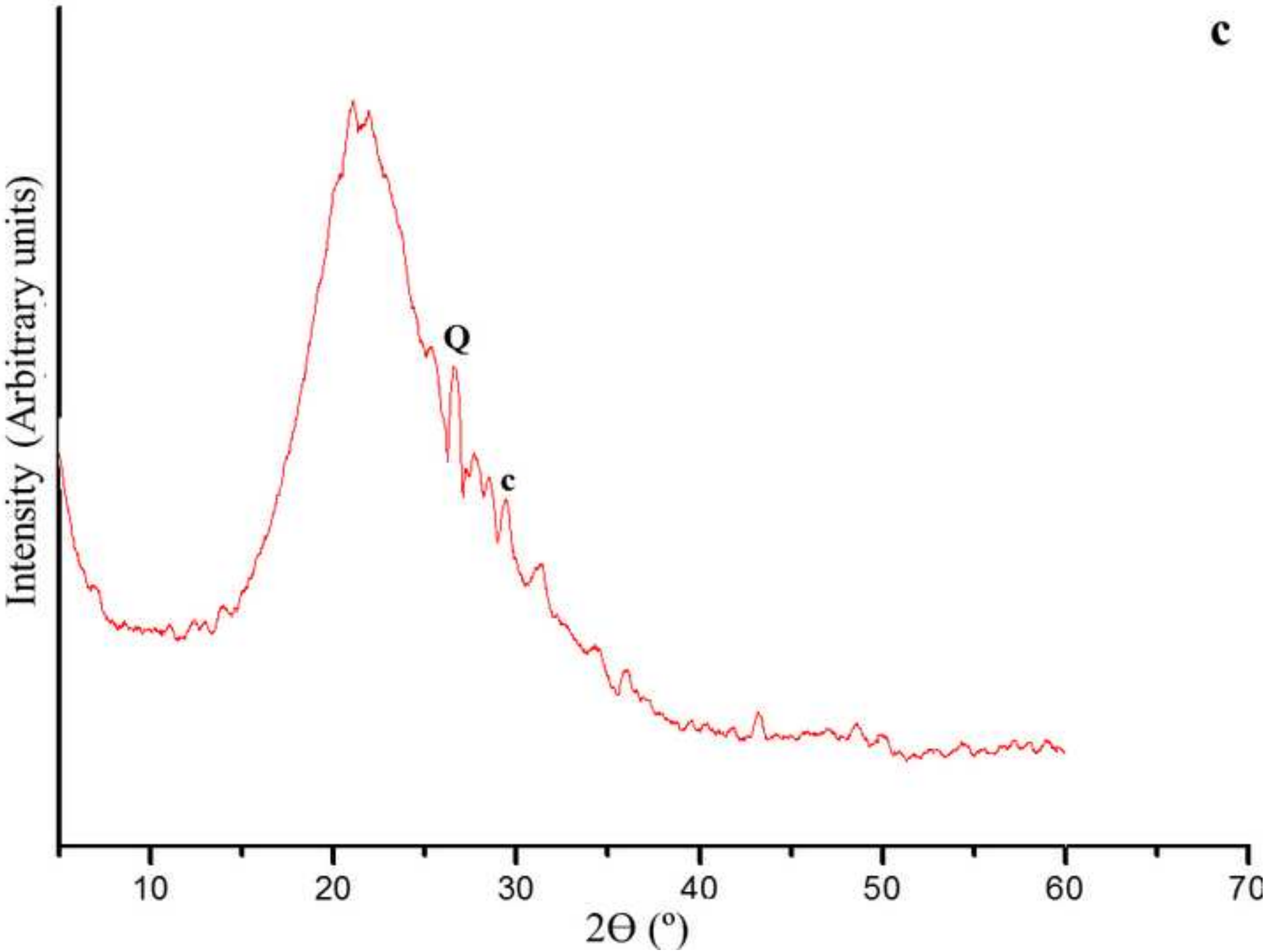

Figure 1d

Click here to download high resolution image

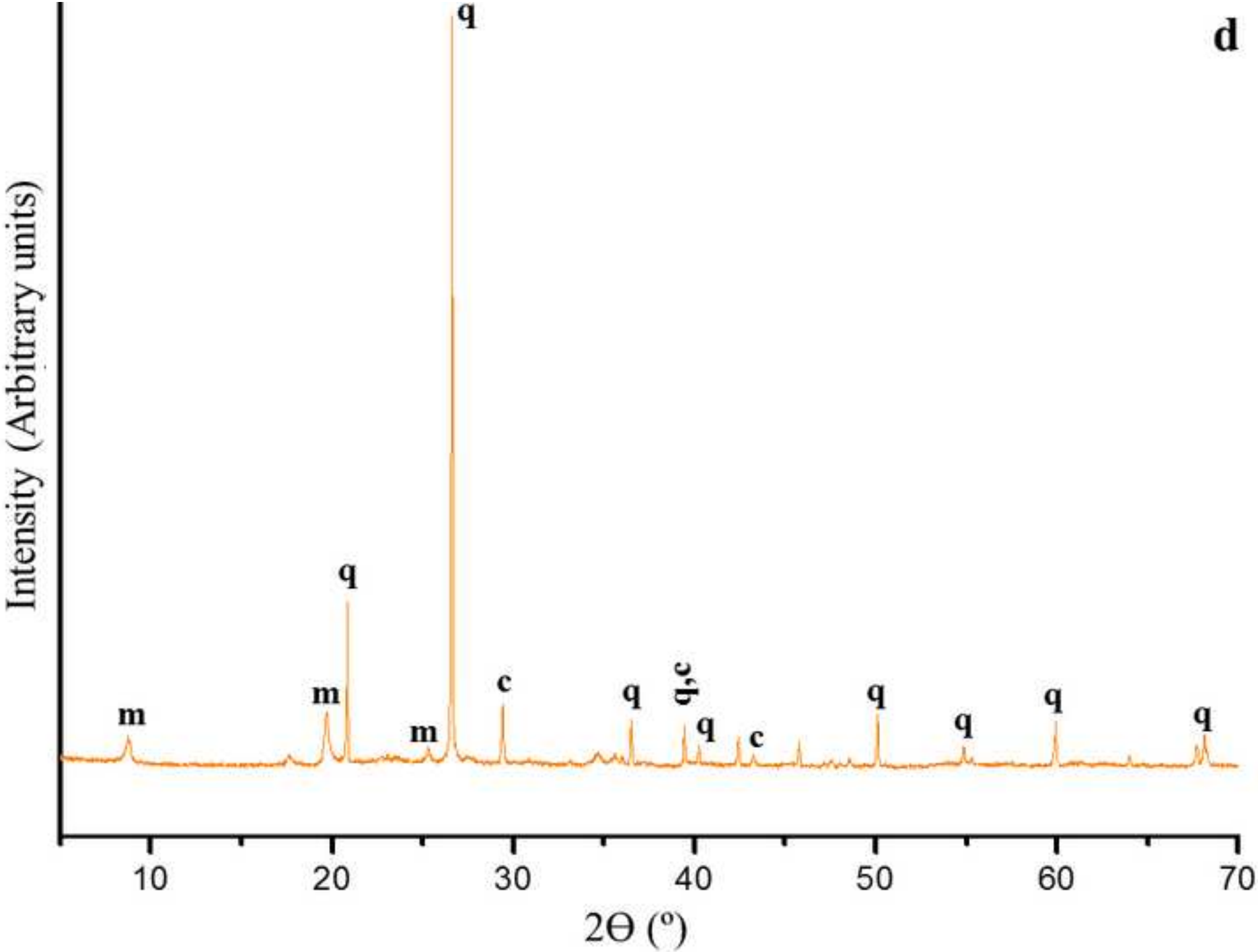

Figure 2

Click here to download high resolution image

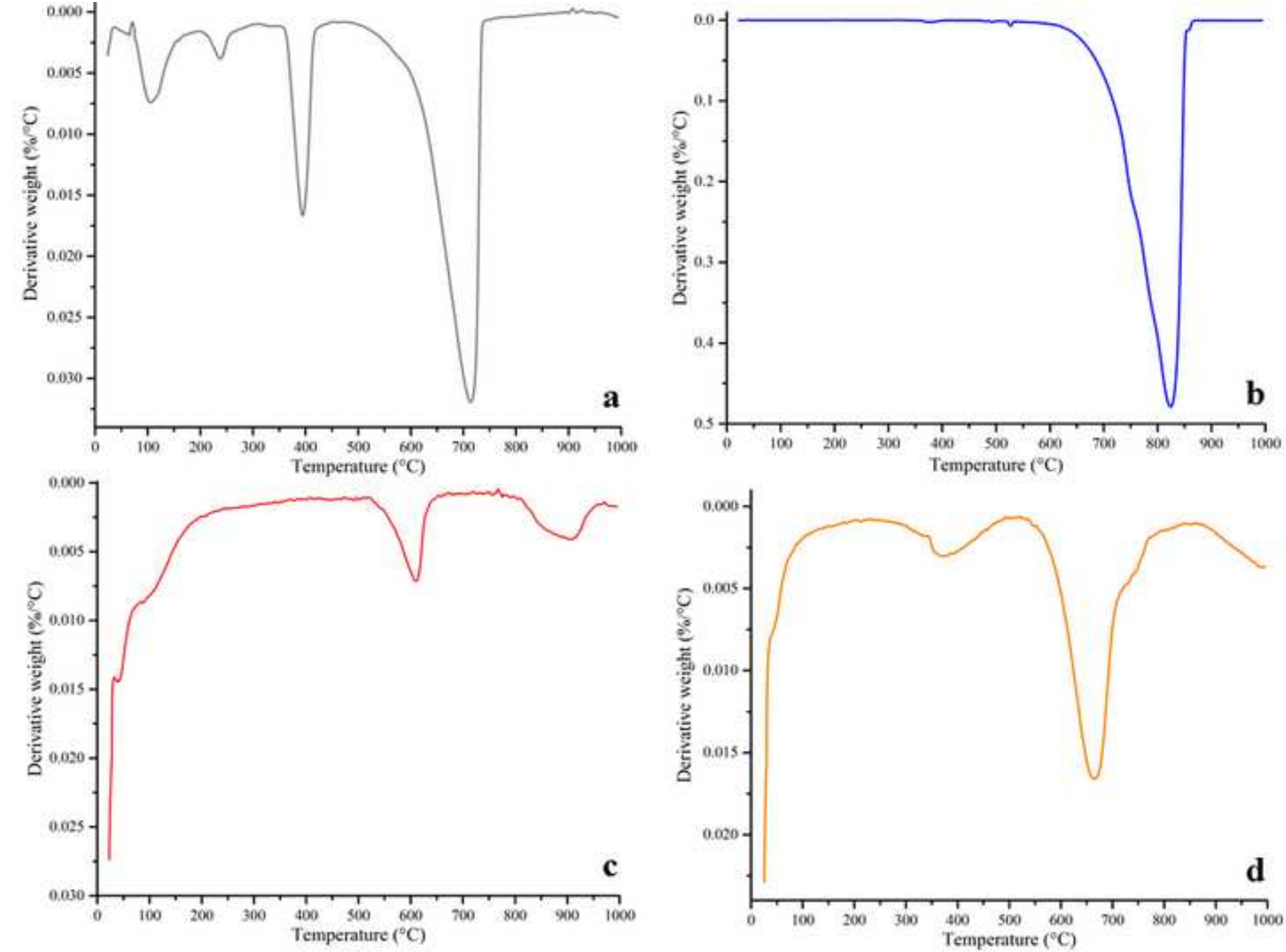

Figure 2a

Click here to download high resolution image

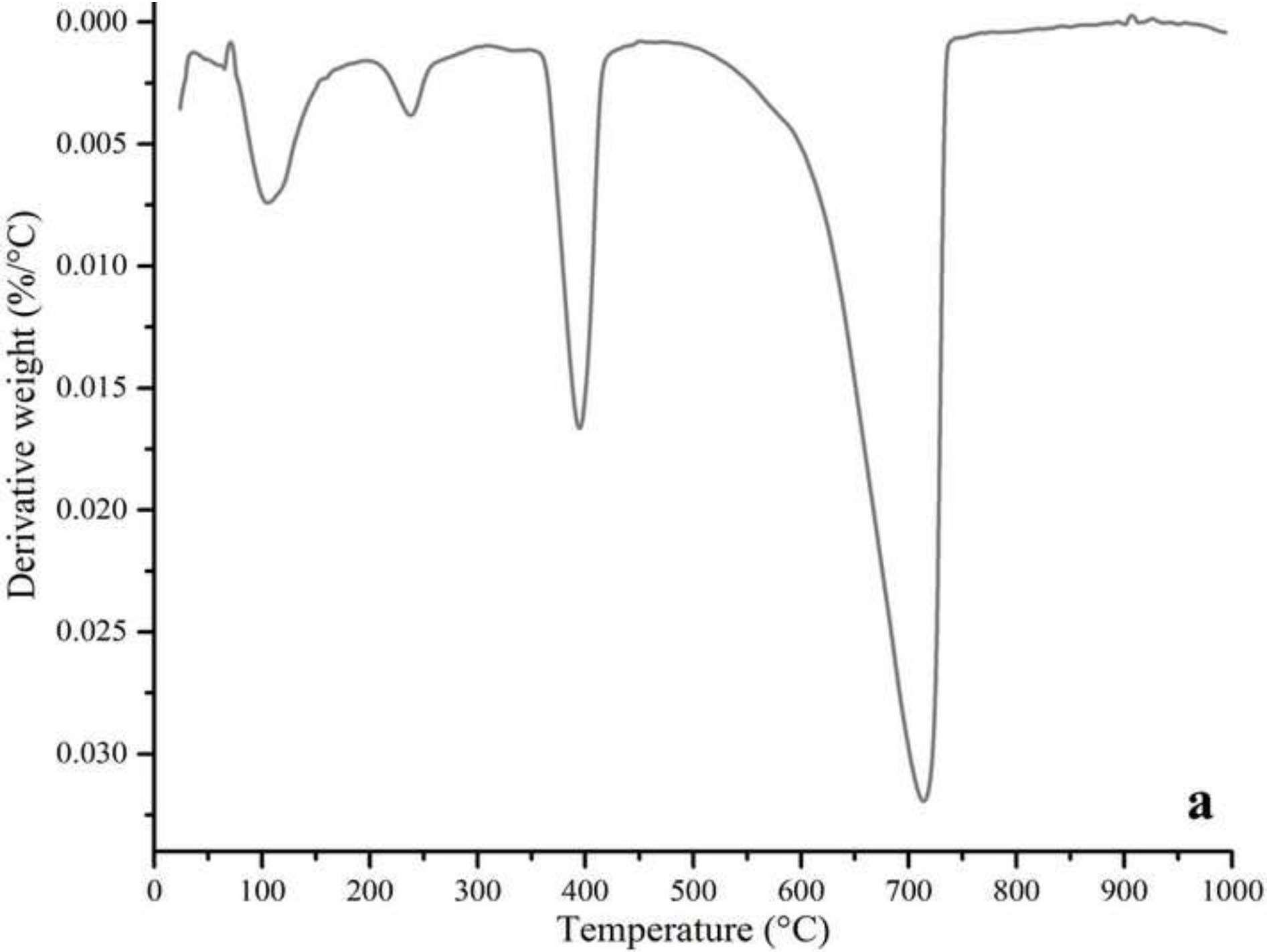

Figure 2b

Click here to download high resolution image

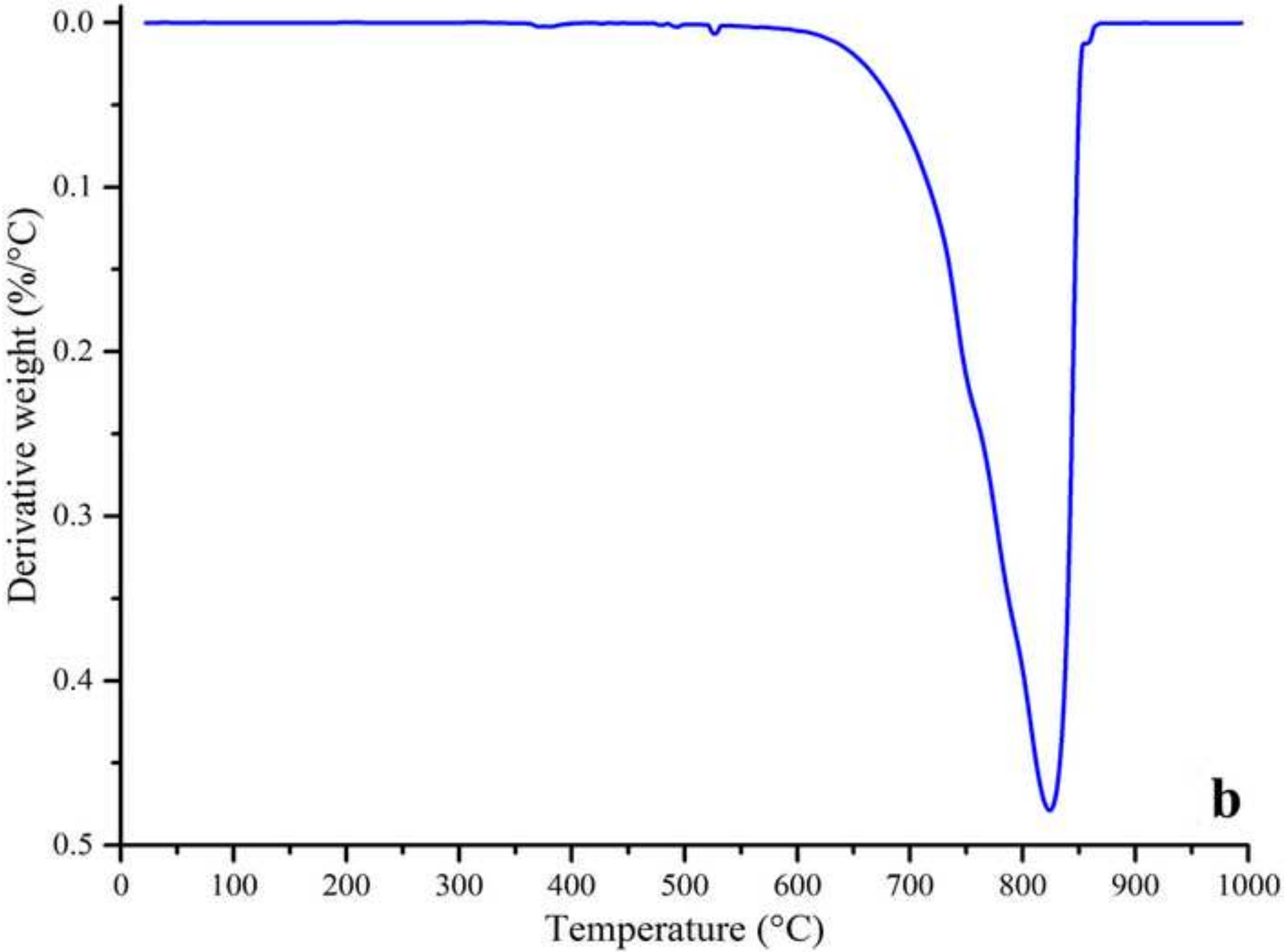

Figure 2c

Click here to download high resolution image

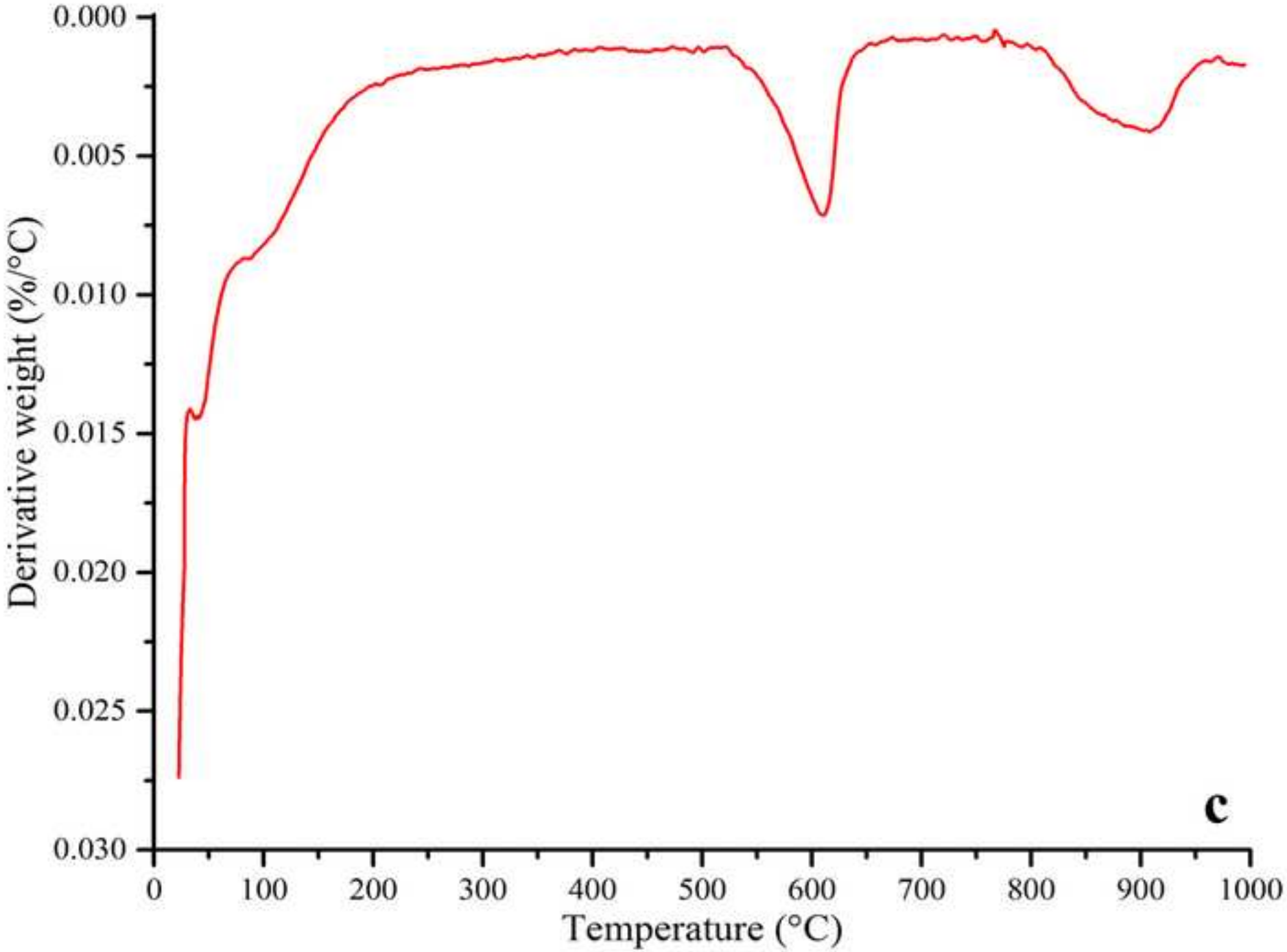

Figure 2d
Click here to download high resolution image

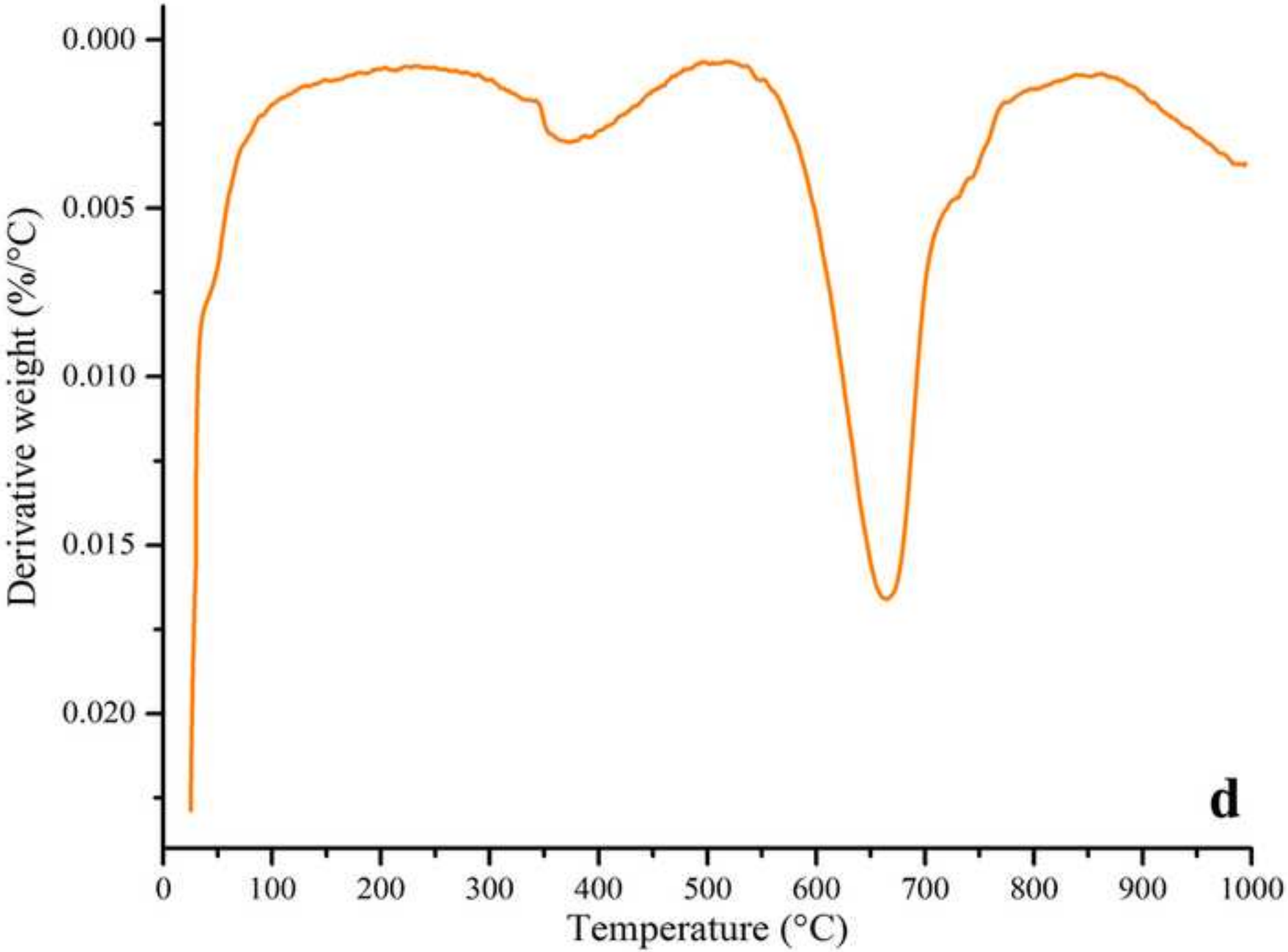

Figure 3

Click here to download high resolution image

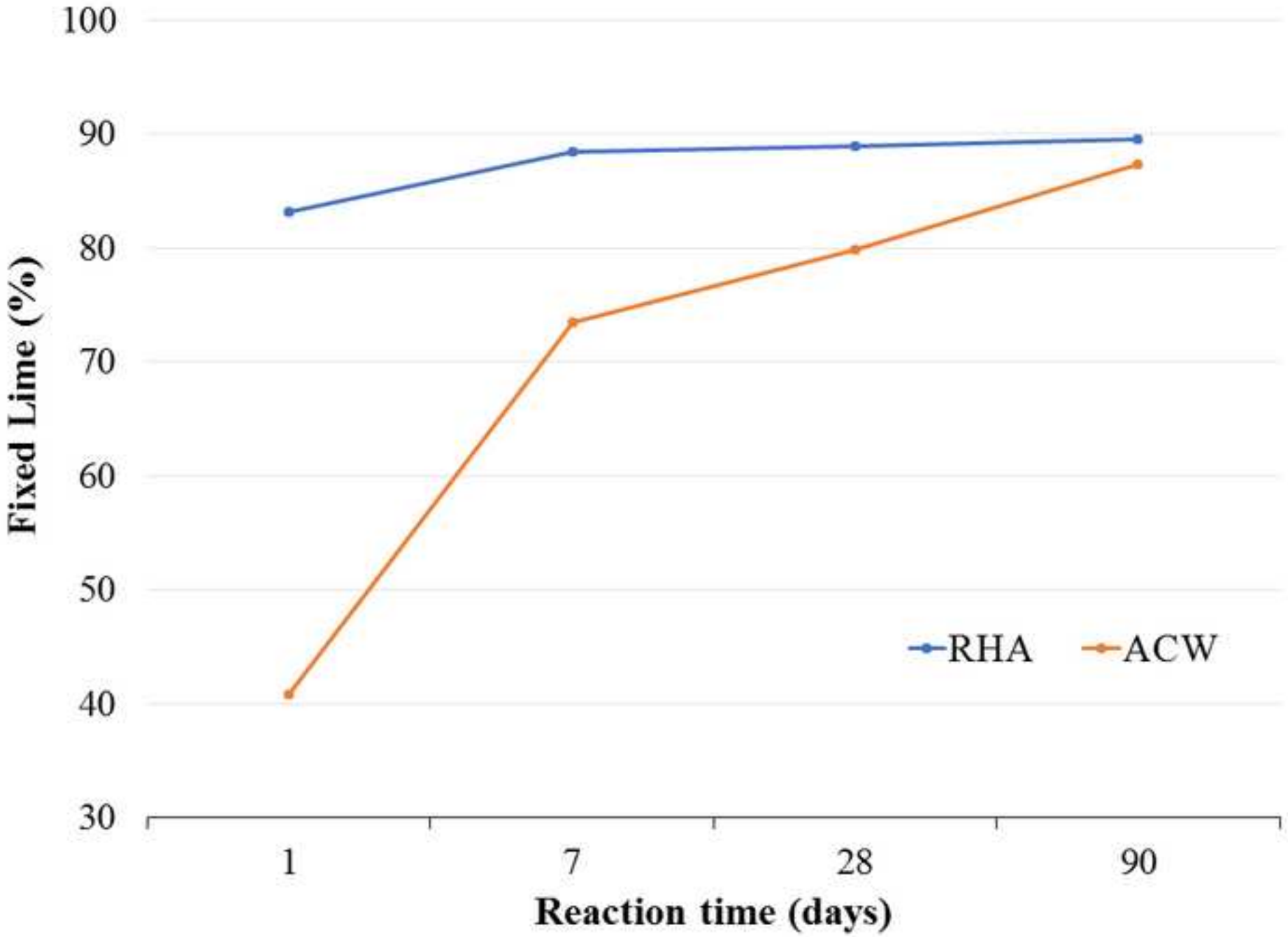

Figure 4

Click here to download high resolution image

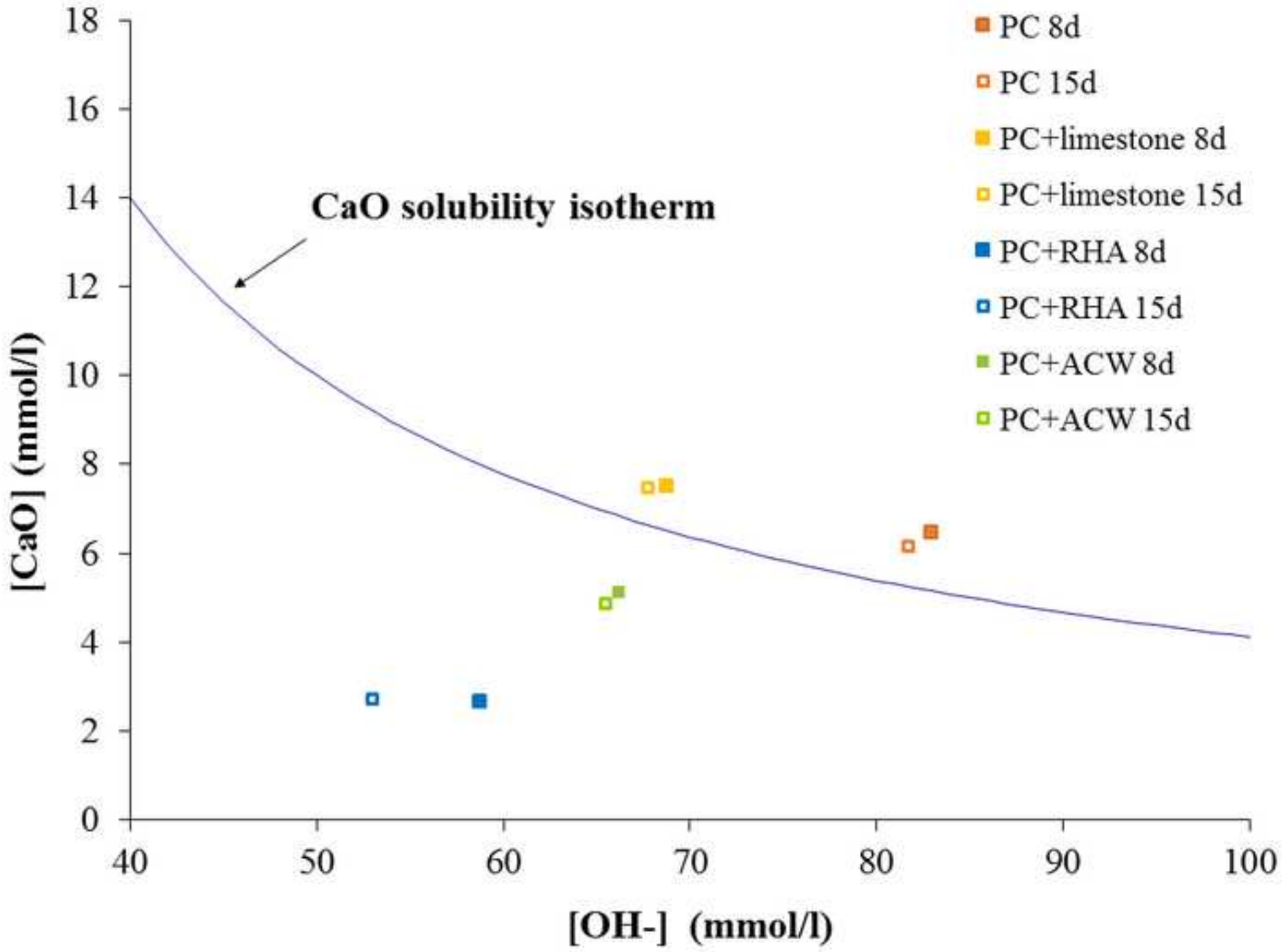

Figure 5

Click here to download high resolution image

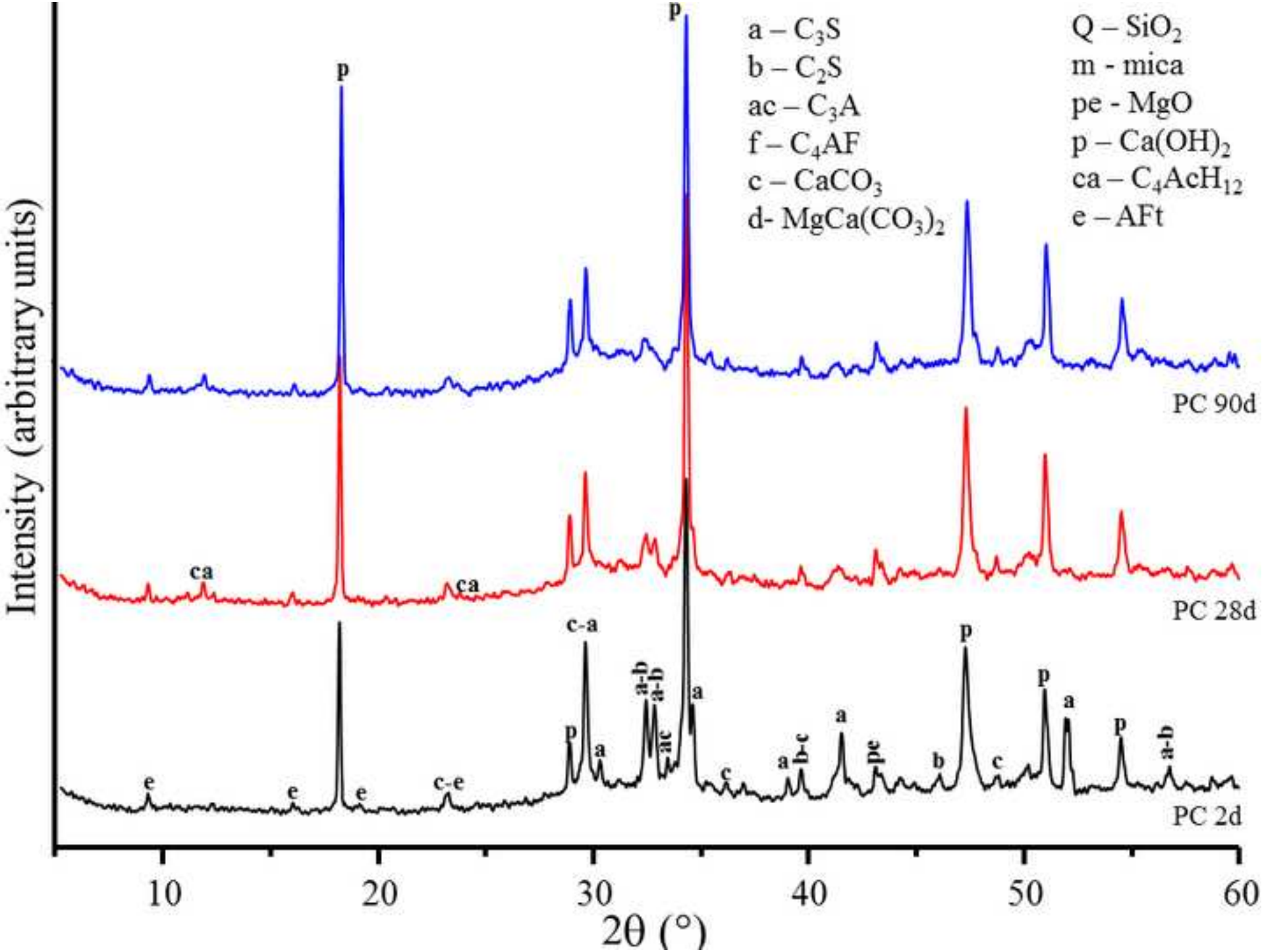

Figure 6

Click here to download high resolution image

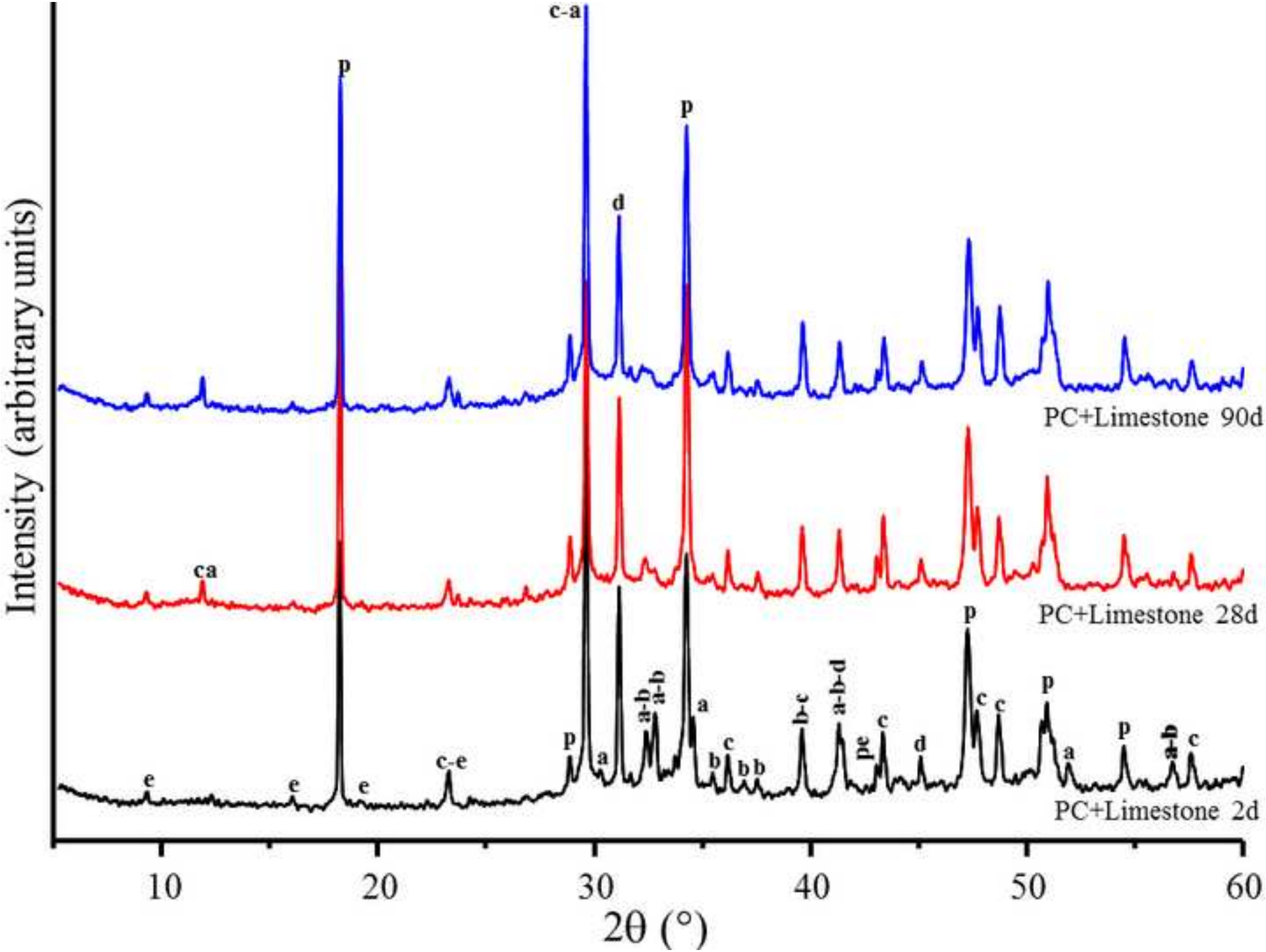

Figure 7

Click here to download high resolution image

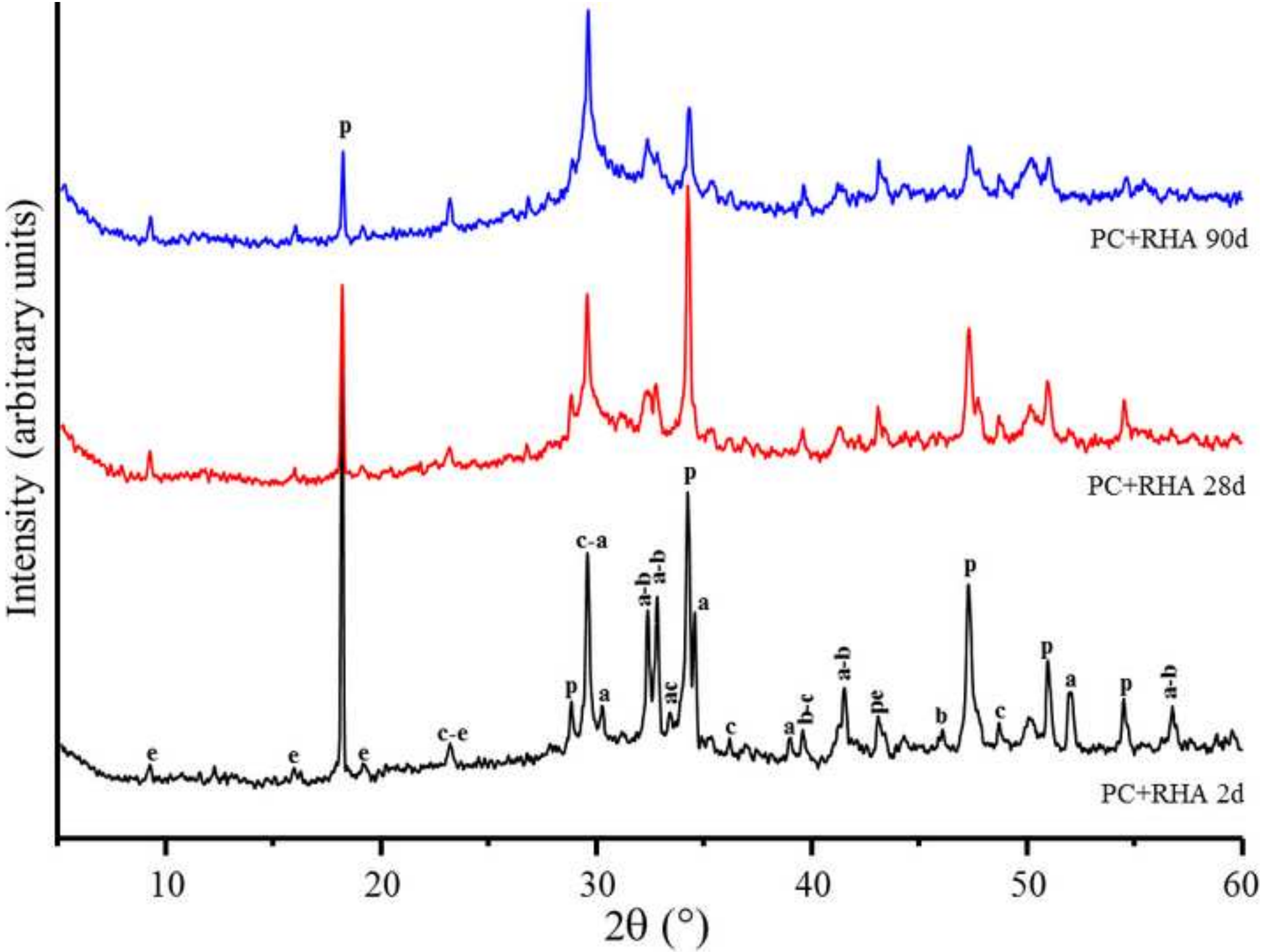

Figure 8

Click here to download high resolution image

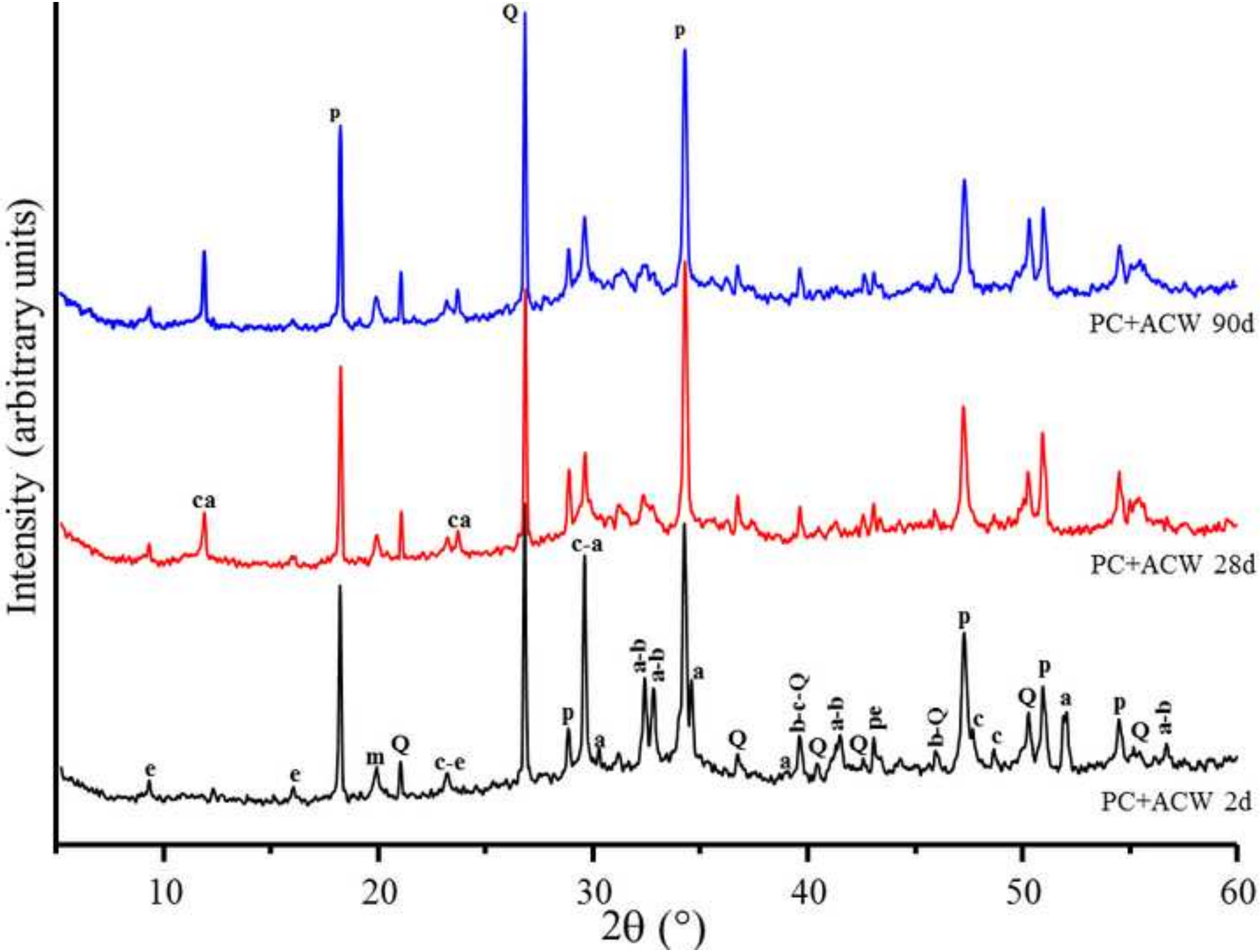

Figure 9

Click here to download high resolution image

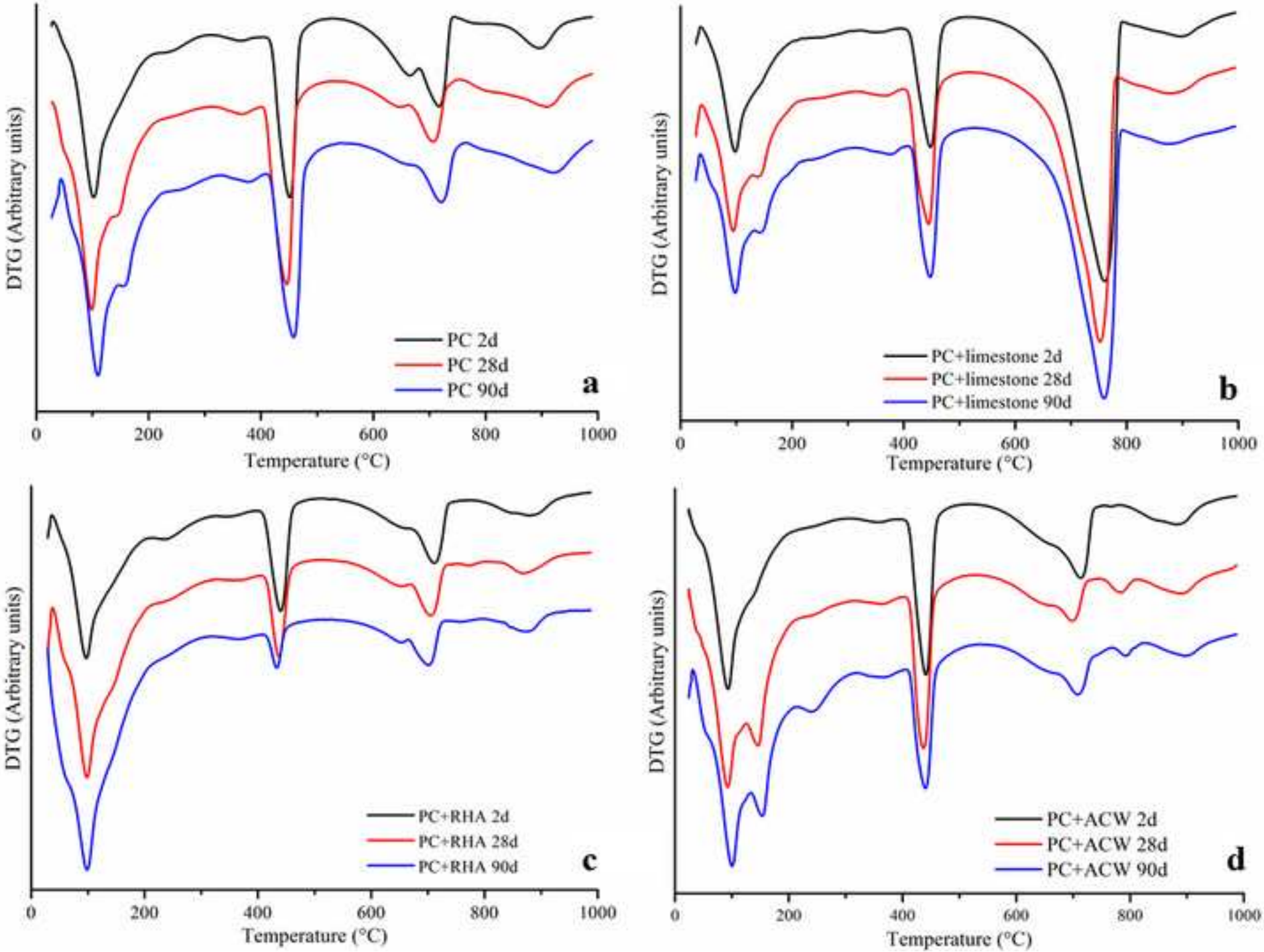

Figure 9a

Click here to download high resolution image

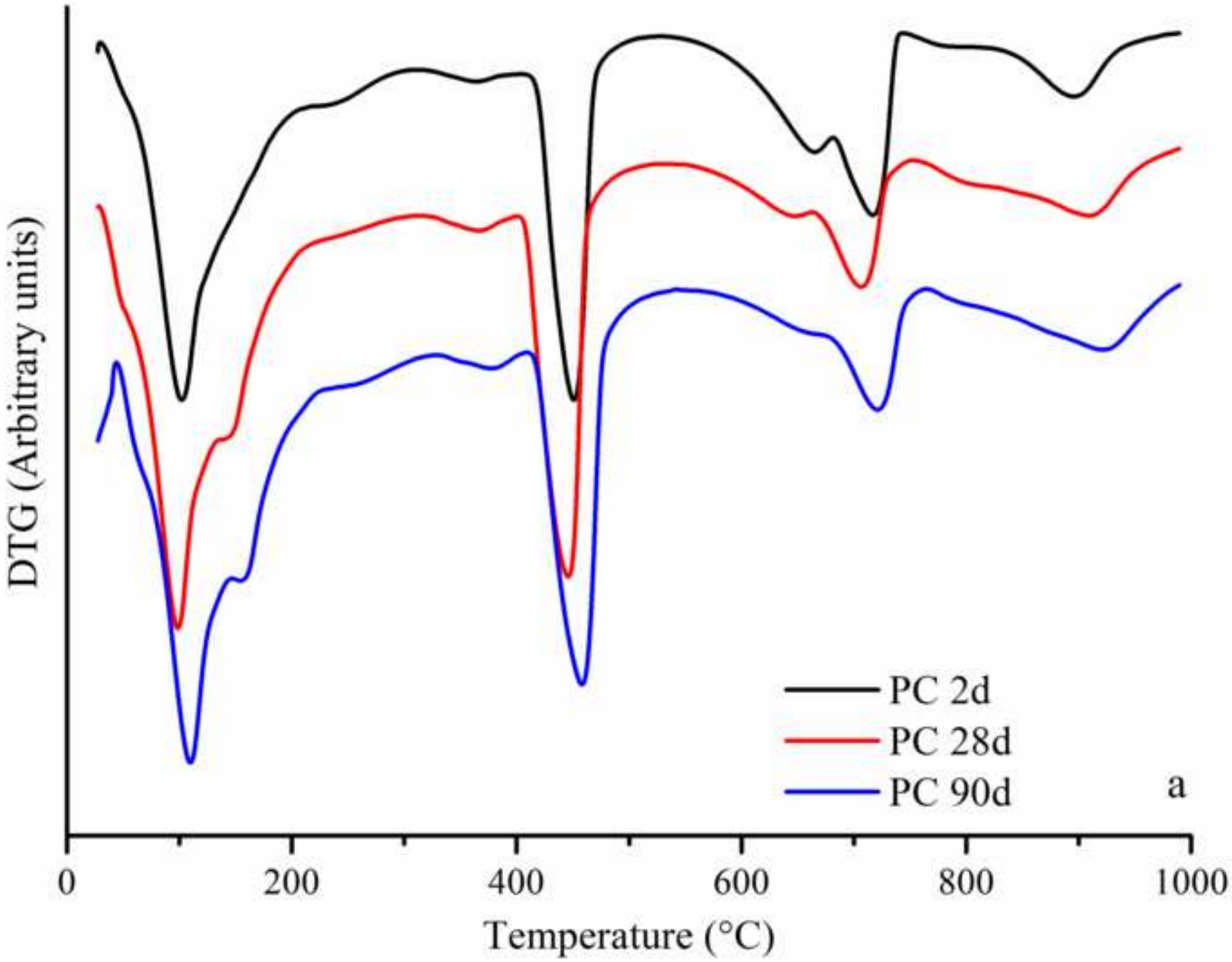

Figure 9b

Click here to download high resolution image

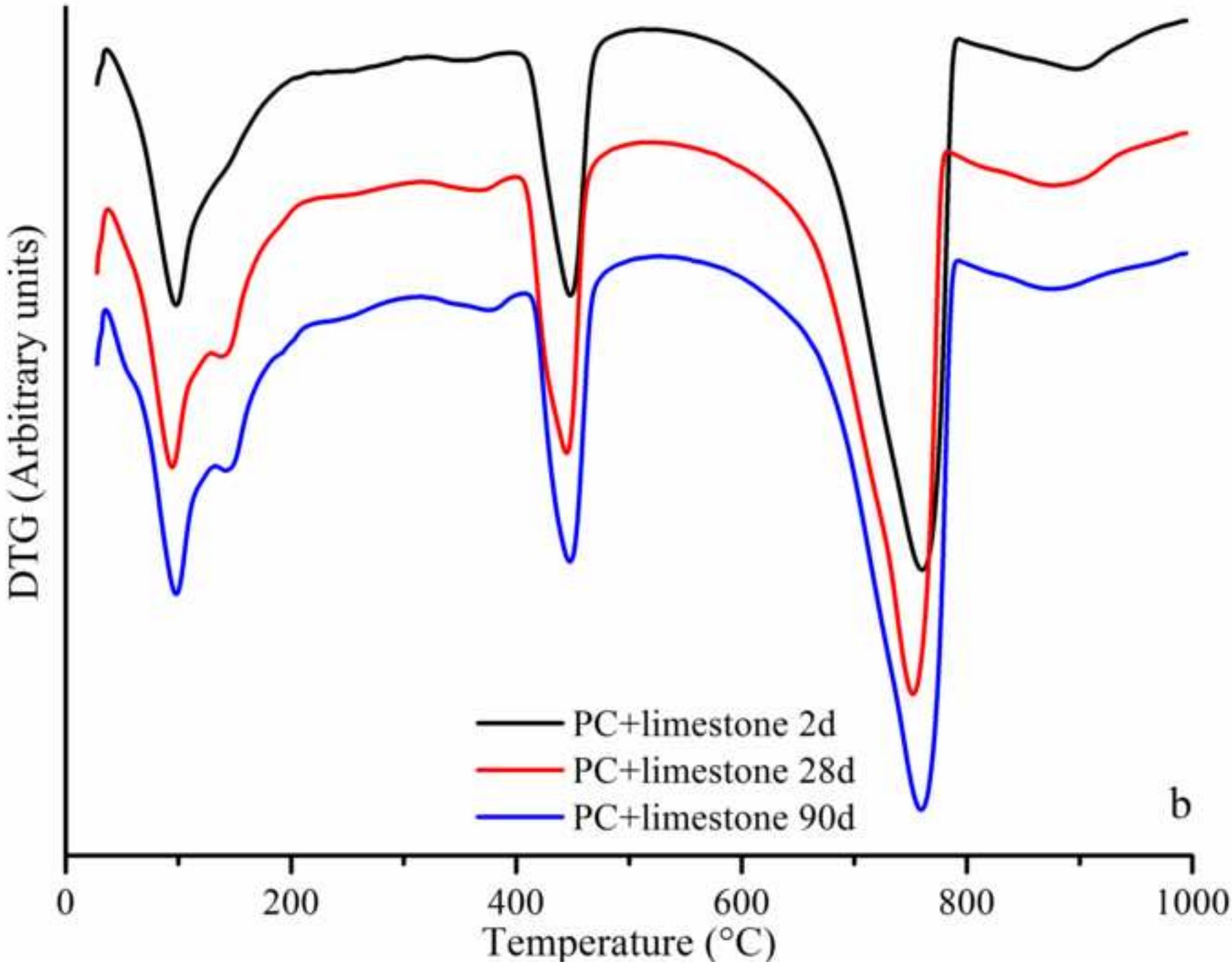

Figure 9c

Click here to download high resolution image

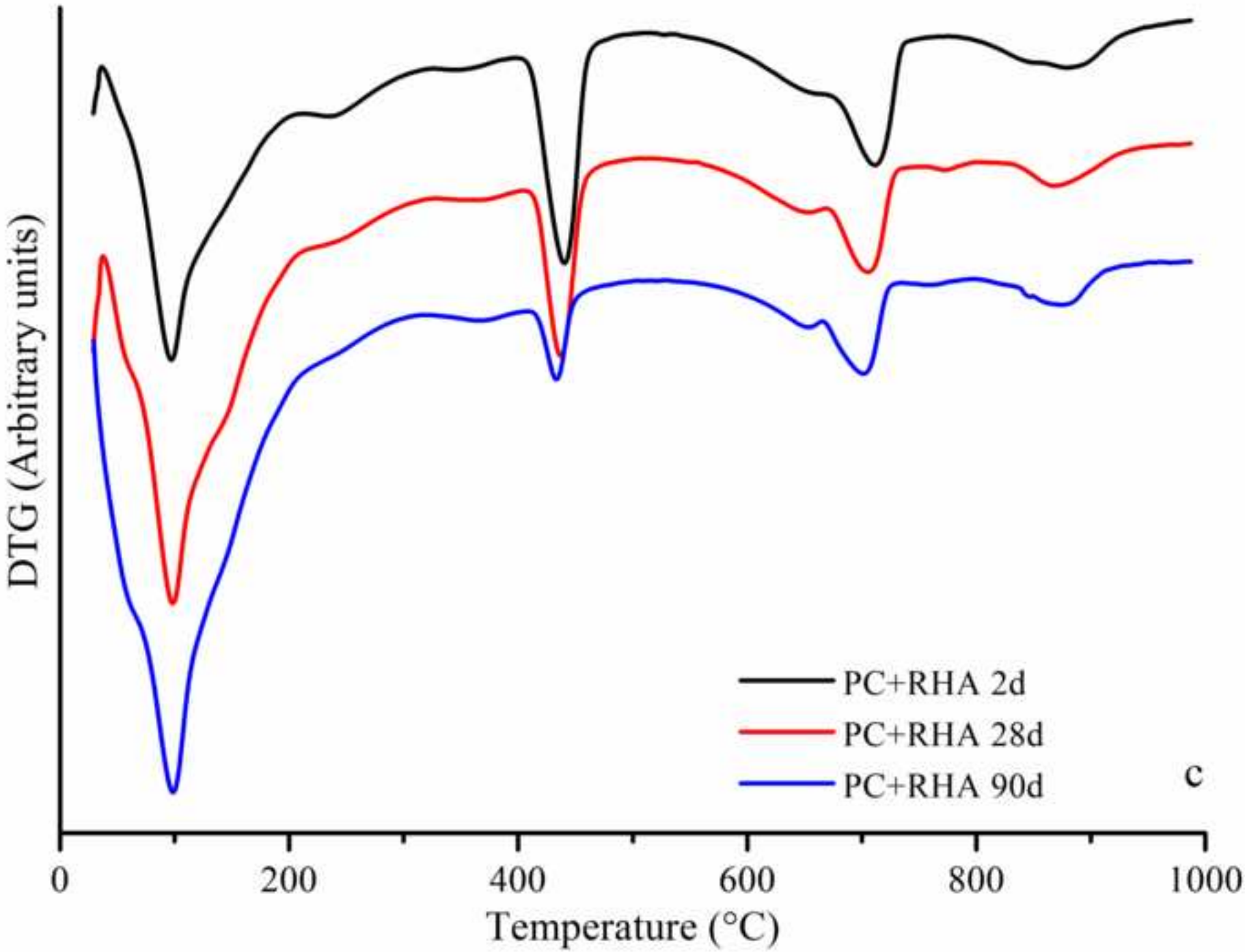

Figure 9d

Click here to download high resolution image

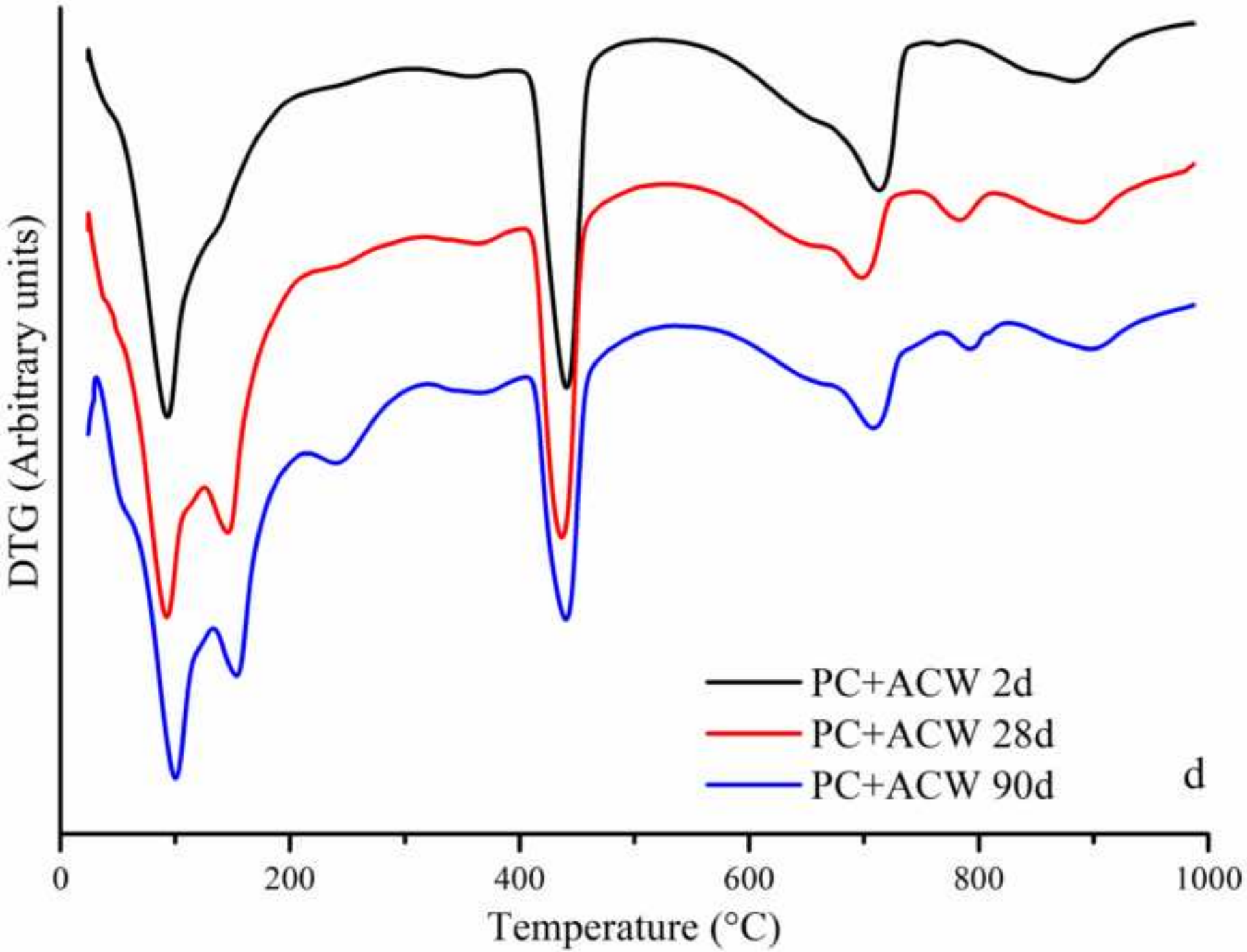

Figure 10

Click here to download high resolution image

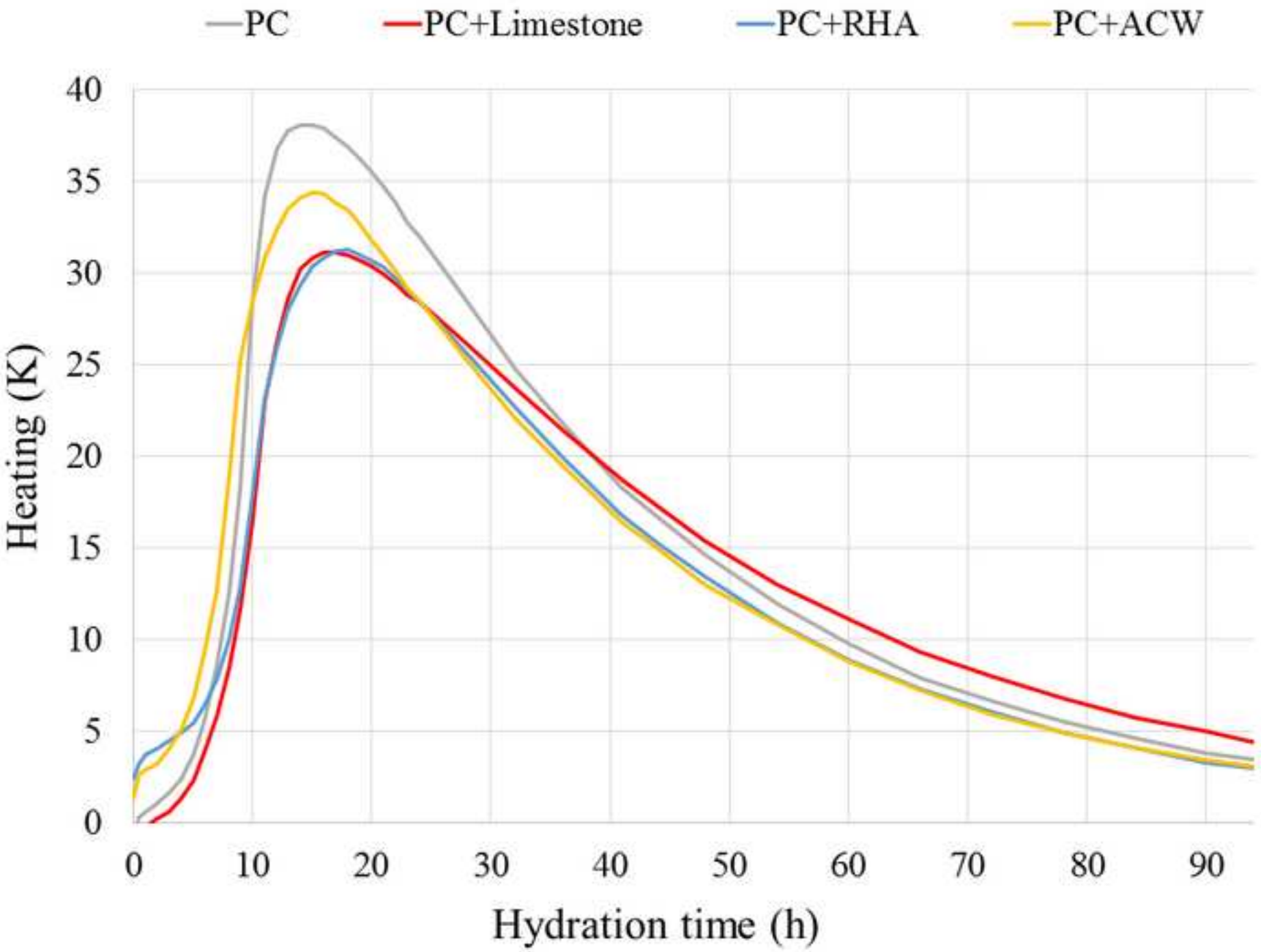

Figure 11

Click here to download high resolution image

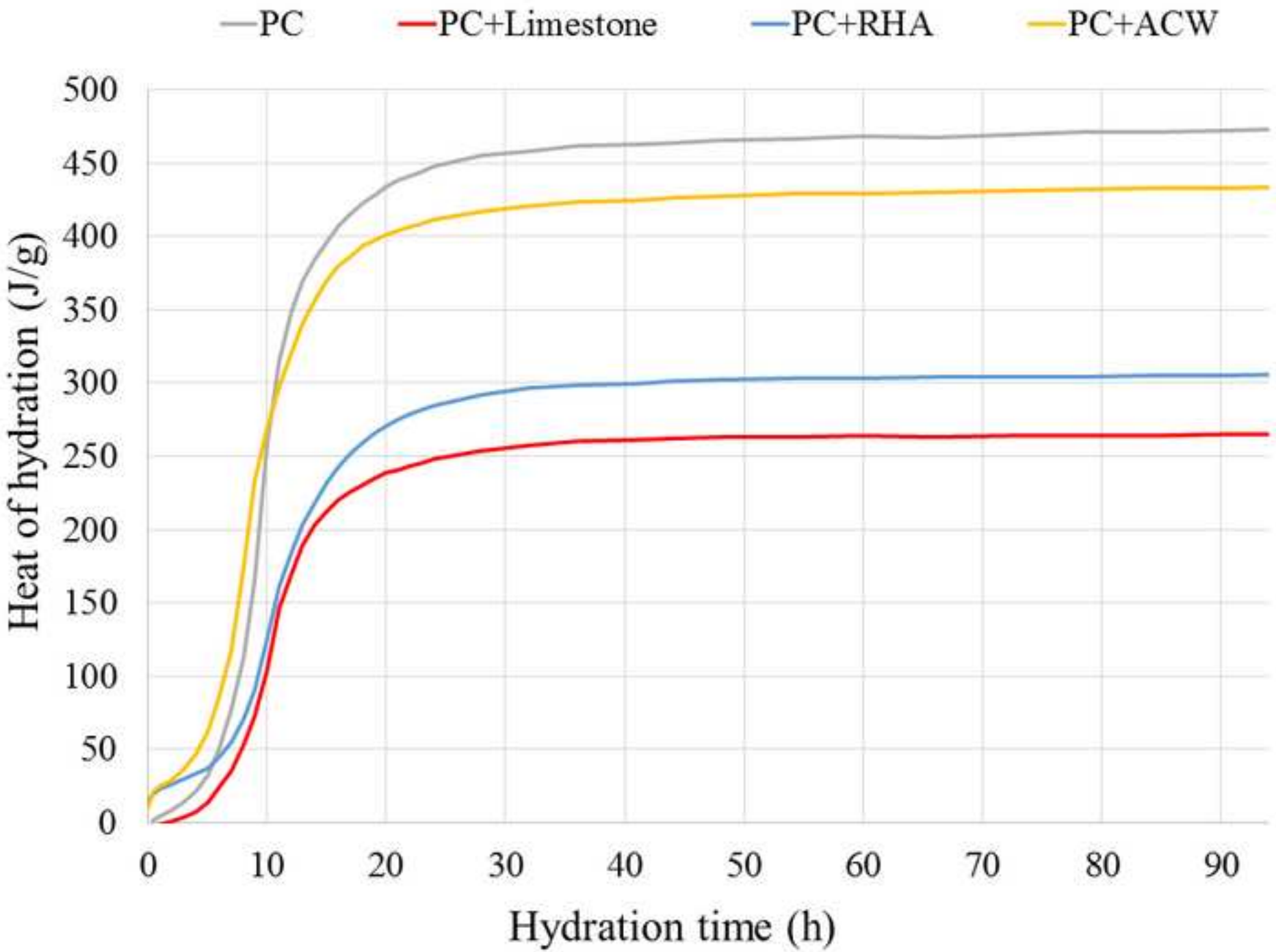

Figure 12

Click here to download high resolution image

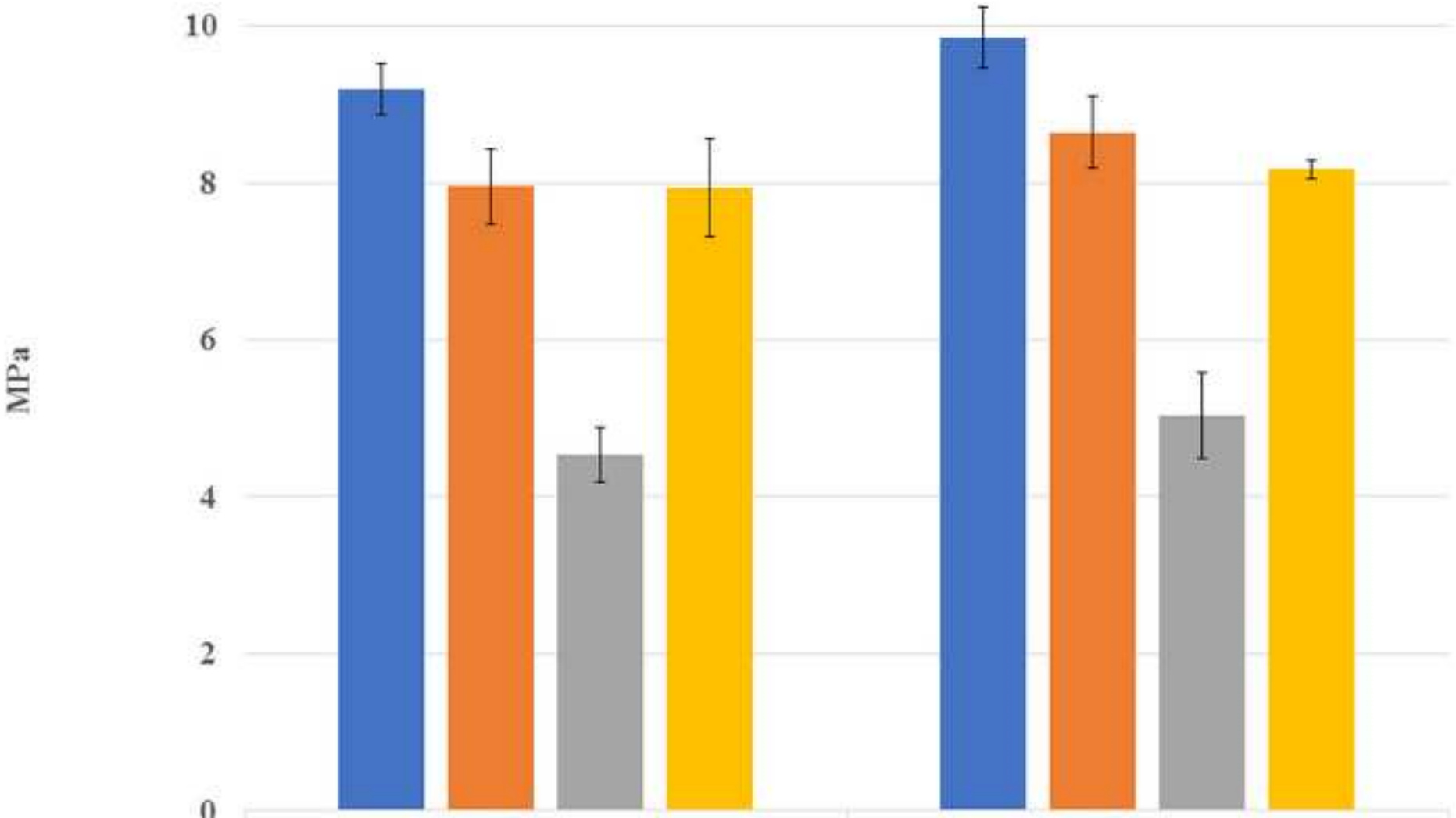

	7 days	60 days
PC	9.20a	9.86a
PC+limestone	7.95b	8.65ab
PC+RHA	4.54c	5.04c
PC+ACW	7.95b	8.17b

Figure 13

Click here to download high resolution image

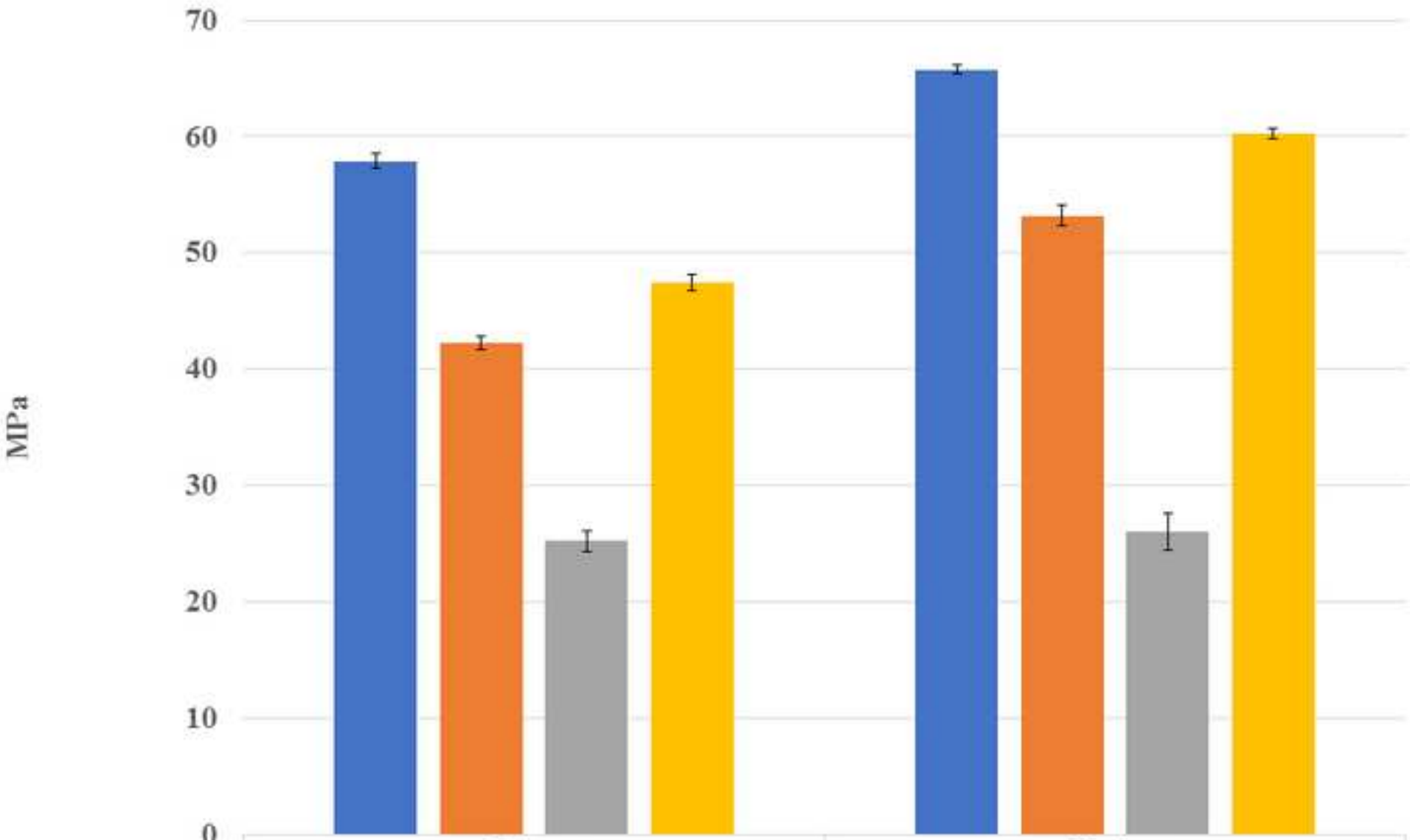

	7 days	60 days
PC	57.90a	65.73a
PC+limestone	42.29b	53.19b
PC+RHA	25.21c	26.03c
PC+ACW	47.41d	60.24d

Figure 14

Click here to download high resolution image

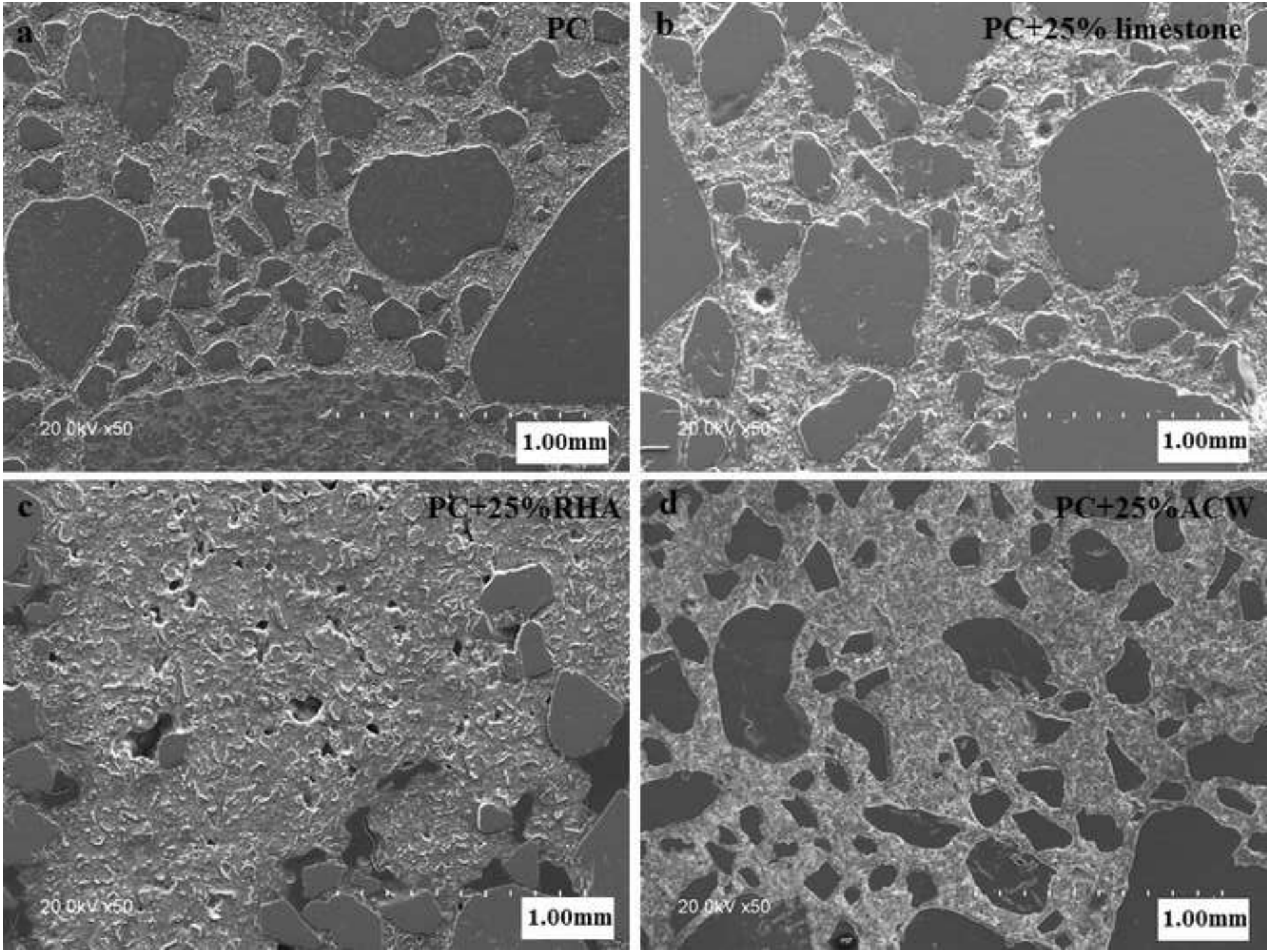

Figure 14a

Click here to download high resolution image

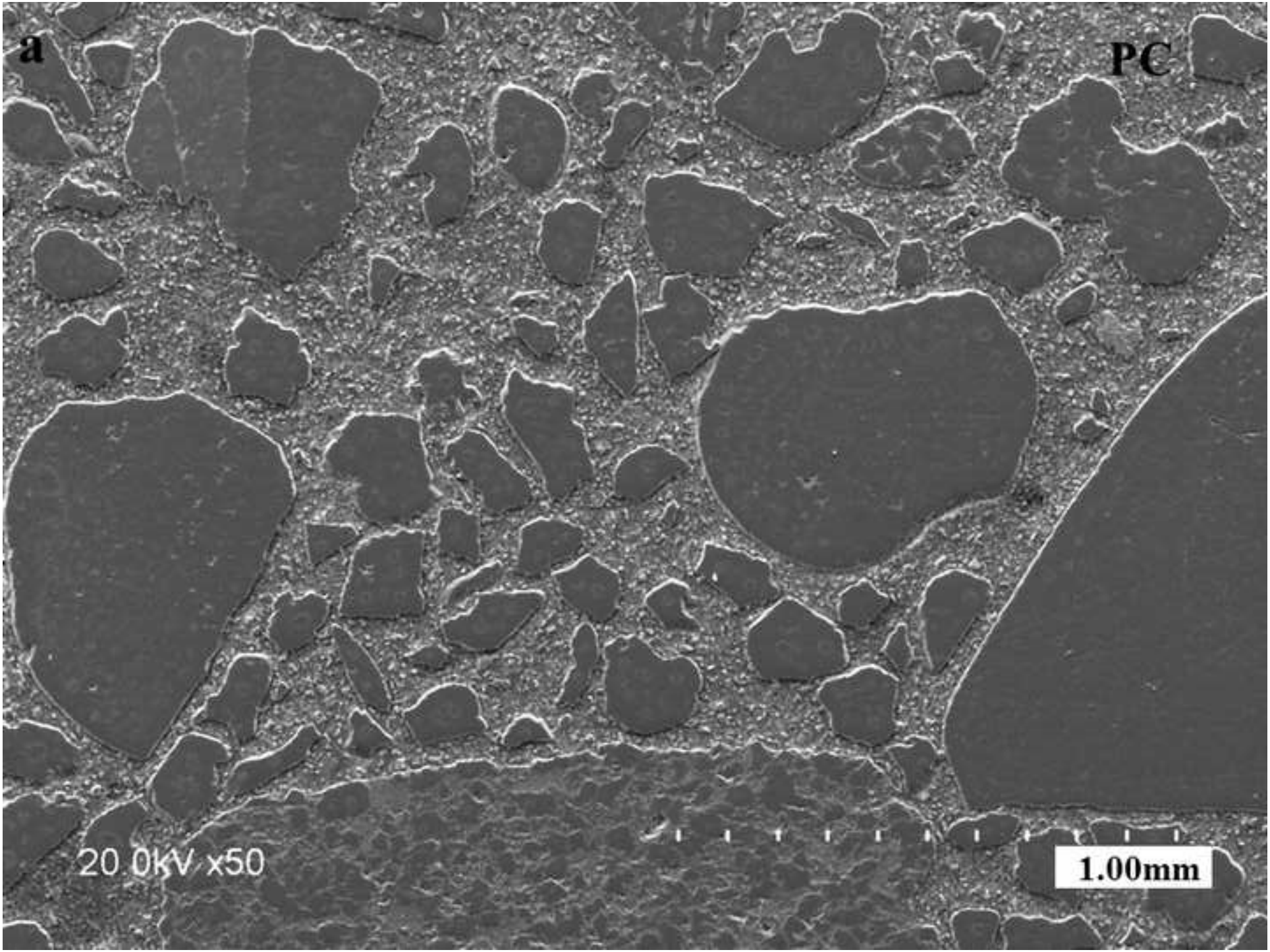

Figure 14b

Click here to download high resolution image

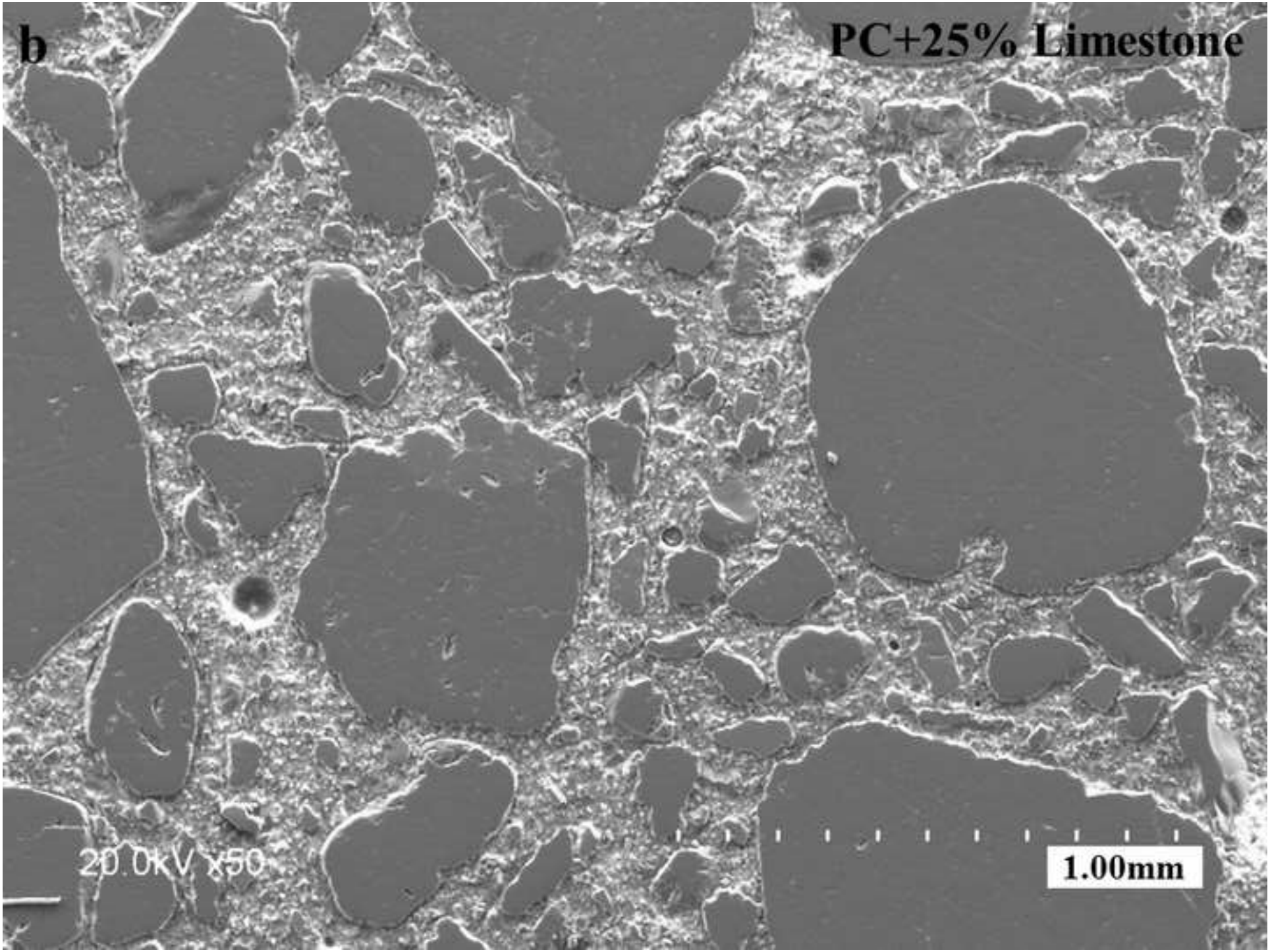

Figure 14c

Click here to download high resolution image

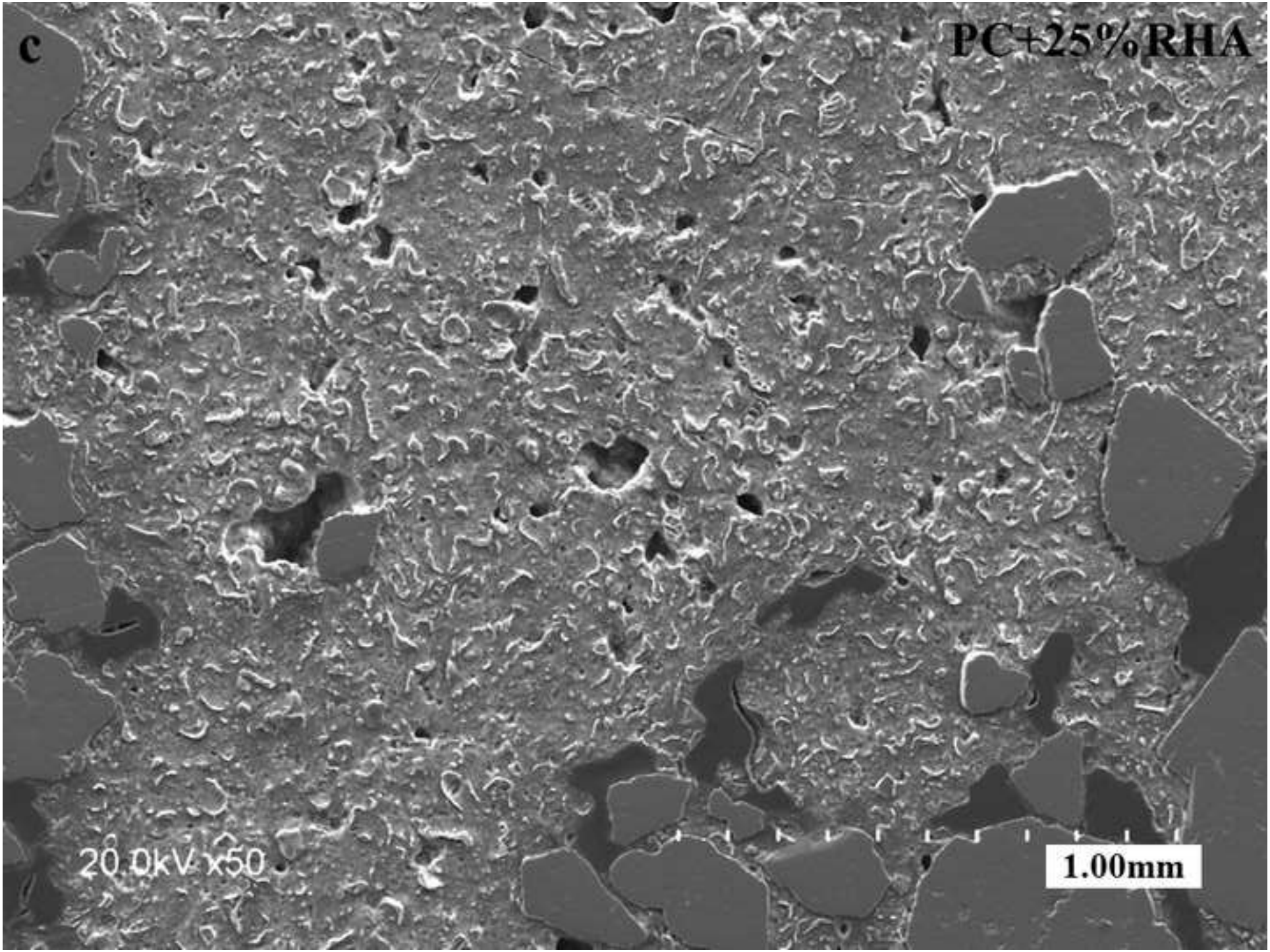

Figure 14d

Click here to download high resolution image

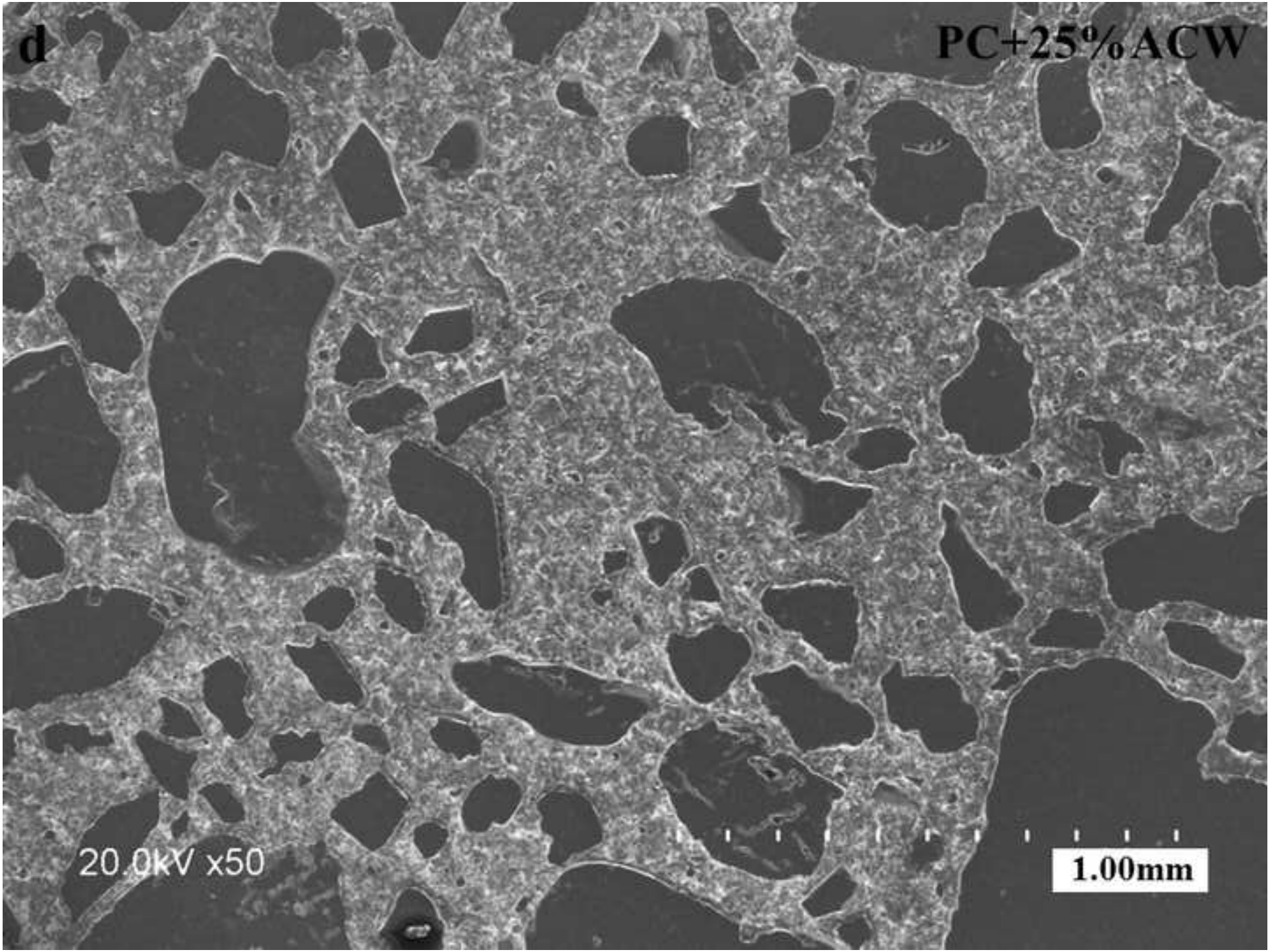

Figure 15

Click here to download high resolution image